Control of Ocean Wave Energy Converters with Finite Stroke

by

Yejun Lao

A dissertation submitted in partial fulfillment
of the requirements for the degree of
Doctor of Philosophy
(Civil Engineering)
in The University of Michigan
2020

Doctoral Committee:

Associate Professor Jeffrey T. Scruggs, Chair
Professor Jerome P. Lynch
Associate Professor Johanna Mathieu
Associate Professor Gabor Orosz

Yejun Lao

waynelao@umich.edu

ORCID iD: 0000-0002-0845-7721

To my family for their love and support

ACKNOWLEDGEMENTS

I would like to firstly thank my advisor, Professor Scruggs, for his mentoring on both my research and work as a graduate student instructor over the last five years. Throughout the years, whether it is a homework question, preliminary test, research problem or conference presentation, Jeff is always there and ready to help me. I have been fortunate enough to have such an advisor who really cares about his students and is willing to invest time and energy in his students. I hope we can continue our collaboration for many years to come.

I want to acknowledge my committee member, Professor Lynch, Professor Mathieu and Professor Orosz , for taking the time to review my work and provide constructive feedbacks. Special thanks to Professor Lynch, whose guidance has motivated me to think more about the real-life application of my research. I also want to thank Dr. Lissa MacVean for her help when I worked as the teaching assistant in CEE 265.

I would also like to thank my girlfriend Joan. Joan's support and understanding help me go through these stressful years. Joan also really cared about my emotional wellbeing. I enjoy the time when we go out for a running, hiking, traveling and skiing and can not wait for our next adventures.

I also want to say thank you to my family, especially my parents. As the only child in my family and an international student, I know that my parents have sacrificed a lot to make me pursue my degree in the United States possible. My parents have been supportive throughout the years and hopefully, I can make them proud.

I have made a lot of friends over the years. Alyssa and Brenden, my lab-mates,

TABLE OF CONTENTS

LIST OF FIGURES

Figure

LIST OF ABBREVIATIONS

WEC   Wave Energy Converter

PTO   Power Take-Off

OWC   Oscillating Water Column

MPC   Model Predictive Control

LQG   Linear Quadratic Gaussian

LMI   Linear Matrix Inequality

LTI   Linear Time-Invariant

LS   Lyapunov Stable

AS   Asymptotically Stable

PR   Positive Real

SPR   Strictly Positive Real

OSP   Output Strictly Passive

OSPR   Output Strict Positive Real

IID   Independent, Identically-Distributed

DFT   Discrete Fourier Transform

SVD   Singular Value Decomposition

CARE   Continuous-time Algebraic Riccati Equation

DARE Discrete-time Algebraic Riccati Equation

LTR Loop Transfer Recovery

LIST OF SYMBOLS

$\mathbb{R}$ The set of real numbers

$\mathbb{C}$ The set of complex numbers

$\mathbb{Z}$ The set of integers

$\mathbb{R}_{\geqslant 0}, \mathbb{R}_{>0}, \ldots$ The set of real numbers in interval $[0, \infty)$, $(0, \infty)$, $\ldots$

$\mathbb{R}^{n \times m}, \mathbb{R}^n$ the set of $n \times m$ real matrices, n-length real vectors

$\| \cdot \|$ A generic norm

$\| \cdot \|_F$ Frobenius norm

$\langle \cdot, \cdot \rangle$ A generic inner product

$\mathcal{L}$ Inner product space

$\mathcal{L}_e$ Extended inner product space

$\mathcal{L}_2$ The Lebesgue space

$\mathcal{L}_{2e}$ The extended Lebesgue space

ℓ_2 The discrete-time Lebesgue space

ℓ_{2e} The discrete-time extended Lebesgue space

$\mathrm{Tr}(\cdot)$ Trace

$(\cdot)^T$ Transpose

$(\cdot)^H$	Complex conjugate transpose
$H(s)$	Transfer function
$P = P^T > 0$	Matrix P is positive definite. Positive semi-definite, negative definite and negative semi-definite is denoted similarly.
$(\cdot)^{-1}$	Inverse
$\lambda_i(\cdot)$	Eigenvalue of a matrix
$\mathrm{Re}(\cdot)$	Real part of a complex number
$\mathrm{Im}(\cdot)$	Imaginary part of a complex number
$\mathbb{B}_H(s_0)$	Blocking space of transfer function associated with the zero s_0
$\cup$	The union of sets
$\mathcal{E}\{\cdot\}$	Expectation
δ	Kronecker delta
$x \mapsto y$	Mapping from x to y
$a \to b$	a approaches b
$\mathrm{null}\{\cdot\}$	Nullspace
$\mathrm{sgn}(\cdot)$	Sign function

ABSTRACT

In the design of ocean wave energy converters, proper control design is essential for the maximization of power generation performance. However, in practical applications, this control must be undertaken in the presence of stroke saturation and model uncertainty. In this dissertation, we address these challenges separately.

To address stroke saturation, a nonlinear control design procedure is proposed, which guarantees to keep the stroke within its limits. The technique exploits the passivity of the wave energy converter to guarantee closed-loop stability. The proposed technique consists of three steps: 1) design of a linear feedback controller using multi-objective optimization techniques; 2) augmentation of this design with an extra input channel that adheres to a closed-loop passivity condition; and 3) design of an outer, nonlinear passive feedback loop that controls this augmented input in such a way as to ensure stroke limits are maintained. The discrete-time version of this technique is also presented.

To address model uncertainty, in particular we consider the nonlinear viscosity drag effect as the model uncertainty. This robust control design problem can be regarded as a multi-objective optimization problem, whose primary objective is to optimize the nominal performance, while the second objective is to robustly stabilize the closed-loop system. The robust stability constraint can be posed using the concept of circle criterion. Because this optimization is non-convex, Loop Transfer Recovery methods are used to solve for sub-optimal solutions to the problem.

These techniques are demonstrated in simulation, for arrays of buoy-type wave

energy converters.

CHAPTER 1

Introduction

1.1 History of Harvesting Ocean Wave Energy

The history of harvesting ocean wave energy has unfolded over more than a century, during which many different devices for utilizing wave power have been proposed. The earliest idea related to the Ocean Wave Energy Converter (WEC), to the author's knowledge, is due to Stahl [1]. The operating principle was to use the motion of a cylindrical float, which is attached to a fixed structure to generate power. However, people at that time were doubtful about the feasibility of this idea, and no real energy converter model was constructed. As petroleum became the most important energy resource after the First World War, the interest of wave energy faded [2]. In the late 1940s, a Japanese wave energy pioneer Yoshio Masuda started to investigate several different types of WECs, and surmised that buoy-type converters have relatively high reliability. The converters had a very long lifetime, some of which operated more than 20 year at sea [3]. A European wave energy pioneer, Stephen Salter from the University of Edinburgh initiated wave energy research in 1973. His group built the "Edinburgh Duck" models and came up with several techniques to improve the performance by controlling the device movement [3]. At the same time, two Norwegian scientists Kjell Budal and Johannes Falnes focused on the point absorber type converters, which can achieve the maximal power extraction by tuning

the resonant frequency to the characteristic frequency of the incoming waves [4]. In the US, Michael E. McCormick was one of the early wave-energy researchers and his book Ocean Engineering Mechanics provided useful insight into the interaction between waves and converters [5].

In the years following the oil crisis in 1973, many institutions and researchers turned their attention to wave energy and focused on the possibility of increasing the amount of power extracted from waves. During the late 1970s, larger government-funded research programs were started at UK, Norway and many other countries. During this time, Dr. David Evans at Bristol University proposed a submerged cylinder device constrained by the springs and dampers to make small oscillations both vertically and horizontally, which can be very efficient in absorbing the energy from the waves. This type of device was also tested experimentally and the result was promising [6]. In Japan, Masuda led the sea test of the Kaimei ship, which consisted of 22 oscillating water column chambers open at the bottom [7]. The oscillation of the water level inside each chamber can provide airflow to the turbines. The Kaimei was connected to the grid and was able to supply power for household use to the coastal community of Yura in Yamagata prefecture in Japan. In the early 1980s, when the petroleum price declined, the funding for wave energy research drastically reduced.

The situation in Europe dramatically changed by the decision made in 1991 by the European Commission of including wave energy in their R&D program in renewable energies. During the 90s, around thirty wave energy projects are funded by the European Commission. In 2001, the International Energy Agency established an Implementing Agreement on Ocean Energy Systems (IEA-OES), whose goal is to advance the wave energy research, development and demonstration through international cooperation. The IEA-OES provides annual reports which are generally the surveys of ongoing activities on wave energy worldwide [8]. More recently, a growing interest in wave energy is taking place in North America (the U.S. and Canada), with

the funding support from the national and regional departments [9].

1.2 Potential of Ocean Waves

A large amount of waves are generated when a strong wind blows along the surface of the ocean. In the deep water, the dissipation rate of energy stored in the waves is low, enabling the waves to travel much farther than the wind that creates them. Furthermore, since the density of sea water is three orders of magnitude higher than air, energy delivered by waves is more concentrated than wind energy [10].

The total available wave energy is just a small portion of the wind energy, which in turn is just a small portion of solar energy. Nevertheless, the wave energy does have its own advantages. As solar energy is converted to wind energy, the energy density changes from 0.1-0.3kW/m^2 horizontal surface to 0.5kW/m^2 area perpendicular to wind direction. As wind energy is converted to wave energy, even more energy concentrated spatially. The average power flow below the ocean surface is at 2-3kW/m^2 area perpendicular to wave direction [2]. The wave power is more persistent than the wind and solar energy. The energy from waves can supply power up to 90% of the time, compared to 20~30% of the time for wind and solar energy [11].

It is estimated that between 2000 and 4000 TWh/year of energy can be extracted worldwide from waves. The greatest potential for wave energy exists where the strongest winds are found at the latitudes between 40° and 60° north and south, on the eastern boundaries of the oceans [12]. One of the richest nations in terms of the potential of wave energy is U.K., along with the north of Scotland having particularly high potential. The global distribution of wave power resources is in Figure 1.1. To get a sense of the available energy levels (the unit is the same as the one in Figure1.1), about 37kW/m can be seen in the U.S. Northern Pacific coast, compared with about 33 kW/m in the U.S. Northern Atlantic coast. Over 70 kW/m can be found in the west coast of Scotland, about 50 kW/m in Norway, about 40 kW/m in

Wave power levels are approximate and given as kW/m of wave front
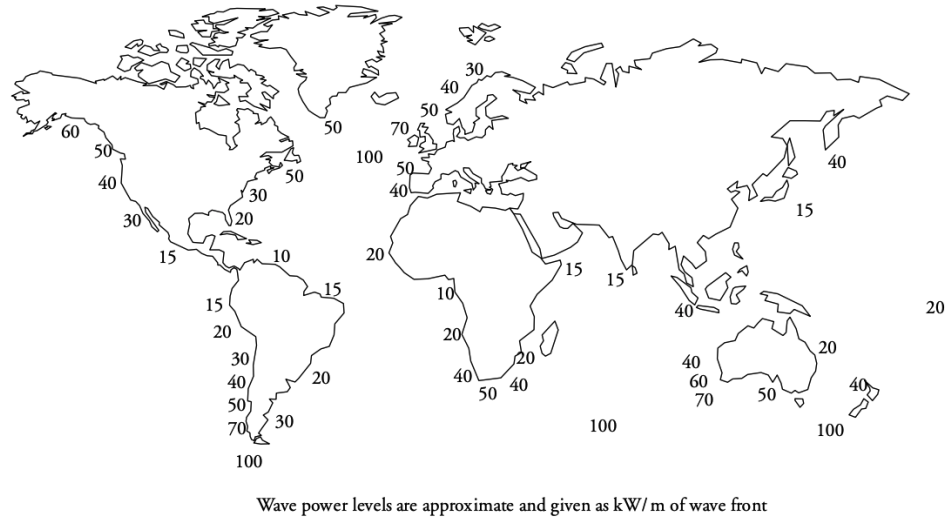
Figure 1.1: Global Distribution of Deep Water Wave Power Resources [13]

Portugal, and about 12-15 kW/m in the Pacific coast of Japan, while further south approaches or exceeds 70 kW/m, especially in the southern part of Australia and Chile.

In general, more wave power can be found in the high northern and southern latitudes, especially during the winter months. As the energy demand is always higher in the winter due to the heating, locally generated power from waves is a natural fit in these regions. Compared with other renewable energy types, wave energy is considered to have the lowest environmental impact [13]. If the wave energy capture technology is fully developed, the market potential is enormous.

1.3 Challenges

To achieve the potential of wave energy and make it economically competitive, several technical difficulties need to be overcome.

A significant challenge is to convert the slow and random oscillatory motion into the driving force of a generator that can output reliable electricity for commercial use. Although the average power generation can be calculated in advance, converting

4

this random input into smooth electrical output requires energy storage systems. Additionally, the wave direction can be highly unpredictable, so the wave devices have to align themselves on compliant moorings, or need to be symmetrical to extract the power [14].

Another big challenge is that a WEC needs to survive under extreme events such as hurricanes and storms. To operate efficiently, WECs are designed to achieve optimal performance under most frequent wave conditions. Moreover, WECs also need to survive the infrequent, or extreme wave conditions.

Since WECs are mainly offshore devices, the maintenance cost is correspondingly higher compared with other renewable energy industries [15]. The structure of the WEC needs to be designed reliable to minimize the maintenance cost.

1.4 Wave Energy Converters

There are over 1000 wave energy conversion technologies have been patented around the world. Most of them include an oscillating body(sometimes water level in a chamber), whose oscillation in response to waves drives subsequent energy conversion stages. Based on the relative direction between the principal axis of the oscillating body and the wave propagation direction, the WECs can be categorized into three dominant types: Point Absorber, Attenuator and Terminator. This is shown in Figure1.2. For attenuator and terminator, they are mainly floating devices. However, for point absorber, it can be a floating or submerged device.
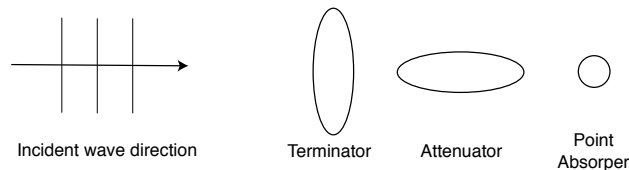
Figure 1.2: Orientation and scale of a Terminator, Attenuator and Point Absorber [10]

1.4.1 Point Absorber

A point absorber is a device that is usually axisymmetric and possesses small dimensions relative to the incident wavelength. They can be submerged below the sea surface or floating structures that heave up and down on the surface of the water. Since they are axisymmetric, wave direction is not important for these devices.
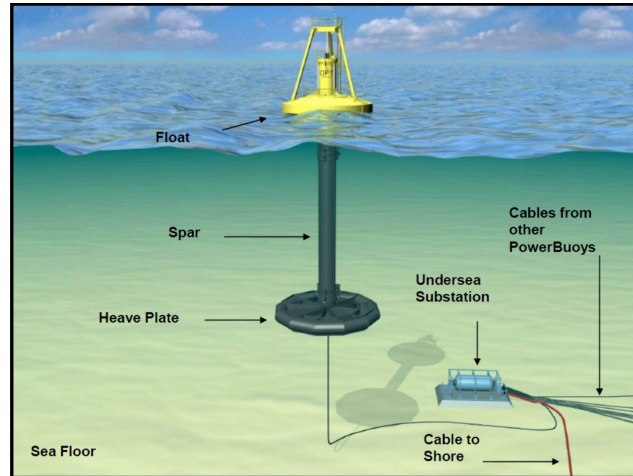
Figure 1.3: PowerBuoy Prototype from Ocean Power Technology [16]

There are numerous examples of the point absorbers. One of them is the Powerbuoy from Ocean Power Technology. The Powderbuoy is a floating oscillating body, the structure of which is shown in Figure1.3. A mooring keeps the Powerbuoy on station in the ocean. At the surface, the float oscillates along the spar with a reduced response to ocean waves due to the heave plate below. The relative motion between the float and the spar drives a rod into the spar. A mechanical actuator converts this linear motion into a rotary motion that drives an electric generator, which in turn outputs three-phase unregulated AC power. A power management and conditioning system converts and conditions AC power into DC power. Ultracapacitor technology is used to remove the transient nature of wave power. The first prototype PB3 was used by US Navy project to provide power to coastal security networks and survived rigorous sea trials [16]. In order to supply a certain amount of steady power, a wave

farm needs to be constructed, which contains an array of Powerbuoys. This concept is illustrated in Figure1.4.
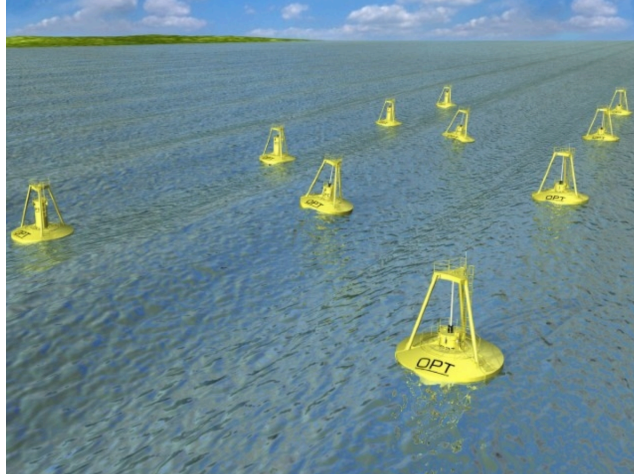
Figure 1.4: Wave farm from Ocean Wave Technology [14]

Another interesting example is the WaveStar device, currently being tested on the coast of Denmark [17]. The Wavestar WEC in Figure1.5 utilizes the idea of multiple point absorbers. This test device has two rows of floaters attached to a pier structure, secured to the sea bed by steel piles. These floaters are directed towards dominant wave direction, and oscillate as waves pass, pumping hydraulic fluid into a hydraulic system through which an electric generator will be driven.

Figure 1.5: WaveStar WEC device [17]

1.4.2 Attenuator

An attenuator lies parallel to the predominant wave direction with its beam much smaller than its length and oscillates laterally in response to waves. Attenuators are mainly connected lightweight bodies, for example, contouring rafts. The motion of the attenuator is asymmetric about the device's mid-point , so that the fore and aft portion of the device works equally hard. Power absorption is through the relative motion between the adjacent portions.
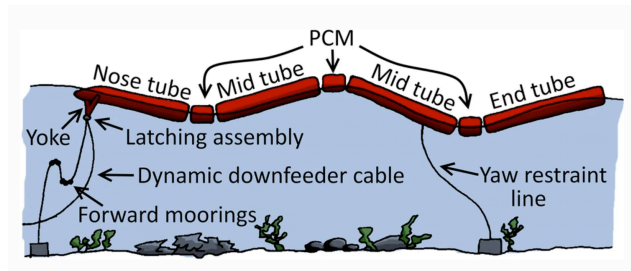
Figure 1.6: Sketch of Pelamis components [18]

The Pelamis WEC belongs to the WEC of attenuator type, as it extracts energy by the relative motion between separated sections of the tube. It is a semi-submerged "snake-like" offshore device, and developed by Pelamis Wave Power Ltd. It was the first WEC to be installed at a commercial scale, with the P1 model successfully launched at Aguçadoura, Portugal, in 2008.

The Figure1.6 illustrates that the Pelamis WEC has four steel cylinder sections linked by three power conversion modules at the hinge points. The moorings allow the WEC to face ocean waves' direction and the joints flex vertically and horizontally as the wave passes. This motion is resisted by hydraulic rams, and it turns out that this resistance can be tuned to provide a resonant response to maximize power

generation [18].

1.4.3   Terminator

Terminator devices have their principal axis perpendicular to the predominant wave direction can be rigid or compliant. Rigid terminators generate energy by physically intercepting waves. Compliant terminators have almost the same hydrodynamic behavior as attenuators. The only difference is that the incident wave directions differ by a right angle.

A famous example is the "Edinburgh Duck" model. The duck is one of the earliest "terminator" type device that can absorb most energy when waves approach from a predominant direction. Multiple sections were laid end to end along the wave predominant crest lines. Each section consisted of the duck that performed pitch oscillations around a central cylindrical unit. Neighboring units were jointed together to allow relative oscillation. The central sections formed a long spine, and the phase lag between the different incoming waves reaching different parts of the spine caused it to remain approximately in place to reduce mooring loads. For full-scale operation, high-pressure hydraulic systems were used to power conversion. The relative heave and surge oscillation of the duck and the spine segments were used to generate the power [10].

1.5   Power Take-off System

In order to convert the irregular mechanical movement of the oscillators to another form of energy that can drive an electric generator, a Power Take-Off (PTO) system is needed. The PTO is sometimes called as the device of secondary energy conversion. The primary energy converters are usually comprised of an oscillator and a reference. An oscillator may be a floating buoy and the corresponding reference is the sea floor, the relative motion of which can be used by PTO for secondary energy conversion.
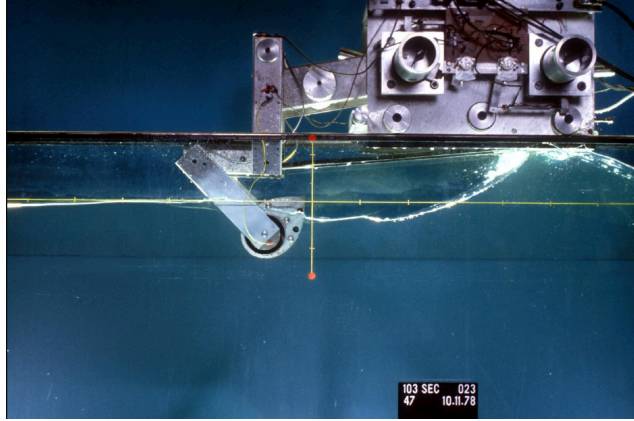
Figure 1.7: Edinburgh duck was tested in a narrow tank [14]

Because the wave input is irregular, an intermediate energy storage system such as a battery is generally required, the supply of electric energy to the location of use is smooth. The PTO plays an essential role in converting the mechanical form of energy to electrical power. There are different types of PTO used in the wave energy area, and we introduce several well studied types of WEC here.

1.5.1 Direct Drive - Linear Generators

It is advantageous to use linear systems for applications that involve linear or reciprocating motion, as the mechanical interface can be reduced compared with systems on rotating machines. The use of linear generators is called the direct drive approach, and its working principle is shown in Figure1.8. The direct drive WEC has relatively fewer moving parts and offers potential for cost-saving [19].

One of the first concepts where the linear generator can be used as PTO in the WEC, was filed for a patent in US at 1985 by Neuenschwander [20]. However, it was changed to a rotary generator later. The main problem at that time is that the linear generator would reciprocate in the slow speed of the actual device and at such speed, the force reacted by the generator needs to be large, which in turns requires the generator to be a large machine. However, thanks to the improvement in the
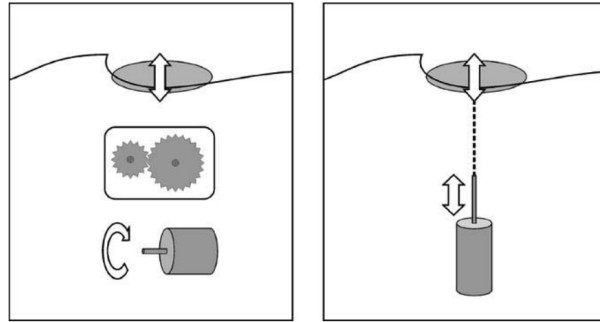
Figure 1.8: Comparison between linear generator and rotary generator in wave energy conversion [19]

magnetic material and power electronics, the linear generator has become one of the most commonly used PTO methods in the WEC design [21, 22].

The basic principles are illustrated in Figure1.9. The translator is a moving part on which magnets are mounted with alternating polarity. The stationary part is a stator with the windings of conductor. Between the translator and the stator, there is an air gap . As the translator oscillates, a voltage is generated in the windings following Faraday's law.
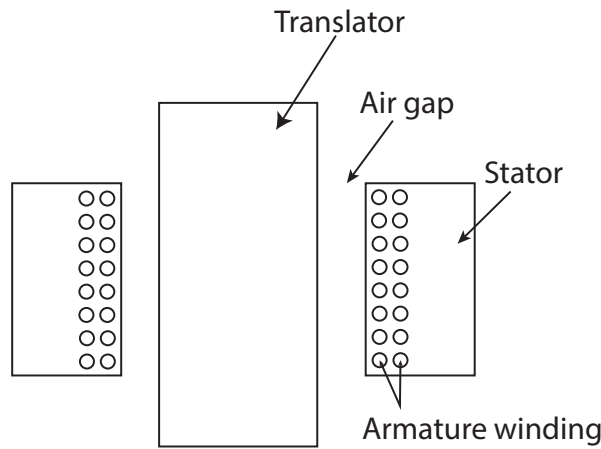
Figure 1.9: Basic principles of a linear generator [19]

1.5.2 Hydraulics

Hydraulics are well-suited for wave energy conversion, since the waves apply large force at slow speeds and the hydraulic machines can absorb energy efficiently at this scenario. Moreover, hydraulics can achieve short-term energy storage with the use of high-pressure gas accumulators, which can contribute to the smooth electricity production of the WEC [18].

Hydraulic PTO was firstly introduced in WEC applications in the Edinburgh Duck [23], the idea of which is to employ a hydraulic system into the WEC interface. Typically, a hydraulic PTO uses high-pressure oil hydraulic pumps or rams to convert the reciprocating mechanical oscillation to an oil hydraulic pressure head, which can drive hydraulic motors at the constant and high speed. The electric generator driven by the hydraulic motors may be a high-speed induction or synchronous generator [10].

A typical hydraulic circuit diagram is in Figure1.10. The rod of the hydraulic cylinder is forced up and down by the oscillation of a floating buoy, which put the fluid through check valves to hydraulic motors. The hydraulic motor can drive the generator to generate electric power at a certain speed. High pressure and low pressure accumulator are included in the circuit to provide energy storage and maintain constant flow to the hydraulic motor [14].

The Pelamis WEC is one of the full-size WEC examples that employs such hydraulic circuit. The PTO in Pelamis is separated by the high-pressure accumulator. The first part called the primary transmission, consisting of the hydraulic cylinders and their controls, converts the irregular wave motion to stored energy in the hydraulic accumulators. The second part called secondary transmission has hydraulic motors coupled to electric generators and transfers the stored energy into electricity transmitted to the shore. It is noted that through careful design, the energy loss in Pelamis PTO can be well under 20% over a wide range of operation conditions [18].
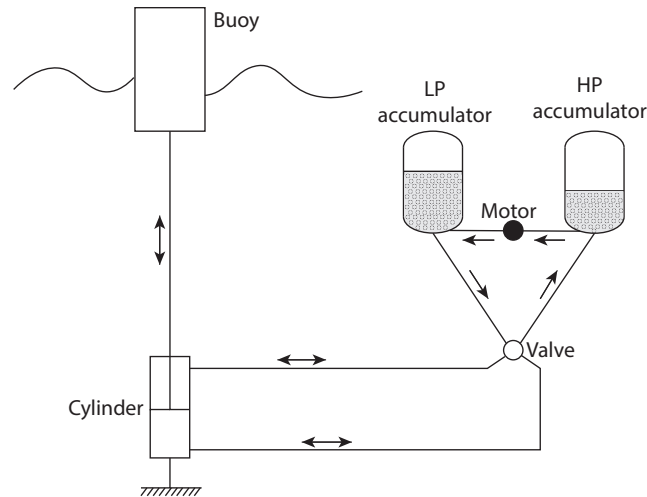
Figure 1.10: A typical hydraulic circuit [14]

1.5.3 Air Turbine

Air turbines are mostly used in Oscillating Water Column (OWC) wave energy converter systems. The working principle of a typical air turbine is that wave motion causes a reciprocating airflow under pressure. To produce unidirectional airflow, the reciprocating airflow needs to be rectified by a series of non-return valves [24]. The unidirectional airflow will drive the turbine which is coupled with the generator. Such device shares a lot similarity as the wind turbine, which has been thoroughly researched [25,26]. A practical example of OWC is the navigation buoy in Figure1.11 [27], which is proposed by the Japanese wave energy pioneer Yoshio Masuda. More than 3000 navigation buoys were produced after 1965, some of which have served more than 30 years.

However, the air turbine with non-return valves is complicated and hard to maintain, which is not ideal in the large scale wave energy converters [24]. Many kinds of the self-rectifying air turbine have been proposed. One of them is called Wells turbine with symmetric blades profiles, invented by Professor Alan Wells of Queen's University [28]. Impulse turbine patented by Ivan A. Babintsev in 1975 is more efficient than Wells turbine, which has the asymmetric blades profiles and guide vanes
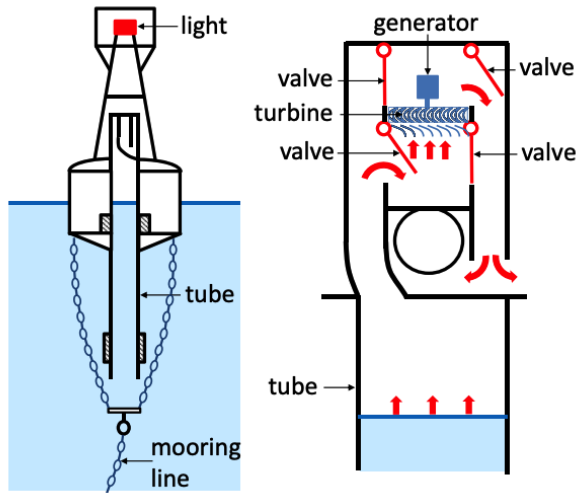
Figure 1.11: A navigation buoy using the air turbine. On the right hand side, details through the turbine and rectifying valves [27]

to rectify the air flow direction.

1.5.4 Energy Storage

Some form of energy storage is usually incorporated in a PTO system, as the fluctuations in absorbed wave power will result in a very variable electrical power output, which is unsuitable for the grid [29]. The energy storage system supports the bi-directional power flow between the buoys and the system, but only single directional power flow to the grid onshore, which smoothes out the power sent to the grid. Accumulators can function as short-term energy storage as part of the hydraulic system. By storing energy, accumulators would help the system deal with the high level of variance, reducing the capital cost and power losses of all subsequent powertrain elements [30].

1.6 Control

Over the last four decades, a great deal of progress has been made in the area of wave energy conversion. However, large scale wave energy conversion is still more ex-

pensive than wind or solar energy. The use of control techniques can bring about a three to five-fold improvement in cost-effectiveness as measured in dollars per kilowatt-hour of electric power to the consumers. Such gains could make wave energy commercially attractive even in weaker wave climates and parts of the world where other renewable energy options already exist [10].
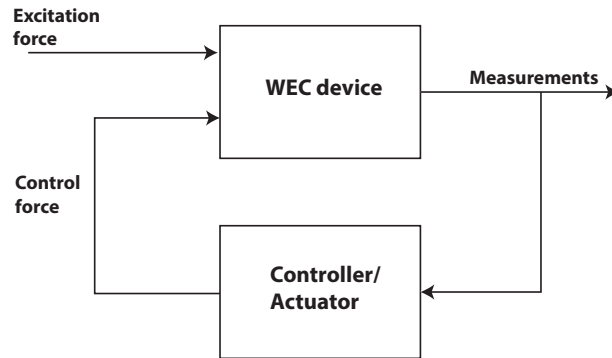
Figure 1.12: System diagram illustrates the role of the controller/actuator in WEC
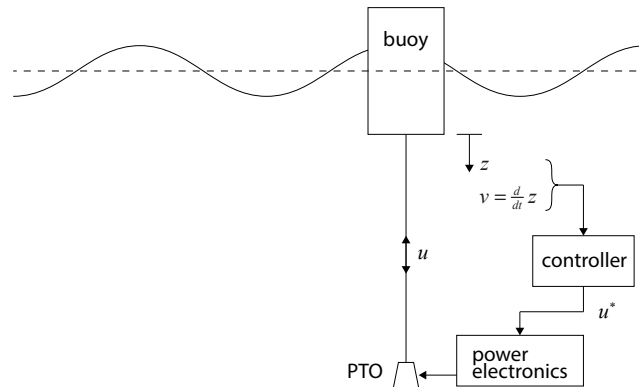
Figure 1.13: A simple point absorber type WEC with the controller

The controller or actuator in Figure 1.12 [10] mainly focuses on controlling the oscillation body's behavior to achieve the optimal performance of power generation. Here, we use a simple point absorber type WEC to illustrate how the controller works in real operation. Figure 1.13 is a floating buoy model, connected with the seafloor mounted PTO and generator by a pretension tether cable. The PTO used here is the direct drive. We assume the PTO applies the controller force u in the cable. The controller determines $u^\star$ based on the measurements of the floating buoy (i.e., velocity

15

v and displacement z). The cable force u is regulated by the power electronics to track the controller output $u^\star$. The dynamics of the closed-loop system is dependent on the controller, which can be carefully tuned to achieve maximum power extraction.

In regular waves (i.e., a sinusoidal wave), the optimal power absorption can be achieved when the natural frequency of the WEC is the same as the wave frequency. While off-resonance, the conversion rate can decrease significantly. For narrow bandwidth devices like point absorbers, it is essential to use control techniques to achieve resonance. However, for larger WEC devices such as attenuators and terminators, with broad bandwidth, the benefit of applying optimal control can be marginal [31].
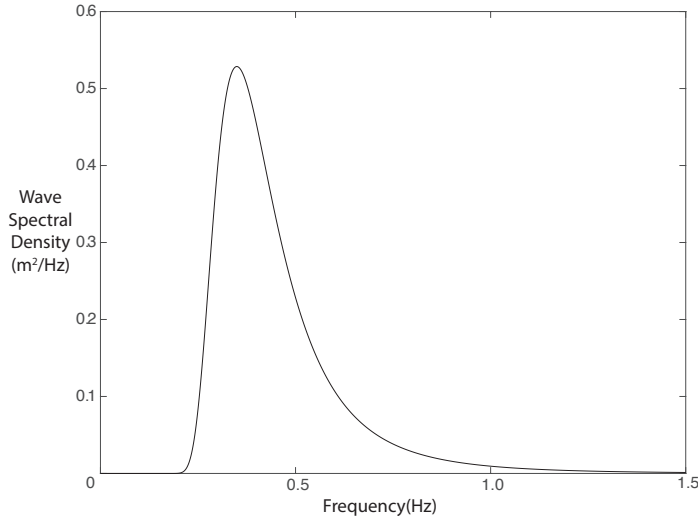
Figure 1.14: JONSWAP spectrum of a developed sea

Real waves, however, are stochastic and exhibit significant power over a continuous spectrum of frequencies. For example, a commonly used ocean wave spectrum named JONSWAP spectrum [32] in Figure 1.14 gives the distribution of the energy among different frequencies. This requires that a WEC device should behave as if resonant over the wide range of frequencies.

Many control techniques on harvesting real waves have been proposed in the last few decades and we will review a few of them.

1.6.1 Reactive Control

Reactive control is first proposed by Salter [33] and Budal [34] in the mid 1970s. For practical implementation, it was proposed to use a controllable PTO, the goal of which is to achieve the optimal phase and amplitude of the oscillation. In other words, optimal control means to control the behavior of the oscillation to maximize power generation. It was found that the WEC device can be "tuned" to resonate at a chosen frequency using the feedback of the device displacement or velocity [3]. In addition, using velocity feedback, the damping coefficient of the PTO can be adjusted to balance the radiation damping of the device at each frequency to maximize wave energy absorption.

Since the control force in this method is in phase with the velocity, this method is called "reactive control". We can use a simple single-degree point absorber to explain this method. Assuming the wave amplitude is small, the dynamic equation of this device can be expressed as:

$$m\ddot{z} + kz = f_f + f_r + f_c \tag{1.1}$$

Where m is the mass of the point absorber(primary converter), and k as the hydrostatic stiffness for the device. We also assume that the applied damping of the point absorber is so small that it can be negligible. In the right side of the equation (1.1), there are three terms: the first term is the excitation(diffraction) force f_f, the second term is the radiation damping force f_r, and the third term is the force f_c applied on the device by the actuator. The equation (1.1) can also be applied to multiple WEC devices (e.g., an array of floating buoys).

We can also express the radiation damping force f_r in frequency domain:

$$\hat{f}_r(i\omega) = -\left[i\omega(\hat{m}_r(\omega) + m_\infty) + \hat{c}_r(\omega)\right]\hat{v}(i\omega) \tag{1.2}$$

17

Where m_∞ is the infinite added mass, $\hat{m}_r(\omega)$ is the frequency dependent added mass, and $\hat{c}_r(\omega)$ is the frequency dependent radiation damping. $\hat{v}(i\omega)$ is the frequency response of the device's velocity. Using the equation (1.2), the system dynamic equation in frequency domain can be represented as:

$$G_{vf}(i\omega)\hat{v}(i\omega) = \hat{f}_f(i\omega) + \hat{f}_c(i\omega) \tag{1.3}$$

Where

$$G_{vf}(i\omega) = G_{vfr}(\omega) + iG_{vfi}(\omega)$$

$$G_{vfr}(\omega) = Re\{G_{vf}(i\omega)\} = \hat{c}_r(\omega)$$

$$G_{vfi}(\omega) = Im\{G_{vf}(i\omega)\} = \omega[m + m_\infty + \hat{m}_r(\omega)] - \frac{1}{\omega}k$$

In reactive control, the feedback measurements can be displacement or velocity, which are provided by the sensors, the general form of the control force in frequency domain can be

$$\hat{f}_c(i\omega) = -Y(i\omega)\hat{v}(i\omega) \tag{1.4}$$

The equation (1.3) becomes:

$$(G_{vf}(i\omega) + Y(i\omega))\hat{v}(i\omega) = \hat{f}_f(i\omega) \tag{1.5}$$

The power generation can be maximized by setting

$$Y(i\omega) = G_{vf}^\star(i\omega) \tag{1.6}$$

This is also called the complex conjugate control, which is optimal in regular waves [35]. This method is simple and easy to be implemented. However, in irregular waves, the implementation of reactive control suffers both theoretical and practical

limitations. The theoretical limitation is that the reactive control technique is non-causal, which means that it needs the future information of the wave motion. The practical limitation is that it requires large amount of power flowing up and down the energy conversion chain.

1.6.2 Latching Control

Latching control is another popular control technique in point absorbers, firstly introduced by Budal and Falnes [36]. Consider a simple heaving buoy shown in figure1.13, with the horizontal dimensions sufficiently small to be considered as a point absorber and tuned optimally for maximum power in a regular sea. Respectively, for a small device, the excitation force $f_f(t)$ can be obtained by integrating the pressure due to incident waves over the device. This means that $F_D(t)$ is in phase with the incident waves, with its magnitude proportional to the magnitude of the incident wave motion. The tuning equation (1.6) requires that the velocity is in phase with the excitation force, which means the displacement lags the surface wave elevation by $\frac{\pi}{2}$. As the wave elevation approaches its equilibrium point, the displacement of the WEC will increase to a value that exceeds its physical constraint.
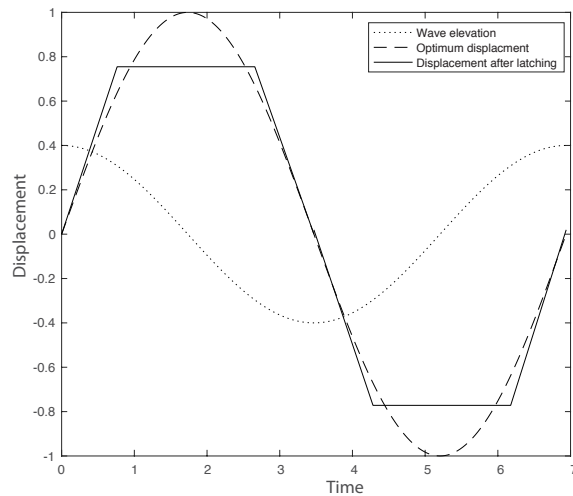
Figure 1.15: Wave elevation, optimal displacement and actual displacement under latching control [19]

However, the use of latching control can address this concern while maintaining the small displacement assumption of the point absorber. The concept of this control technique is explained in figure 1.15. The three curves in figure 1.15 show the wave elevation, displacement under optimal control, and displacement under latching control. This figure shows that once the WEC displacement arrives at a certain value, the latching control strategy immediately halts the motion of the device. As the power output is $f_c(t)v(t)$, the WEC cannot generate power until it is released. This approach can be an effective way to avoid large displacement in heaving point absorber devices [37]. Moreover, the latching control strategy allows the existence of the device whose natural frequency is higher than the exciting wave force frequency.

Latching control is a suboptimal approach and can be extended to irregular waves with the future information of the wave motion at some distance [36]. Falcao proposed an alternative on-off control technology, which requires no future wave information, with the application on the point absorbers equipped with a hydraulic PTO [38]. Despite of the widespread popularity in WEC design, however, the latching control technique has several limitations. In particular, its suitability on the point absorber with the electric PTO has not been fully assessed; moreover, it may fail to work well on arrays of point absorbers since the optimum phase condition doesn't hold where there is more than one oscillator.

New control approaches are required. The development of better PTO systems, such as linear electric generators and novel variable-displacement hydraulics, has opened the possibility of applying real-time control techniques. Model Predictive Control (MPC) is one of these advanced control techniques that are suitable in the wave energy area.

1.6.3 Model Predictive Control

The idea of applying MPC techniques in the wave energy area was proposed by Gieske [39], and this novel idea was revisited by many researchers [40–43]. It is possible to develop a real-time controller that maximizes the power generation within the constrained set [44]. In [44], MPC was applied to a heaving, semi-submerged sphere constrained to oscillate over a finite stroke. The model developed by Hals [44] stems from the linearized wave-structure interaction, which includes a low-order linear state space model of the radiation damping effect. The dynamic trajectory of the future incident wave force is forecast in real-time, based on past and present measured values. Then, each time the forecast is updated, the objective function (i.e., the amount of energy generated), is optimized over the receding prediction horizon. The initial portion of the optimizing trajectory for the PTO force is then implemented in real-time, until it is superseded by a subsequently-optimized trajectory.

MPC techniques are advantageous, because they can accommodate the nonlinearities (such as viscous drag forces and nonlinear buoyant force) in system dynamics and mechanical constraints (such as PTO force constraints). And an MPC controller can be regarded as optimal on a wave-to-wave time scale. One main drawback of the MPC techniques is that the optimal performance of the controller depends on how precise the wave forecast algorithm is [44].

1.7 Causal Control

All of the aforementioned control strategies need the future wave excitation forecast, which is not ideal since it is difficult to provide a precise wave forecast model. A number of causal controller have been proposed over the years [45, 46], most of which are the approximation of the anti-causal controller and only sub-optimal. New research work of optimal causal control design in WEC are needed.

In some situations where nonlinearities and hard constraints are not overly restrictive, it is advantageous to use a causal feedback controller that can be implemented based on some easy-to-measure signals such as the displacement and the velocity of the primary energy converter. The idea of this new causal control design was proposed by Scruggs and has been shown to result in a very good optimal performance that is almost as high as that of the anticausal controller [47]. The causal control design is a constrained control problem, where the constraint is that the linear feedback law should be causal and the objective function is the expectation of the power absorption over a certain time interval. In this problem, we assume the stationary wave spectrum $S_a(\omega)$ is known, together with a vector of output measurements $y(t)$. Denoting $u(t)$ as the control input to the PTO, the control problem becomes a constrained optimization problem that is shown below.

$$
\text{OP}: \begin{cases} \text{Maximize:} & \bar{p} \\ \text{Domain:} & \text{Causal feedback law } K : y \mapsto u \end{cases}
$$

Where $\bar{p}$ is the average power generation, the detailed description of which will be introduced in Chapter 3. It was recently shown in [47] that, under the assumption of linear dynamics and stationary stochastic sea state, the optimal causal control of WEC system is a non-standard Linear Quadratic Gaussian (LQG) control problem. The closed-form solution can therefore be found, assuming an accurate models are available for the WEC dynamics and the wave spectrum.

In the context of causal control, it is possible to extend this idealized LQG framework to a more realistic model. In the case in which nonlinearities in the WEC dynamics are significant, Gaussian Closure techniques to approximate system dynamic behavior with the synthesis of optimal feedback law is applied. The optimal controller can be computed by the simple and efficient gradient-based algorithm through a gaussian approximation of the stationary stochastic system response. Additionally,

this technique can also accommodate complex transmission loss models [48]

The LQG theory for optimal energy harvesting can be naturally extended to an adaptive control framework, for problems in which a priori model is unavailable for the characterization of the stochastic behavior of the incident waves . This has been examined in [49], for the situation in which uncertainty is presumed to exist for the wave spectrum $S_a(\omega)$ and for the resultant incident wave forces. The method proposed in [49] accomplishes the adaptation indirectly. By identifying the stochastic system for the disturbance, re-optimizing the feedback law using the principle of certainty equivalence.

Another common problem in the control design of WEC, whether the controller is causal or not, is that the dynamic response of the WEC can be too large to satisfy the small oscillation assumption. In such cases, it is necessary to put constraints on the displacement of the WEC. In [50], multi-objective control techniques is applied with the main objective is to maximize power absorption under causal control domain and the competing objective is to restrain the displacement of the WEC (i.e., $\mathcal{E}\{z^2\} < \mu$, where $z(t)$ is the displacement response of the WEC). Such control problem can be formulated in the form of Linear Matrix Inequality (LMI) techniques, which are the convex optimization problems and can be solved efficiently using numerical software [51].

1.8   Research Objectives

The objective of this research is to modify the above causal control technique such that it can achieve a relatively high performance in the presence of model uncertainty and stroke saturation.

1.8.1 Model Uncertainty

In the previous literature, Gaussian Closure technique have been applied to the model uncertainty [48]. However, this method is approximate and the controller generated from it might not be optimal under different characterizations of the model uncertainties. An actual WEC system is very complex, while the model we used in design is a highly simplified version of it. The discrepancy between the actual WEC system and the linearized model can be regarded as uncertainty in the design process. It is important that the control system designed using simplified model, be insensitive to this uncertainty.

In this proposed research, we assume the nonlinearity of the system comes from the viscosity drag effect. The nonlinear viscosity effect can be described by an experience law proposed by Morison [52]. We use the concept of absolute stability to impose a constraint on the controller such that it stabilizes the system when the viscosity damping force is introduced. Combining with the objective to maximize the power generation, a robust controller can be designed using multi-objective control techniques.

1.8.2 Stroke Saturation

Another essential issue that needs to be addressed is the fact that the PTO has a finite feasible stroke [44]. In [50], the constraint is imposed on the variance of the displacement but the stroke violation can still happen. Finite stroke requires that at any time, the stroke can not exceed its maximum allowable displacement (i.e., $|z(t)| \leq z_m, \forall t \geq 0$ where z_m is the maximum stroke). For example, if the PTO is a hydraulic ram, placed between two rectilinear degrees of freedom, this stroke limit is obvious. The same can be said that it is a direct-drive linear permanent magnet synchronous machine, or a rotational machine interfaced with linear motion through a rack-and-pinion or ball-screw mechanism. For flap-type converters that extract

energy from surge, the PTO is often a rotational pump that impose torque on the flap hinge. In this case, there is clearly an angular stroke limit. Observance of these stroke limits are challenging because they are often in conflict with the primary objective of maximizing power generation. In strong waves, it may be the case that theoretical performance maximization algorithm requires the WEC to respond so vigorously that the PTO exceeds its maximum allowable stroke value at some time. In such situation, stroke limits should be explicitly accommodated in control design [53].

The stroke constraint can be achieved by a "two-stage" control system design method. First stage is to design a linear controller whose primary objective is to maximize the power generation and associate objective is to lower the variance of the stroke. Second stage is to impose an outer nonlinear controller which enforce the stroke constraint at any time interval. We will provide more details for this method in later Chapters. Moreover, we presented versions of this method in both continuous-time and discrete-time WEC control designs.

1.9   Outline

The rest of this document is outlined as follows: In Chapter 2, we overview the fundamental concepts which will be used in this thesis. In particular, we review Passivity, Optimization, and Linear System Theory. Chapter 3 will introduce the dynamic behavior of the WEC system and surrounding fluids. It will discuss how we generate state-space models for WEC system and surrounding fluids using subspace-based system identification techniques. In chapter 4, a new modified subspace-based spectral factorization algorithm is proposed. Using the same amount of data, it can provide a more accurate state-space model than the standard algorithm. Chapter 5 focuses on the comparison between causal control and anticausal control techniques in the unconstrained WEC control problem. It shows that for a point absorber type WEC, causal control can be a good substitute for anticausal control techniques. Chapter

6 proposes a "two-stage" control strategy of WEC system with finite stroke in the continuous time domain. It demonstrates that such control strategy can satisfy the stroke constraint while still results in high power generation. The proof of global stability of the closed-loop system is provided. In Chapter 7, the control strategy from Chapter 6 is implemented in the discrete time WEC system. The main difference is the design of the nonlinear controller, which requires a one-step-ahead predictor in discrete time. In Chapter 8, we propose the robust control design methodology for WECs considering nonlinear dynamic behavior. The circle criterion and Loop Transfer Recovery (LTR) method are used to tackle this robust control design problem. Chapter 9 gives some conclusions and discusses future work.

CHAPTER 2

Preliminary Knowledge

The work of this thesis relies heavily on the passivity, optimization and linear system theory. This chapter will give a brief summary of the basic concepts used in each area. In particular, Section 2.1 is concerned with the passivity theory. Section 2.2 covers convex optimization and LMIs. Section 2.3 focuses on linear system theory.

2.1 Signals and Passivity

The system's input and output are signals, so we introduce the basic definition of vector space, norm function (in particular, Euclidean Norm) and inner product space. We also introduce the concept of matrix norm, which is heavily used in Chapter 4, Chapter 6 and Chapter 7. The behavior of system input and output determines system properties, e.g., passivity.

2.1.1 Vector Spaces and Norms

Definition 2.1.1. (Vector Space [54]) Suppose $\mathcal{V}$ is a nonempty set and $\mathbb{F}$ is a field, the operation of vector addition and scalar multiplication are defined here:

1. for every pair $u, v \in \mathcal{V}$, a unique element $u + v \in \mathcal{V}$ are assigned as their sum;

2. for each $\alpha \in \mathbb{F}$, there is a unique element $\alpha v \in \mathcal{V}$ called their product.

Then $\mathcal{V}$ is a *Vector Space* if the following properties hold for all $u, v, w \in \mathcal{V}$ and all $\alpha, \beta \in \mathbb{F}$, for addition:

1. there exists a zero element in $\mathcal{V}$, denote by 0, such that $v + 0 = v$;

2. there exists a vector $-v \in \mathcal{V}$, such that $v + (-v) = 0$;

3. the association $u + (v + w) = (u + v) + w$ is satisfied;

4. the commutativity relationship $u + v = v + u$ holds.

For multiplication:

1. scalar distributivity $\alpha(v + u) = \alpha v + \alpha u$ holds;

2. vector distributivity $(\alpha + \beta)v = \alpha v + \beta v$ holds;

3. the associative rule $(\alpha\beta)v = \alpha(\beta v)$ for scalar multiplication holds;

4. for the unit scalar $1 \in \mathbb{F}$ the equality $1v = v$ holds.

Definition 2.1.2. (Vector Norm [54]) A norm $\|\cdot\|$ on a vector space $\mathcal{V}$ is a function that maps $\mathcal{V} \mapsto \mathbb{R}_{\geqslant 0}$, for all $u \in \mathcal{V}$ such that

1. $\|u\| = 0$ if and only if $u = 0$;

2. $\|au\| = a\|u\|$ for all $a \in \mathbb{F}$;

3. triangle inequality $\|u + v\| \leqslant \|u\| + \|v\|$ holds, for all u and $v \in \mathcal{V}$

Definition 2.1.3. (Vector p-norm [55]) For all $u \in \mathcal{V}$, the *vector p-norm* of u is defined as:

$$\|u\|_p = \left(\sum_{i=1}^{n} |u_i|^p \right)^{\frac{1}{p}}, \quad \text{for} \quad 1 \leqslant p \leqslant \infty \tag{2.1}$$

Remark 2.1. In this document, we will mainly focus on Euclidean norm (when $p = 2$) and Infinity norm (when $p = \infty$).

Euclidean norm:

$$\|u\|_2 = \sqrt{\sum_{i=1}^{n} |u_i|^2} \tag{2.2}$$

Infinity norm:

$$\|u\|_\infty = \max_{1 \leqslant i \leqslant n} |u_i| \tag{2.3}$$

Definition 2.1.4. (Induced matrix p-norm [55]) Suppose a p-norm for vectors ($1 \leqslant p \leqslant \infty$) is used both for $\mathbb{R}^m$ and $\mathbb{R}_n$, the *norm of matrix* $A \in \mathbb{R}^{m \times n}$ induced by a vector p-norm is defined as:

$$\|A\|_p = \sup_{x \neq 0} \frac{\|Ax\|_p}{\|x\|_p} \tag{2.4}$$

Remark 2.2. In fact, A can be viewed as a mapping from a vector space $\mathbb{R}^n$ with a vector norm $\| \cdot \|_p$ to another vector space $\mathbb{R}^m$ equipped with a vector norm $\| \cdot \|_p$. In particular, the induced matrix 2-norm can be computed as

$$\|A\|_2 = \sqrt{\lambda_{\max}(A^T A)} \tag{2.5}$$

Definition 2.1.5. (Frobenius norm [55]) The *Frobenius norm* of matrix $A \in \mathbb{R}^{m \times n}$ is defined as:

$$\|A\|_F = \sqrt{\mathrm{Tr}(A^T A)} = \sqrt{\sum_{i=1}^{m} \sum_{j=1}^{n} |a_{ij}|^2} \tag{2.6}$$

2.1.2 Inner Product Space

Definition 2.1.6. (Inner Product [54]) A inner product $\langle \cdot, \cdot \rangle$ on a vector space $\mathcal{V}$ is a function mapping $\mathcal{V} \times \mathcal{V} \mapsto \mathcal{F}$ such that

1. for all $u, v \in \mathcal{V}$, $\langle u, v \rangle = \overline{\langle v, u \rangle}$ (where overbar means complex conjugate)

2. for all $u \in \mathcal{V}$, $\langle u, u \rangle \geqslant 0$, $\langle u, u \rangle = 0$ if and only if $u = 0$;

3. for all $u, v, w \in \mathcal{V}$ and $a, b \in \mathbb{F}$, $\langle u, av + bw \rangle = a \langle u, v \rangle + b \langle u, w \rangle$. This condition implies that the mapping $u, v \to \langle u, v \rangle$ is linear in $\mathcal{V}$.

Definition 2.1.7. (Inner Product Space [56]) Give an inner product $\langle \cdot, \cdot \rangle : \mathbb{R}^n \times \mathbb{R}^n \mapsto \mathbb{R}$, an inner product space, $\mathcal{L}$, is defined as:

$$\mathcal{L} = \left\{ x : \mathbb{R} \to \mathbb{R}^n \mid \|x\|^2 = \int_0^\infty \langle x(t), x(t) \rangle dt < \infty \right\} \tag{2.7}$$

The extended inner product space, $\mathcal{L}_e$, is defined as:

$$\mathcal{L}_e = \left\{ x : \mathbb{R} \to \mathbb{R}^n \mid \|x\|^2 = \int_0^T \langle x(t), x(t) \rangle dt < \infty, \forall T \in \mathbb{R}_{\geqslant 0} \right\} \tag{2.8}$$

Definition 2.1.8. (Lebesgue Space [56]) The Lebesgue space, $\mathcal{L}_2$, is an inner product space, and is given by all square integrable functions defined by:

$$\mathcal{L}_2 = \left\{ x : \mathbb{R}_{\geqslant 0} \to \mathbb{R}^n \mid \|x\|_2^2 = \int_0^\infty x^T(t) x(t) dt < \infty \right\} \tag{2.9}$$

The extended Lebesgue space, $\mathcal{L}_{2e}$, is defined by

$$\mathcal{L}_{2e} = \left\{ x : \mathbb{R}_{\geqslant 0} \to \mathbb{R}^n \mid \|x\|_{2,T}^2 = \int_0^T x^T(t) x(t) dt < \infty, \forall T \in \mathbb{R}_{\geqslant 0} \right\} \tag{2.10}$$

Definition 2.1.9. (Discrete-time Lebesgue Space [56]) The Discrete-time Lebesgue space, ℓ_2, is given by all square summation functions defined by:

$$\ell_2 = \left\{ x : \mathbb{Z}_{\geqslant 0} \to \mathbb{R}^n \mid \|x\|_2^2 = \sum_{k=0}^\infty x_k^T x_k dt < \infty \right\} \tag{2.11}$$

The extended Discrete-time Lebesgue space, ℓ_{2e}, is defined by

$$\ell_{2e} = \left\{ x : \mathbb{Z}_{\geqslant 0} \to \mathbb{R}^n \mid \|x\|_{2,T}^2 = \sum_{k=0}^T x_k^T x_k dt < \infty, \forall T \in \mathbb{Z}_{\geqslant 0} \right\} \tag{2.12}$$

2.1.3 Passivity

Definition 2.1.10. (Passivity [54]) A system $H : \mathcal{L}_e \mapsto \mathcal{L}_e$, whose input and output are denoted as u and y, is said to be passive if

$$\int_0^{T_1} u^T y \, dt \geqslant 0 \qquad \forall u \in \mathcal{L}_e, \forall T_1 \in \mathbb{R}_{\geqslant 0} \tag{2.13}$$

Definition 2.1.11. (Output Strictly Passive (OSP) [54]) A system $H : \mathcal{L}_e \mapsto \mathcal{L}_e$, whose input and output are denoted as u and y, is said to be Output Strictly Passive if there exist $\beta \in \mathbb{R}_{\geqslant 0}$, such that

$$\int_0^{T_1} u^T y \, dt \geqslant \beta \int_0^{T_1} y^T y \, dt \qquad \forall u \in \mathcal{L}_e, \forall T_1 \in \mathbb{R}_{\geqslant 0} \tag{2.14}$$

2.2 Optimization and LMIs

Optimization plays an essential role is this thesis work, particularly convex optimization with LMI constraints. Convex optimization is heavily used in Chapter 4, Chapter 6 and Chapter 7.

2.2.1 Convex Sets

Definition 2.2.1. (Convexity [57]) A set, $\mathcal{S}$, in a real inner product space is convex if for all $x, y \in \mathcal{S}$ and $\alpha \in [0,1]$, $\alpha x + (1 - \alpha)y \in \mathcal{S}$. A function , f, is said to be convex if for all $x, y \in \mathcal{S}, \alpha \in [0,1]$, $f(\alpha x + (1 - \alpha)y) \leqslant \alpha f(x) + (1 - \alpha)f(y)$.

2.2.2 Linear Matrix Inequality

Definition 2.2.2. (Matrix Definiteness) Let $A \in \mathbb{R}^{n \times n}$ and A is a symmetric matrix. The matrix A is said to be *postive definite* if

$$x^T A x > 0, \text{for all nonzero } x \in \mathbb{R}^n \tag{2.15}$$

it is *positive semidefinite* if

$$x^T A x \geqslant 0, \text{for all nonzero } x \in \mathbb{R}^n \tag{2.16}$$

Conversely, the matrix A is *negative definite* if

$$x^T A x < 0, \text{for all nonzero } x \in \mathbb{R}^n \tag{2.17}$$

It is *negative semidefinite* if

$$x^T A x \leqslant 0, \text{for all nonzero} x \in \mathbb{R}^n \tag{2.18}$$

Definition 2.2.3. (Linear Matrix Inequality [58]) A Linear Matrix Inequality has the form

$$F(x) \triangleq F_0 + \sum_{i=1}^m x_i F_i \geqslant 0 \tag{2.19}$$

where $x \in \mathbb{R}^m$ is the vector variable and the symmetric matrices $F_i = F_i^T \in \mathbb{R}^{n \times n}, i = 0, \ldots, m$ are given.

Proposition 2.2.4. (Convexity of LMI [58]) A LMI, $F : \mathbb{R}^m \mapsto \mathbb{R}^{n \times n}$, is *convex.*

Proof. Consider $x, y \in \mathbb{R}^m$ and $\alpha \in [0, 1]$, the LMI F is convex since

$$
\begin{aligned}
F(\alpha x + (1 - \alpha)y) &= F_0 + \sum_{i=1}^m (\alpha x_i + (1 - \alpha)y_i)F_i \\
&= \alpha \left(F_0 + \sum_{i=1}^m x_i F_i \right) + (1 - \alpha) \left(F_0 + \sum_{i=1}^m y_i F_i \right) \\
&= \alpha F(x) + (1 - \alpha)F(y) \tag{2.20}
\end{aligned}
$$

$\square$

Although the LMI (2.19) may seem to have a specialized form, it can represent

a wide variety of convex constraints on x. In particular, linear inequalities, (convex) quadratic inequalities , matrix norm inequalities and constraints that arise in control theory, such as Lyapunov and convex quadratic matrix inequalities, can all be cast in the form of an LMI [58].

Lemma 2.3. *(Schur Complement Lemma [58]) Consider the matrix $A = A^T \in \mathbb{R}^{n \times n}$, $C = C^T \in \mathbb{R}^{m \times n}$, and $B \in \mathbb{R}^{n \times m}$. The following conditions are equal.*

1. $\begin{bmatrix} A & B \\ B^T & C \end{bmatrix} < 0$

2. $A - BC^{-1}B^T < 0$, $C < 0$

3. $C - B^T A^{-1} B < 0$, $A < 0$

2.3 Linear System Theory

The majority of the controller synthesis methodology developed in this dissertation requires the knowledge of the state-space form of the Linear Time-Invariant (LTI) system. A review of linear system theory is provided in this section, in particular the stability of LTI system, passivity of the system, and the zeros of LTI transfer matrices.

Definition 2.3.1. (Continuous-time LTI System) A *Continuous-time linear time-invariant* system can be represented by the following set of equations:

$$S_{c,LTI} : \begin{cases} \dot{x}(t) & = Ax(t) + Bu(t), \quad x(t_0) = x_0 \\ y(t) & = Cx(t) + Du(t) \end{cases} \tag{2.21}$$

Where $x(t) \in \mathbb{R}^n$ is the state vector, $x(t_0)$ is the initial condition of the system, $u(t) \in \mathbb{R}^m$ is the input vector, $y(t) \in \mathbb{R}^p$ is the output vector, $A \in \mathbb{R}^{n \times n}$, $B \in \mathbb{R}^{n \times m}$, $C \in \mathbb{R}^{p \times n}$, $D \in \mathbb{R}^{p \times m}$.

Definition 2.3.2. (Discrete-time LTI System) The *Discrete-time linear time-invariant* system can be represented by the following set of equations:

$$S_{d,LTI} : \begin{cases} x_{k+1} & = Ax_k + Bu_k \\ y_k & = Cx_k + Du_k \end{cases} \tag{2.22}$$

Where $x_k \in \mathbb{R}^n$ is the state vector, x_0 is the initial condition of the system, $u_k \in \mathbb{R}^m$ is the input vector, $y_k \in \mathbb{R}^p$ is the output vector, $A \in \mathbb{R}^{n \times n}$, $B \in \mathbb{R}^{n \times m}$, $C \in \mathbb{R}^{p \times n}$, $D \in \mathbb{R}^{p \times m}$ for all $k \in \mathbb{Z}$.

Definition 2.3.3. (Markov Parameter) Consider the discrete-time, LTI system in (2.22), the matrix impulse response with initial condition $x_0 = 0$ is:

$$H_k = \begin{cases} D, & k = 0 \\ CA^{k-1}B & k > 0 \end{cases} \tag{2.23}$$

2.3.1 Stability of Linear System

Definition 2.3.4. (Lyapunov stability and asymptotical stability [56]) Assume that in (2.21), there is no input. The equilibrium point $x = 0$ of (2.21) is

- Lyapunov Stable (LS) if, for each $\epsilon > 0$, there exists $\delta = \delta(\epsilon) > 0$ such that

$$\|x(0)\| < \delta \Rightarrow \|x(t)\| < \epsilon, \quad \forall t \geqslant 0 \tag{2.24}$$

- Asymptotically Stable (AS) if it is LS and δ can be chosen such that

$$\|x(0)\| < \delta \Rightarrow \lim_{t \to \infty} x(t) = 0 \tag{2.25}$$

Theorem 2.4. *(Lyapunov Stability for LTI System in Continuous-time Domain [56])*

Let $A \in \mathbb{R}^{n \times n}$ and assume there exists $P \in \mathbb{R}^{n \times n}$, where $P = P^T > 0$, satisfying

$$A^T P + PA \leqslant 0 \tag{2.26}$$

Then $Re\{\lambda_i(A)\} \leqslant 0, i = 1, \ldots, n$, and the equilibrium point $x = 0$ of the system $\dot{x} = Ax$ is LS.

Theorem 2.5. *(Lyapunov Stability for LTI System in Discrete-time Domain [56])*
Let $A \in \mathbb{R}^{n \times n}$ and assume there exists $P \in \mathbb{R}^{n \times n}$, where $P = P^T > 0$, satisfying

$$A^T PA - P \leqslant 0 \tag{2.27}$$

Then $|\lambda_i(A)| \leqslant 1, i = 1, \ldots, n$, and the equilibrium point $x = 0$ of the system $x_{k+1} = Ax_k$ is LS.

Theorem 2.6. *(Asymptotical Stability for LTI System in Continuous-time Domain [56]) Let $A \in \mathbb{R}^{n \times n}$ and assume there exists $P \in \mathbb{R}^{n \times n}$, where $P = P^T > 0$, satisfying*

$$A^T P + PA < 0 \tag{2.28}$$

Then $\operatorname{Re} \lambda_i(A) < 0, i = 1, \ldots, n$, the matrix A is Hurwitz and the equilibrium point $x = 0$ of the system $\dot{x} = Ax$ is AS.

Theorem 2.7. *(Asymptotical Stability for LTI System in Discrete-time Domain [56])*
Let $A \in \mathbb{R}^{n \times n}$ and assume there exists $P \in \mathbb{R}^{n \times n}$, where $P = P^T > 0$, satisfying

$$A^T PA - P < 0 \tag{2.29}$$

Then $|\lambda_i(A)| < 1, i = 1, \ldots, n$ and the equilibrium point $x = 0$ of the system $x_{k+1} = Ax_k$ is AS.

2.3.2 Passivity and Output Strictly Passivity

Theorem 2.8. *(Positive Real (PR) Lemma [59]) Let the LTI system be defined by the equation (2.21) where (A, B) is controllable and (A, C) is observable. The system is passive if and only if there exist a $P \in \mathbb{R}^{n \times n}$ and $P = P^T > 0$, such that*

$$\begin{bmatrix} A^T P + PA & PB - C^T \\ B^T P - C & -D^T - D \end{bmatrix} \leqslant 0 \qquad (2.30)$$

Theorem 2.9. *(Positive Real Lemma in Discrete-time [60]) Let the discrete-time LTI system defined by the equation (2.22) where (A, B) is controllable and (A, C) is observable. The system is passive if and only if there exist a $P \in \mathbb{R}^{n \times n}$ and $P = P^T > 0$, such that*

$$\begin{bmatrix} A^T PA - P & A^T PB - C^T \\ B^T PA - C & -D^T - D + B^T PB \end{bmatrix} \leqslant 0 \qquad (2.31)$$

Theorem 2.10. *(Output Strict Passivity [61]) Assume that the LTI system is defined by (2.21), we denote H as the transfer function of the system. We also assume that (A, B) is stabilizable and (A, C) is detectable. Let E_o be a full-row-rank matrix with a null space equal to the unobservable subspace of (A, C). The statements below are equal:*

1. *The LTI system is OSP;*

2. *$H(s)$ is Output Strict Positive Real (OSPR). i.e., it is analytic for $\mathrm{Re}(s) > 0$ and $\exists \beta \in \mathbb{R}_{>0}$, s.t. $H(s) + H^H(s) \geqslant \beta H^H(s)H(s)$, $\forall s \in \mathbb{C}_{\geqslant 0}$.*

3. $\exists P = P^T \geqslant 0$ and $\beta \in \mathbb{R}_{>0}$ s.t. $E_o P E_o^T > 0$ and

$$
\begin{bmatrix}
A^T P + PA & PB - C^T & C^T \\
B^T P - C & -D^T - D & D^T \\
C & D & -\frac{1}{\beta} I
\end{bmatrix} \leqslant 0
\tag{2.32}
$$

Proof. The detailed proof of Theorem 2.10 can be found at the appendix in [61]. $\square$

Theorem 2.11. *(Output Strict Passivity in Discrete-time [61]) Assume that the Discrete-time LTI system is defined by (2.22), we denote Z as the transfer function of the system. We also assume that (A, B) is stabilizable and (A, C) is detectable. Let E_o be a full-row-rank matrix with a null space equal to the unobservable subspace of (A, C). The statements below are equal:*

1. *The LTI system is OSP;*

2. *$Z(z)$ is OSPR. i.e., it is analytic for $|z| \geqslant 1$ and $\exists \beta \in \mathbb{R}_{>0}$, s.t. $Z(\alpha e^{j\theta}) + Z^T(\alpha e^{-j\theta}) \geqslant \beta Z^T(\alpha e^{-j\theta}) Z(\alpha e^{j\theta})$, $\forall \theta \in [0, 2\pi)$ and all $|\alpha| \geqslant 1$.*

3. *$\exists P = P^T \geqslant 0$ and $\beta \in \mathbb{R}_{>0}$ s.t. $E_0 P E_0^T > 0$ and*

$$
\begin{bmatrix}
A^T PA - P & A^T PB - C^T & C^T \\
B^T PA - C & -D^T - D + B^T PB & D^T \\
C & D & -\frac{1}{\beta} I
\end{bmatrix} \leqslant 0
\tag{2.33}
$$

2.3.3 Zeros of Linear Systems

Definition 2.3.5. (Blocking Zero [62]) A causal LTI system represented by the transfer function $H(s) \in \mathbb{C}^{n \times n}$ has a blocking zero at $s_0 \in \mathbb{C}$ if $H(s_0) = 0$.

Definition 2.3.6. (Output Blocking Zero) A causal LTI system represented by the transfer function $H(s) \in \mathbb{C}^{n \times n}$ has an output blocking zero at $s = s_0$ if $\exists$ nonzero vector $\eta \in \mathbb{C}^n$, s.t. $\eta^H H(s_0) = 0$.

Definition 2.3.7. (Blocking Space) A causal LTI system whose transfer function is $H(s) \in \mathbb{C}^{n \times n}$ has a output blocking zero s_0, the set $\{\eta \in \mathbb{C}^n : \eta^H H(s_0) = 0\}$ is the blocking space associated with s_0, and is denoted as $\mathbb{B}_H(s_0)$

Definition 2.3.8. (Simple Zero) A finite output blocking zero is said to be simple if $\lim_{s \mapsto s_0} \eta^H H(s)(s - s_0)^{-1} \neq 0, \forall \eta \in \mathbb{B}_H(s_0)$. While for an infinite zero, $\lim_{s \mapsto \infty} \eta^H H(s)s \neq 0, \forall \eta \in \mathbb{B}_H(\infty)$.

Lemma 2.12. *For LTI system in* (2.21) :

1. *Suppose $s_0 \in \mathbb{C}$, s.t. $A - s_0 I$ is nonsingular. Then the system has a finite zero at $s = s_0$ with nonzero blocking vector $\eta \in \mathbb{C}^n$ if and only if $\exists$ a vector ϵ s.t.*

$$
\begin{bmatrix} \epsilon \\ \eta \end{bmatrix}^T \begin{bmatrix} A - s_0 I & B \\ C & D \end{bmatrix} = 0 \tag{2.34}
$$

2. *the system has a zero at $s = \infty$ with nonzero blocking vector $\eta \in \mathbb{C}^n$ if and only if $\eta^H D = 0$*

Definition 2.3.9. The LTI system in (2.21) is minimum phase if its poles and finite zeros are in $\mathbb{C}_{\leqslant 0}$

Theorem 2.13. *Let the LTI system in* (2.21) *be OSP, and its transfer function $H(s)$ be nonsingular for almost all $s \in \mathbb{C}$. Then all imaginary zeros of the LTI system is simple and H is minimum-phase*

Proof. The detailed proof can be found at [61]. □

Theorem 2.14. *Let H and G denotes two LTI systems which have finite gain in open loop, i.e. $H, G \in \mathbb{H}_\infty$. Let H be as in Theorem 2.13. Let Ω_H and Ω_G be the sets of all imaginary zeros for H and G, respectively. If $\Omega_H \subseteq \Omega_G$ and for each $s_0 \in \Omega_H$, $\mathbb{B}_H(s_0) \subseteq \mathbb{B}_G(s_0)$, then $H^{-1}G \in \mathbb{H}_\infty$.*

Proof. The detailed proof can also be found at [61]. □

<center>

CHAPTER 3

Mathematical Modeling

</center>

3.1   An Oscillating Body in Waves

First, we assume the propagating waves have the small amplitudes to simplify the oscillation behavior of a buoy in waves. Specifically, the wave height-to-length ratio is less than an order of magnitude smaller than one. This assumption enables us to do the analysis based on linear differential equations, allowing for the use of the linear superposition. In general, an oscillation body in waves has six modes (three translation modes surge, sway and heave, and three rotational modes roll, pitch and yaw). To help with the basic concept understanding, we only consider single-degree-of-freedom device for this chapter. Extensions to multi-degree-of-freedom devices can be straightforward using matrix methods.

An oscillating body that is submerged in deep water may lose some energy due to the viscous friction in the boundary layer of the fluid surrounding the body, and therefore generates the opposite damping force. In addition, when the body oscillates up and down, so does the surrounding fluid. To simplify this oscillation motion, we can assume the body only moves in the heave mode in an unbounded fluid, the equation of motion can be expressed as:

$$m\ddot{z} + c\dot{z} + kz = f_f(t) + f_r(t) \qquad (3.1)$$

<center>39</center>

Here m is the body mass, c is the applied damping and k is the hydrostatic stiffness constant. On the right side of the equation, f_f is the incident wave force and f_r is the radiation wave force. For such a submerged oscillation body, the maximum power generation can be achieved by applying complex conjugate control.

However, in most WEC devices, the WEC is oscillating close to the water surface (or "free surface"). The reason is that waves are the free-surface perturbation and the effect of such a perturbation on the body decreases exponentially with the depth of the submergence of the body. As long as the oscillation body is close enough to the free surface to respond to waves, it will create waves because of its own oscillation and thus generate the radiation force f_r.

WEC devices utilizing mechanical oscillation of a body must generate the waves from surrounding fluid in response to the incoming waves. The force on the water by the body is oscillatory and exhibits an exchange of energy that contains a reactive and a nonreactive or resistive part. The reactive part is the oscillatory acceleration of the water of the free surface and did not involve any energy loss, while the nonreactive part is the propagation of energy along the free surface away from the body. The former can be interpreted as an added mass or inertia for the body oscillating near the free surface and the latter as radiation damping, which can be much larger than the effect of viscous damping.

3.1.1 Regular Waves

We first consider the harmonic wave input, which is a single frequency and amplitude. For convenience, we choose a cylindrical body that is moored tightly enough and only has the heave motion. The dynamic equation of such an oscillating body can be written as the equation (3.1). The applied damping constant c can be negligible since it is very small compared to the radiation damping. We also assume that the viscosity damping can also be negligible. $f(t)$ is the total force on the body in the

presence of waves. Other forces are ignored, and we assume the body is in equilibrium in the absence of waves. The solution of $z(t)$ can be found by setting $z(t) = \hat{z}(i\omega)e^{i\omega t}$, where the complex amplitude $\hat{z}(i\omega)$ can be determined using the following equation:

$$[-\omega^2 m + k]\hat{z}(i\omega) = \hat{f}(i\omega) \tag{3.2}$$

For the case where waves and oscillatory motion are small enough, linear superposition holds. The force term on the right side of the equation (3.2) is the linear combination of the incident wave force (also called the diffraction force or excitation force) as $\hat{f}_f(i\omega)$, and the radiation force as $\hat{f}_r(i\omega)$. In general, both forces are six-component vectors, although here we consider them as complex scalars in heave motion.

$$\hat{f}(i\omega) = \hat{f}_f(i\omega) + \hat{f}_r(i\omega) \tag{3.3}$$

The incident wave force $\hat{f}_f(i\omega)$ depends on the geometry of the body and its submergence depth. For the bodies with a characteristic diameter sufficiently small compared to wavelength, $\hat{f}_f(i\omega)$ can be obtained by an integration of the incident wave velocity potential over the submerged surface. This is called the Froude-Krylov force. When the characteristic diameter is comparable or larger than wavelength, the excitation force is the solution to some partial differential equations through numerical computation. $\hat{f}_r(i\omega)$ also depends on body geometry and submergence, and needs to be solved by numerical computation. We can write the radiation force $\hat{f}_r(i\omega)$ as:

$$\hat{f}_r(i\omega) = -[\hat{c}_r(\omega) + i\omega\bar{m}_r(\omega)]\hat{v}(i\omega) \tag{3.4}$$

Both $\hat{c}_r(\omega)$ and $\bar{m}_r(\omega)$ are the frequency dependent terms. We note that $\hat{c}_r(\omega)$ is real-valued and multiplies velocity $\hat{v}(i\omega)$. $\hat{c}_r(\omega)$ is called the radiation damping, or added damping in wave energy area. $\bar{m}_r(\omega)$ is also real-valued and attached to the

41

acceleration $i\omega\hat{v}(i\omega)$. We call $\bar{m}_r(\omega)$ the added mass. As $\omega \to \infty$, $\hat{c}_r(\omega) \to 0$ and $\bar{m}_r(\omega) \to m_\infty$, where m_∞ is a positive constant. We can also treat $\bar{m}_r(\omega)$ as the sum of two terms.

$$\bar{m}_r(\omega) = \hat{m}_r(\omega) + m_\infty \tag{3.5}$$

If we express equation (3.1) in terms of the velocity $\hat{v}(i\omega)$ and insert equation (3.3), (3.4) and (3.5) into it, we have:

$$\left[i \left(\omega(m + m_\infty + \hat{m}_r(\omega)) - \frac{1}{\omega}k \right) + \hat{c}_r(\omega) \right] \hat{v}(i\omega) = \hat{f}_f(i\omega) \tag{3.6}$$

In time domain, the equation (3.6) is a second-order differential equation. Since the regular wave is harmonic and only propagated at the single frequency ω, the equation (3.6) can be solved. However, in this subsection, we are not interested in solving this equation but analyzing the dynamic behavior of the WEC device.

3.1.2 Irregular Waves

For simplicity, we still use the same cylindrical body in single-mode motion as an example. Like the case in regular waves, the basic dynamic behavior of the body can be expressed as the time domain equation (3.1), where the applied damping c can be negligible. Since the irregular wave exhibits energy over the broad range of frequencies, we can not treat it in the way like the regular wave. However, at each time t, we can regard the irregular wave input as the impulse input, and the forces acting on the body are generated through the impulse input. The irregular waves input is a succession of such impulse inputs, and the forces can be expressed in the form of convolution integrals based on linear superposition:

$$f_r(t) = - \int_{-\infty}^{\infty} g_r(\tau)v(t - \tau)\mathrm{d}\tau \tag{3.7}$$

42

$$f_f(t) = \int_{-\infty}^{\infty} h_f(\tau)a(t-\tau)\mathrm{d}\tau \qquad (3.8)$$

where $g_r(t)$ is the radiation impulse response function, and $v(t)$ is the velocity vector of the body. $h_f(t)$ is the excitation force impluse response function and $a(t)$ is the wave elevation. We recall from Section 3.1.1 one term m_∞ called infinity mass contributes to the radiation force, and this term is also included in the radiation impulse response function. We can express $g_r(t)$ as:

$$g_r(t) = h_r(t) + m_\infty \frac{d\delta(t)}{dt} \qquad (3.9)$$

Then, by doing the integration by parts,

$$f_r(t) = \int_{-\infty}^{\infty} h_r(\tau)v(t-\tau)d\tau + m_\infty \ddot{z}(t) \qquad (3.10)$$

where the second term is the infinite-frequency added mass times the acceleration, and h_r is the radiation kernel.

Considering the radiation force, there is no force f_r occurs before the first motion and the force present depends only on the motion up to present. It can be concluded that h_r is equal to 0 until $t = 0$, and this results in:

$$f_r(t) = \int_{0}^{\infty} h_r(\tau)v(t-\tau)d\tau + m_\infty \ddot{z}(t) \qquad (3.11)$$

And by using the equation (3.10) and (3.11), we can rewrite the equation (3.1) in the following form:

$$[m + m_\infty]\ddot{z}(t) + \int_{0}^{\infty} h_r(\tau)v(t-\tau)d\tau + kz(t) = f_f(t) \qquad (3.12)$$

Equation (3.12) is called Cummins' equation [63], where there is no restrctive constraint.

43

Applying a fourier transform on both sides gives the frequency domain equation.

$$-\omega^2[m + m_\infty]\hat{z}(i\omega) + i\omega\hat{h}_r(i\omega)\hat{z}(i\omega) + k\hat{z}(i\omega) = \hat{f}_f(i\omega) \tag{3.13}$$

where

$$\hat{h}_r(i\omega) = \int_{-\infty}^{\infty} h_r(t)e^{-i\omega t}dt \tag{3.14}$$

$$\hat{f}_f(i\omega) = \int_{-\infty}^{\infty} f_f(t)e^{-i\omega t}dt \tag{3.15}$$

The frequency-dependent function $\hat{h}_r(i\omega)$ can be written as:

$$\hat{h}_r(i\omega) = i\omega\hat{m}_r(\omega) + \hat{c}_r(\omega) \tag{3.16}$$

Substitute equation (3.14) and (3.16) into the equation (3.13), we can have the frequency domain dynamic equation.

$$[-\omega^2[m + m_\infty + \hat{m}_r(\omega)] + i\omega\hat{c}_r(\omega) + k]\hat{z}(i\omega) = \hat{f}_f(i\omega) \tag{3.17}$$

The excitation force f_f is the net result of the pressure distribution acting over the entire submerged surface. In the ith degrees of freedom, the excitation force f_{fi} can be written as:

$$f_{fi} = \iint_{S_B} pn_i dS \tag{3.18}$$

where p denotes the pressure at a given point on the submerged surface S_B, and n_i is the outward-point unit vector along the direction of ith degree of freedom. In frequency domain, the excitation force can be expressed as:

$$\hat{f}_f(i\omega) = \hat{h}_f(i\omega)\hat{a}(i\omega) \tag{3.19}$$

The complex frequency impulse response function $\hat{h}_f(i\omega)$ can be regarded as the
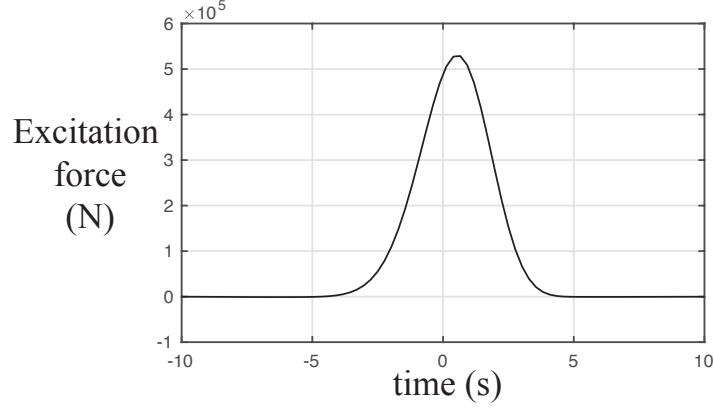
Figure 3.1: Impulse response function of the excitation force f_f in the simple buoy example

excitation force coefficients. In general, $\hat{f}_f$ and $\hat{h}_f$ are 6-dimensional column vectors. Here, since we assume the oscillation is only in heave, $\hat{f}_f$ and $\hat{h}_f$ are scalars. And the corresponding relationship between $\hat{h}_f(i\omega)$ and the impulse response function $h_f(t)$ can be expressed as:

$$h_f(t) = \frac{1}{2\pi} \int_{-\infty}^{\infty} \hat{h}_f(i\omega)e^{i\omega t}d\omega \tag{3.20}$$

The impulse response function $h_f(t)$ is not, in general, causal. This noncausality is partly attributed to the fact that the excitation force might be already applied at the oscillation body before the waves actually arrive at the body [64]. Hence, to determine the value of the present wave excitation force needs not only the past and present values but also the future values of the wave elevation a. Thus, although $h_f(t)$ is a real-valued function, $h_f(t) \neq 0, t \leq 0$ due to its noncausality. This has added to the difficulty of the control system design of the WEC device since this noncausality prohibits us from using the rational finite dimensional function to approximate the behavior of the excitation force. But It turns out in [64] that if we put the incident wave elevation a at a certain distance from the WEC device, the excitation force is actually causal in the dispersion-free wave. Later in [65], the author pointed out that in real waves, it is possible to fit the frequency response of the excitation force well using appropriate causal state-space models.

45

3.2 WEC Arrays

Using a large number of WEC devices to maximize the overall power capture from an approaching wavefront is the idea of a wave farm. Point-absorber arrays have been consider particularly attractive since they are insensitive to the direction of the incoming waves. We consider the point-absorber arrays here. Unlike the single WEC control problem, in order to maximize the power output of the whole WEC arrays, we need to use the interaction between each device to increase the power conversion.

Incident wave direction   WEC arrays
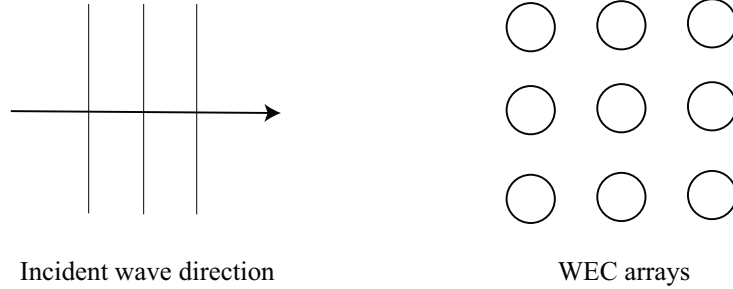
Figure 3.2: Multi arrays of point-absorber type WECs [10]

The dynamic behavior of the whole WEC arrays can still be described by Cummins' equation (3.12).

$$[M + M_\infty]\ddot{z}(t) + \int_0^\infty H_r(\tau)v(t - \tau)d\tau + Kz(t) = f_f(t) \tag{3.21}$$

Where M and M_∞ is the mass matrix and added mass matrix. Both of them are positive diagonal matrices. K is the hydrostatic stiffness matrix, which is also a positive diagonal matrix. We denote z as the WEC arrays displacement vector and v is the velocity vector. $f_f(t)$ is the WEC arrays incident wave force vector. The radiation kernel H_r is not diagonal because each WEC device experiences a force due to the wave radiated by any of the other devices.

The dynamic of WEC arrays in the frequency domain is:

$$-\omega^2[M + M_\infty]\hat{z}(i\omega) + i\omega\hat{H}_r(i\omega)\hat{z}(i\omega) + K\hat{z}(i\omega) = \hat{f}_f(i\omega) \qquad (3.22)$$

In the frequency domain, the incident wave force vector $\hat{f}_f(i\omega)$ is the product of the excitation force coefficients $\hat{H}_f(i\omega)$ and wave amplitude $\hat{a}(i\omega)$. The relationship between them is the same as equation (3.19).

Similarly, the frequency-dependent function $\hat{H}_r(i\omega)$ can be written as:

$$\hat{H}_r(i\omega) = i\omega\hat{M}_r(\omega) + \hat{C}_r(\omega) \qquad (3.23)$$

Where $\hat{M}_r(\omega)$ and $\hat{C}_r(\omega)$ are the matrix form of $\hat{m}_r(\omega)$ and $\hat{c}_r(\omega)$. We define $\bar{M}_r(\omega) = \hat{M}_r(\omega) + M_\infty$. Substitute (3.23) into (3.22), we can have the frequency domain dynamic equation:

$$[-\omega^2[M + M_\infty + \hat{M}_r(\omega)] + i\omega\hat{C}_r(\omega) + K]\hat{z}(i\omega) = \hat{f}_f(i\omega) \qquad (3.24)$$

3.3   Sea State

Sea state is the general condition on the free surface of the ocean, and it can be characterized by a certain wave spectrum density function $S_a(\omega)$. Here, we assume the wave elevation a is a stationary stochastic process with the known spectrum density function $S_a(\omega)$. The mean of the wave elevation a is 0, and the variance of a is σ_a^2, which can be calculated based on the following equation:

$$\sigma_a^2 = \frac{1}{\pi}\int_0^\infty S_a(\omega)d\omega \qquad (3.25)$$

We choose the common JONSWAP spectrum [66] as our wave spectrum $S_a(\omega)$:

$$S_a(\omega) = 155 * \frac{H_{1/3}^2}{T_1^4 \omega^5} \exp\left(\frac{-944}{T_1^4 \omega^4}\right) \gamma^Y \tag{3.26}$$

where

$$Y = \exp\left(-\left(\frac{0.191\omega T_1 - 1}{2^{\frac{1}{2}}\sigma}\right)^2\right) \tag{3.27}$$

and

$$\sigma = \begin{cases} 0.07 & \text{for } w \leq \frac{5.24}{T_1} \\ \\ 0.09 & \text{for } w > \frac{5.24}{T_1} \end{cases} \tag{3.28}$$

The value of sharpness factor γ is usually between 1 and 10 depends on the length of fetch. When γ is 1, it represents a fully developed sea state.
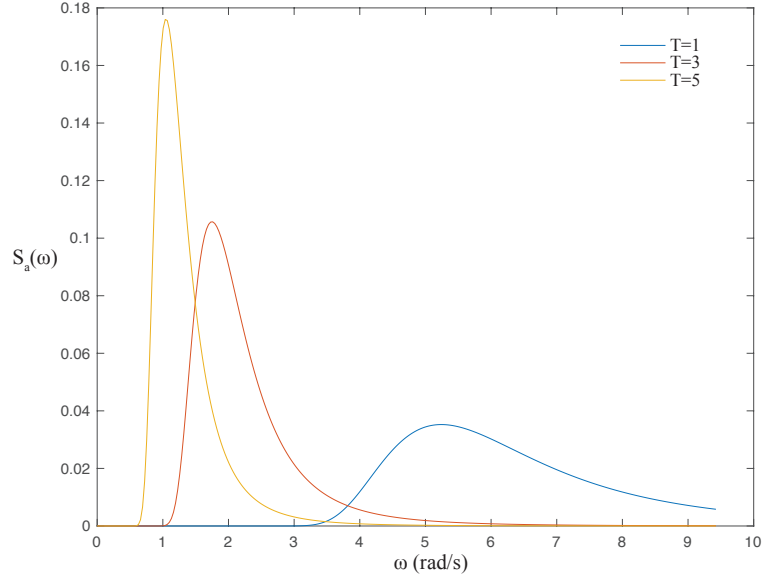
Figure 3.3: Comparison between different mean wave periods while $\gamma = 1$ and $H_{1/3} = 1$m invariant

As we can see in equation (3.26), the wave spectrum $S_a(\omega)$ is determined by three parameters: significant wave height $H_{1/3}$, mean wave period T_1 and sharpness factor γ. The significant wave height $H_{1/3}$ commonly used as a measure of the height of the ocean waves is the mean wave height of the highest third of the waves. The higher
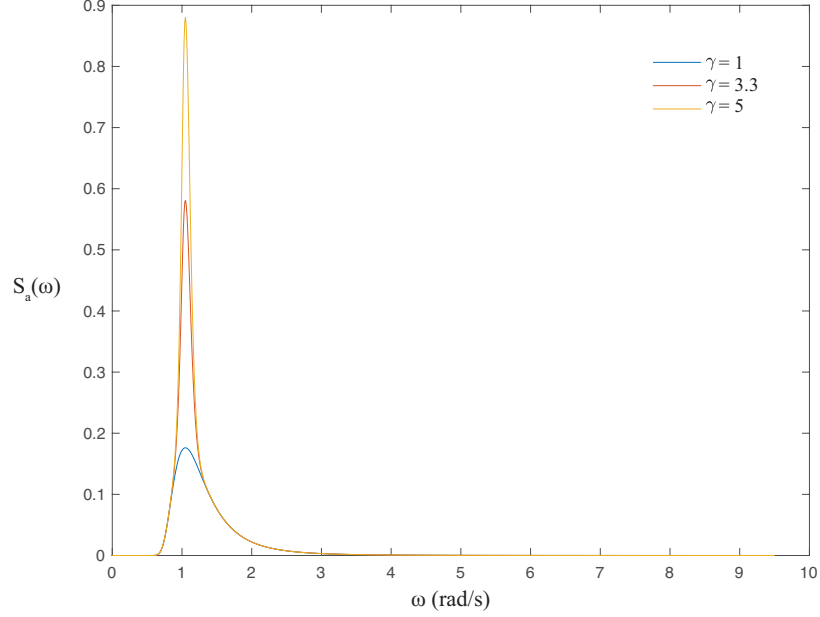
Figure 3.4: Comparison between different sharpness factors while $T = 5$s and $H_{1/3} = 1$m invariant

$H_{1/3}$ is, the more power can be extracted in the ocean waves. The mean wave period T_1 is the mean of all wave periods in a time-series representing a certain sea state. There is another terminology called peak wave period T_p, describing the wave period with highest energy. In JONSWAP spectrum, there is a certain relationship between T_1 and T_p:

$$T_1 = 0.834 T_p \tag{3.29}$$

The sharpness factor γ depends on the fetch. The longer the fetch is, the larger γ will be, resulting in a higher energy sea state.

3.4   Power Generation Model

The power generation model differs in different PTO mechanisms. In this document, we assume our PTO system in each WEC device to be the same direct-drive permanent-magnet machine. We also assume that the generator has linear behavior and minimal core loss, which results in the linear relationship between the WEC

velocity v and the voltage in the generator V:

$$V = k_e v \tag{3.30}$$

where k_e is an electric constant, inherent to the generator. And an equal linear relationship holds between the generator current i and the tether cable force (controller force) u:

$$i = -\frac{1}{k_e} u \tag{3.31}$$

The instantaneous power absorption of the whole WEC array at time t can be calculate using the equation (3.30) and equation (3.31):

$$p_i(t) = V^T i = -u^T v \tag{3.32}$$

The electrical loss in the power generation model is assumed to be dominated by conductive dissipation. In reality, this dissipation is related to the current i through a very complex relationship involving many parameters of the electronic hardware [47]. However, we can upper bound this dissipation term by a quadratic function of the current i:

$$p_{\text{loss}} = i^T R i \tag{3.33}$$

where $R = R^T$ is positive definite. The resistance R includes the stator coil resistance of the generation, and the transmission resistance for the drive. By using equation (3.31), we can express the dissipation energy in terms of the controller force u:

$$p_{\text{loss}} = u^T R_d u \tag{3.34}$$

where $R_d = R_d^T > 0$ can be regarded as the static impedance matrix associated with the power loss.

Combining the instantaneous power absorption and the dissipation energy, the total power generation at time t can be written as:

$$p(t) = -u^T v - u^T R_d u \tag{3.35}$$

In the control system design, our goal is to maximize the power generation performance over a certain time duration. In other words, the control objective is to maximize the average power generation performance.

$$\bar{p} = \mathcal{E}\{-u^T v - u^T R_d u\} \tag{3.36}$$

3.5 State-Space Model

In the WEC device, the external force of the oscillation body includes the wave excitation force and the actuator force, which is applied by the tether cable in the simple buoy example. The WEC arrays dynamic equation (3.22) considering the actuator force can be written in the frequency domain as

$$[-\omega^2 (M + M_\infty)) + i\omega H_r(i\omega) + K]\hat{z}(i\omega) = \hat{f}_f(i\omega) + \hat{u}(i\omega) \tag{3.37}$$

Where $u(t)$ is the vector of the actuator force,

$$\hat{u}(i\omega) = \int_{-\infty}^{\infty} u(t)e^{-i\omega t} dt \tag{3.38}$$

Here, the transfer function $H_r(i\omega)$ is infinite-dimensional since it can be solved by partial differential equations. We can approximate this infinite-dimensional transfer function by the finite state-space model. The method we applied here is called subspace-based system identification techniques which is originally introduced in [67]. There are several advantages of this subspace-based method that does not involve any

iterative procedure and provide balanced truncations of infinite-dimensional systems in discrete-time from frequency domain data. However, the original subspace-based system identification techniques do have several drawbacks: the identified finite state-space model may not be positive real and for a limited number of the frequency-domain data, it may fail to provide an accurate state-space model. We proposed a new version of this technique in [68] that tackles these drawbacks and will present it in the next chapter. For convenience, we will put the updated subspace-based system identification techniques of infinite dimensional transfer functions in Appendix A.

$$H_r(i\omega) \approx D_r + C_r[j\omega I - A_r]^{-1}B_r \qquad (3.39)$$

Based on the state space model for $H_r(i\omega)$, we can propose an augmented state space model that fully characterized the frequency domain dynamic equation (3.22).

$$\begin{cases} \frac{dx_c}{dt} = A_c x_c + B_c(f_f + u) \\ v = C_{cv} x_c \\ z = C_{cz} x_c \\ y = C_{cy} x_c \end{cases} \qquad (3.40)$$

where

$$x_c = \begin{bmatrix} x_r & z & \dot{z} \end{bmatrix}^T, A_c = \begin{bmatrix} A_r & 0 & B_r \\ 0 & 0 & I \\ -M_T^{-1}C_r & -M_T^{-1}K & -M_T^{-1}D_r \end{bmatrix}$$

$$B_c = \begin{bmatrix} 0 & 0 & (M_T^{-1})^T \end{bmatrix}^T, M_T = M + M_\infty$$

$$C_{cv} = \begin{bmatrix} 0 & 0 & I \end{bmatrix}, C_{cz} = \begin{bmatrix} 0 & I & 0 \end{bmatrix}, C_{cy} = \begin{bmatrix} 0 & 0 & I \\ 0 & I & 0 \end{bmatrix}$$

y is the sensor measurements of the WECs. Here we assume that $y = \begin{bmatrix} v^T & z^T \end{bmatrix}^T$.

As for the diffraction force f_f, we can apply the same system identification method to find an approximate finite-dimensional state-space model. With the wave elevation a treated as a stationary stochastic process, the wave excitation force f_f can also be regarded as a stationary stochastic process and its spectrum function has the following relationship with wave spectrum S_a:

$$S_f(\omega) = \hat{H}_f(i\omega) S_a(\omega) \hat{H}_f^T(-i\omega) \tag{3.41}$$

We can find a a finite-dimensional noise filter $W(s)$ such that when excited by the white noise, its power spectrum is close to the wave force spectrum. i.e.,

$$W(i\omega) = D_w + C_w[i\omega I - A_w]^{-1} B_w \tag{3.42}$$

$$S_f(\omega) \approx W(i\omega) W^T(-i\omega) \tag{3.43}$$

Although D_w may be nonzero in the finite-dimensional approximation, it is usually very small and can be discarded. Without loss of generality, we can always make $D_w = 0$. Correspondingly, we can have the finite-dimensional state space model of $W(s)$:

$$\begin{cases} dx_w = A_w x_w dt + B_w dw \\ f_f = C_w x_w \end{cases} \tag{3.44}$$

where $w(t)$ is a Wiener process with zero mean and unit rate; i.e., $\mathcal{E}\, w(t) = 0$ and $\mathcal{E}\, w(t) w^T(\tau) = I \min\{t, \tau\}$. (Note that this is equivalent to stating that $\frac{d}{dt} w(t)$ is white noise with spectral density $S_{\dot{w}} = I$.)

Put the equation (3.44) into the equation (3.40), we can have the following aug-

mented state space model:

$$
\begin{cases}
dx = (Ax + B_u u)dt + Edw \\
v = C_v x \\
z = C_z x \\
y = C_y x
\end{cases}
\tag{3.45}
$$

where

$$
x = \begin{bmatrix} x_c & x_w \end{bmatrix}^T , A = \begin{bmatrix} A_c & B_c C_w \\ 0 & A_w \end{bmatrix}
$$

$$
B_u = \begin{bmatrix} B_c & 0 \end{bmatrix}^T , E = \begin{bmatrix} 0 & B_w \end{bmatrix}^T , C_v = \begin{bmatrix} C_{cv} & 0 \end{bmatrix}
$$

$$
C_z = \begin{bmatrix} C_{cz} & 0 \end{bmatrix} , C_y = \begin{bmatrix} C_{cy} & 0 \end{bmatrix}
$$

3.6 Assumptions

Definition 3.6.1. The transfer function $G_{uv} : u \mapsto v$ is called the *driving-point impedance* of the WEC.

Due to thermodynamic constraints on the physical behavior of the WEC, it is known that its driving point impedance $u \mapsto v$ is passive. (Indeed, otherwise the WEC would be able to generate more energy than it absorbs from the ocean.) This implies that the transfer function

$$
G_{uv}(s) \triangleq C_v (sI - A)^{-1} B_u \tag{3.46}
$$

is positive real.

Assumption 3.6.1. *Driving point impedance* $u \mapsto v$ *is passive, e.g.,*

$$\int_0^T v^T u \, dt \geqslant 0, \quad \forall T \in \mathbb{R}_{\geqslant 0} \tag{3.47}$$

This is equivalent to stating that $G_{uv}(s)$ is is analytic in the open right half plane, real for $s \in \mathbb{R}_{>0}$,and such that it has positive-semidefinite Hermitian component on the imaginary axis; i.e.,

$$G_{uv}(j\omega) + G_{uv}^H(j\omega) \geqslant 0, \quad \forall \omega \in \mathbb{R} \tag{3.48}$$

Assumption 3.6.2. *The mapping* $\{u, w\} \mapsto \{v, y, z\}$ *has bounded* $\mathcal{L}_2$ *gain.*

The Assumption 3.6.2 require the state space model in Equation 3.45 are in $\mathcal{H}_\infty$. Without loss of generality, we also presume a minimal model. e.g.,

Assumption 3.6.3. *System* (3.45) *is a minimal realization of mapping* $\{u, w\} \mapsto \{v, y, z\}$.

Combining the assumption 3.6.2 and 3.6.3 implies that the matrix A is Hurwitz.

3.7 Numerical Example

3.7.1 One Buoy Case

As a simple example, here we consider a single-degree-of-freedom WEC shown in Figure 5.1. The floating cylinder buoy is connected to the linear generator mounted on the sea floor. We assume the buoy only moves in heave. For the model parameters chosen, the natural period is approximately 5.5s. The PTO applies the controller force u through the sensor measurement v. For the sea state, we choose the JOSWAP spectrum with significant wave height $H_{1/3} = 1m$, mean wave period $T_1 = 7s$ and sharpness factor $\gamma = 1$.
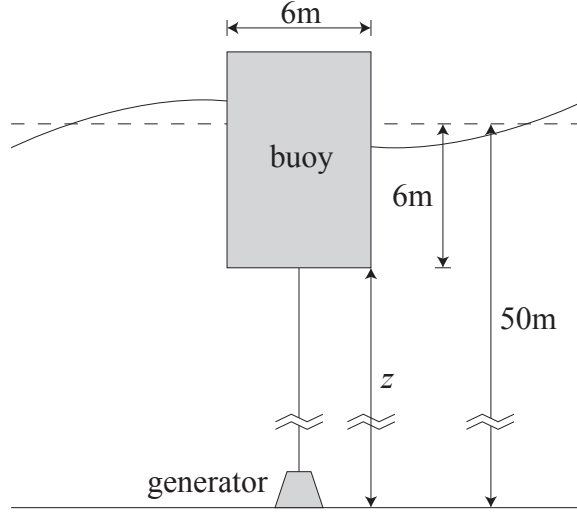
Figure 3.5: A simple floating buoy with the floor-mounted generator. The buoy mass is around 170000 kg. The generator damping is 200N*s/m

Figure 3.6 shows the plot of the frequency dependent added mass $\bar{m}_r(\omega)$, added damping $\hat{c}_r(\omega)$ and excitation force coefficients $\hat{h}_f(i\omega)$. As ω increases, $\bar{m}_r(\omega) \mapsto m_\infty$, added damping and excitation force coefficients approach 0. Figure 3.7 compares the frequency response between the true $\hat{h}_r(i\omega)$ and the approximate state-space model. The state-space model, whose dimensional is equal to 12, approximates $\hat{h}_r(i\omega)$ very well. Based on it, we can construct the state-space model (3.40). In figure 3.8, the frequency response of $S_f(\omega)$ and $W(i\omega)W^H(i\omega)$ are shown. The state-space model of $W(s)$ also has 12 states, the expression of which can be found as in (3.44).

Using the above results, we can have the augmented state-space model (3.45) that fully characterizes the dynamic behavior of the WEC system and surrounding fluid.

3.7.2 Two Buoy Case

In this subsection, we consider the two buoys case. For each buoy, we choose the specification as the same as the one buoy case. The position of two buoys is shown in Figure 3.9. For the sea state, we choose the JONSWAP spectrum with the same parameters from one buoy case.
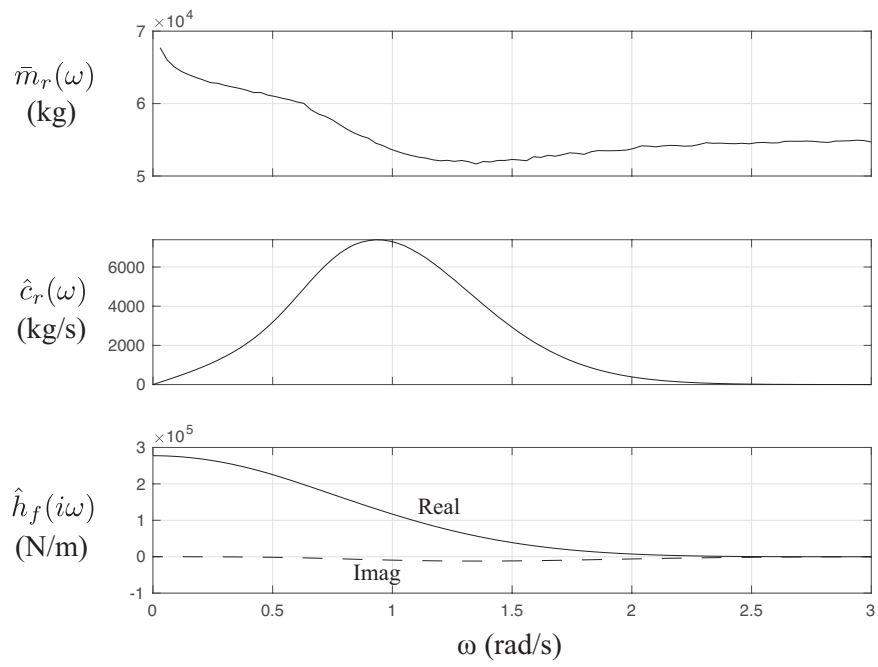
Figure 3.6: Figure of hydrodynamic parameters
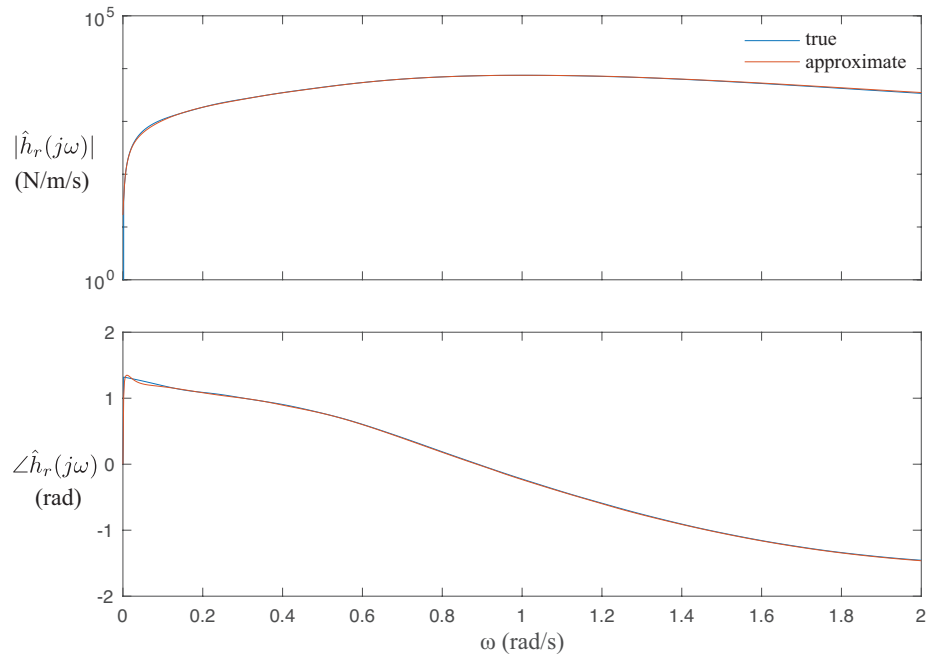
Figure 3.7: System identification of $\hat{h}_r(j\omega)$
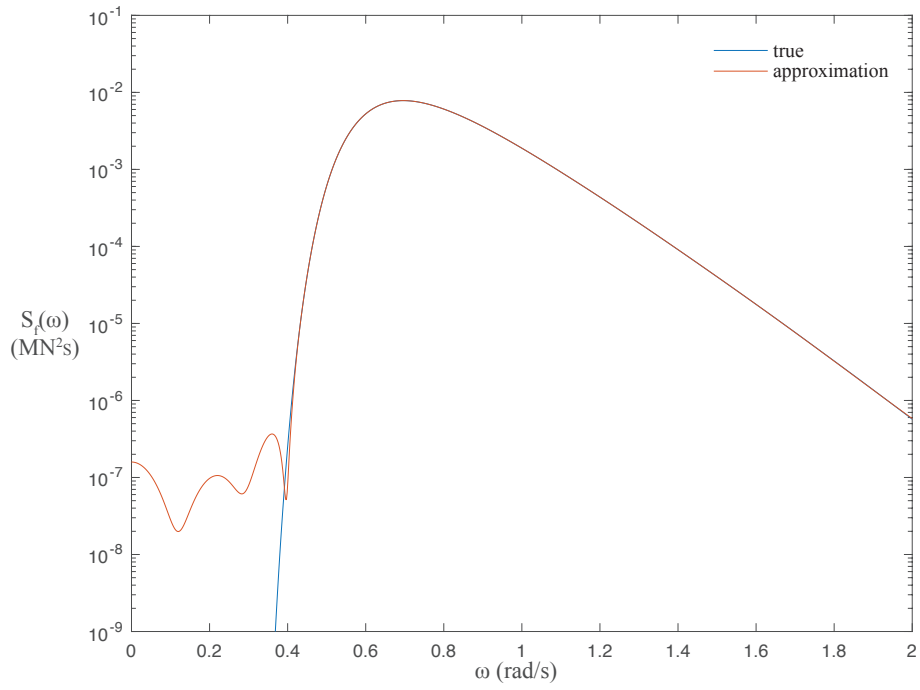
Figure 3.8: System identification of $S_f(\omega)$
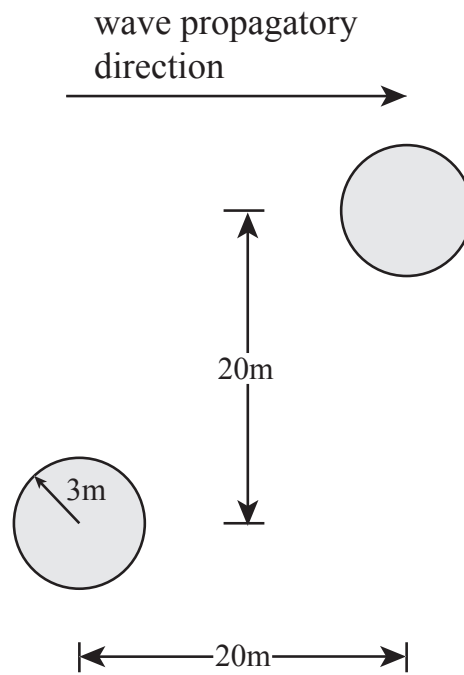
Figure 3.9: 2 buoy position diagram
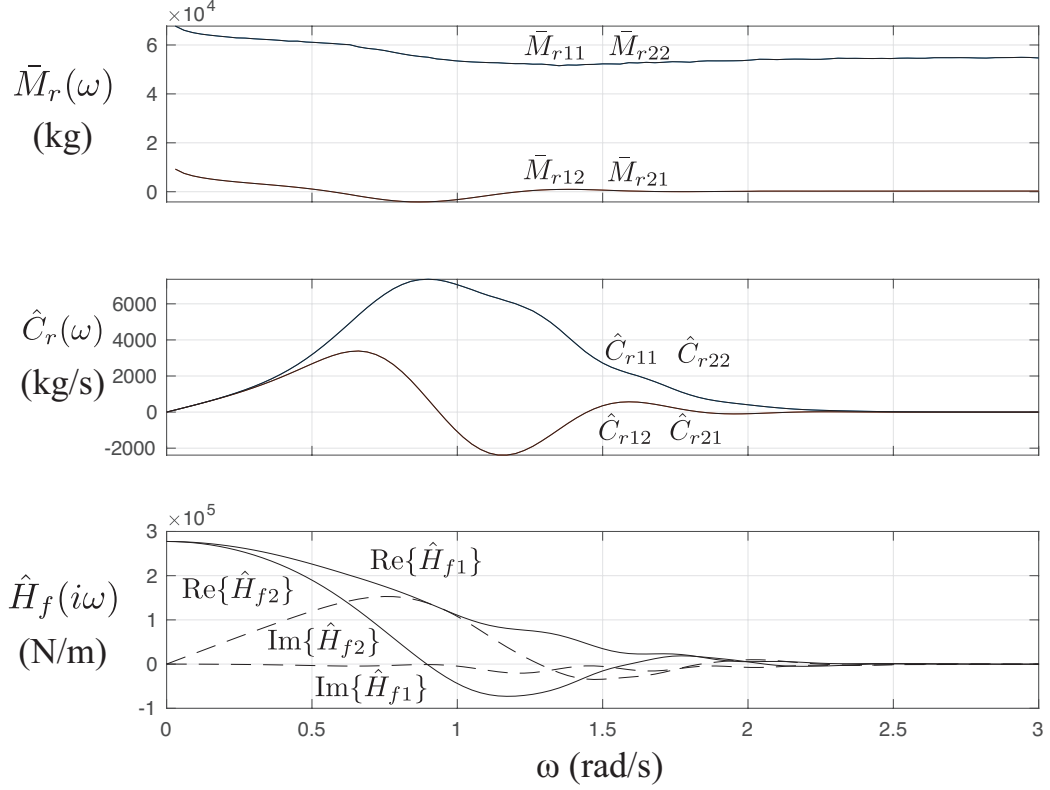
Figure 3.10: Hydrodynamic parameters of two buoys case

Figure 3.10 shows the plot of the frequency dependent added mass $\bar{M}_r(\omega)$, added damping $\hat{C}_r(\omega)$ and excitation force coefficients $\hat{H}_f(i\omega)$. As ω increases, added mass $\bar{M}_r(\omega) \rightarrow M_\infty$, added damping $\hat{C}_r(\omega)$ and excitation force coefficients $\hat{H}_f(i\omega)$ approach **0**. Figure 3.11 compares the frequency response between the true $\hat{H}_r(i\omega)$ and the approximate state-space model. Since at each frequency $\hat{H}_r(i\omega)$ is symmetric and the diagonal terms of it are the same, we can only plot the frequency response of one diagonal term and one off-diagonal term in Figure 3.11. The state-space model, whose dimensional is equal to 18, has a relatively high accuracy of approximating $\hat{H}_r(i\omega)$. Based on it, we can construct the state-space model (3.40). In Figure 3.12 and Figure 3.13, the frequency response of $S_f(\omega)$ and $W(i\omega)W^H(i\omega)$ are shown. Like Figure 3.11, only one diagonal term and one off-diagonal term need to be plotted. The state-space model of $W(s)$ also has 18 states, the expression of which can be found as in (3.44).
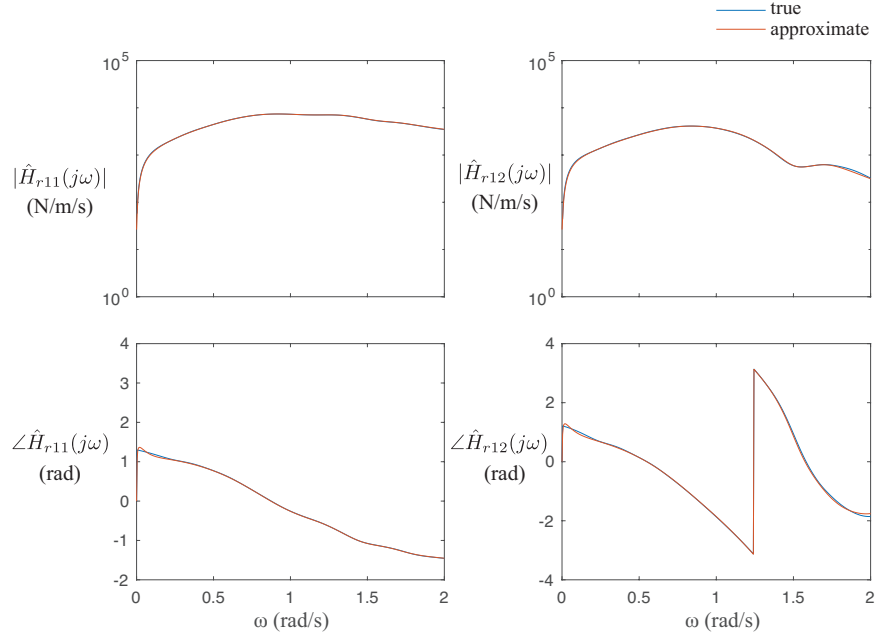
Figure 3.11: System identification of $\hat{H}_r(i\omega)$

Same as the one buoy case, the state-space model that fully characterizes the dynamic behavior of the WEC arrays and surrounding fluid is (3.45).
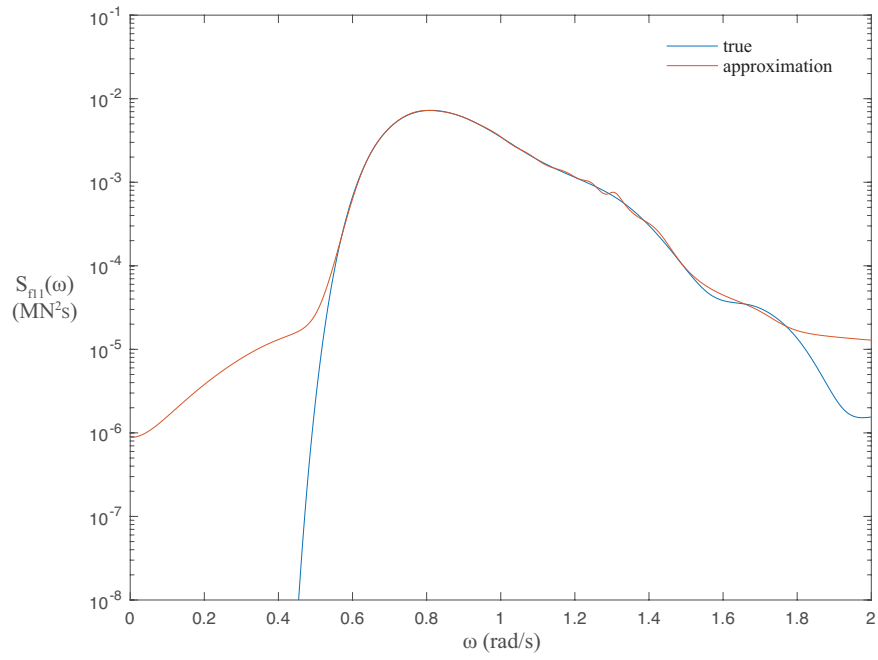
Figure 3.12: System identification of the diagonal term in wave force spectrum $S_f(\omega)$
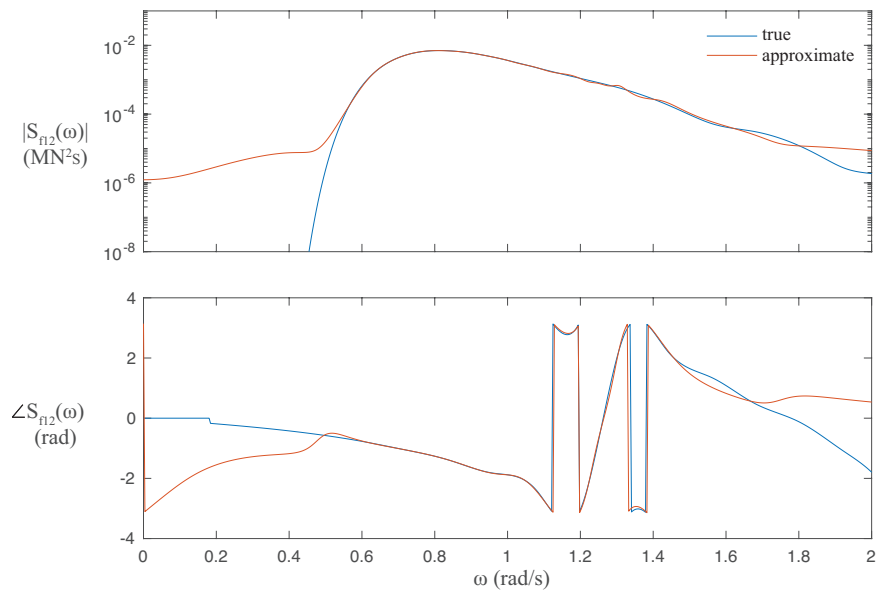
Figure 3.13: System identification of the off-diagonal term in wave force spectrum $S_f(\omega)$

CHAPTER 4

Subspace-based Spectral Factorization of Wave Force Spectrum

4.1 Introduction

In WEC modeling, it is of central importance to characterize the stochastic dynamics of floating rigid bodies subjected to random waves [66]. In Chapter 3, the wave excitation force f_f can be regarded as a stationary stochastic process and its spectrum has the following relationship with wave spectrum S_a:

$$S_f(\omega) = \hat{H}_f(i\omega)S_a(\omega)\hat{H}_f^T(-i\omega) \tag{4.1}$$

where $H_f(i\omega)$ is the impulse response function of the wave excitation force f_f. In many circumstances (such as in response control design) it is useful to approximately decompose this spectrum into rational spectral factors. The problem is made challenging due to the infinite-dimensionality of the system. In particular, infinite-dimensionality arises in two distinct ways. Firstly, $H_f(i\omega)$ constitutes an irrational transfer function. This transfer function must in general be found numerically at each frequency, as the solution to a system of partial differential equations characterizing the interaction between the floating body and the surrounding fluid [69–71]. Secondly, the power spectral density of the wave elevation is, itself, typically an irrational spectrum [72].

Since the transfer function $H_f(i\omega)$ can only be solved numerically at each frequency, we can sample the discrete-time transfer function $H_{fd}(e^{i\Omega_\ell})$ using bilinear transformation.

$$H_{fd}(e^{i\Omega_\ell}) = H_f \left(i\frac{2}{T}\tan(\Omega_\ell/2) \right) \tag{4.2}$$

Where evenly-spaced discrete-time frequencies $\Omega_\ell = 2\pi\ell/2N$, with $\ell = \{0, .., 2N-1\}$, and T is the sampling time. The discrete-time wave spectrum can be generated using bilinear transformation:

$$S_{ad}(\Omega_\ell) = S_a \left(\frac{2}{T}\tan(\Omega_\ell/2) \right) \tag{4.3}$$

Correspondingly, the discrete-time wave force spectrum can be found as:

$$S(\Omega_\ell) = H_{fd}(e^{i\Omega_\ell})S_{ad}(\Omega_\ell)H_{fd}^T(e^{-i\Omega_\ell}) \tag{4.4}$$

Our goal in this Chapter is to find a rational, minimum-phase filter $G(z)$ of desired order n, such that

$$S(\Omega_\ell) \approx G(e^{i\Omega_\ell})G^H(e^{i\Omega_\ell}) \tag{4.5}$$

Many researchers have investigated spectral factorization algorithms that perform an optimization of $G(z)$ over an assumed parametric domain [73, 74]. The objective of such techniques is to minimize a certain error function, such as a weighted norm of the error between the two expressions in (4.5). This type of technique often involves in an associated non-convex optimization problem, which can only be solved iteratively and with no guarantee on the rate of convergence or the global optimality of the attained solution.

The first subspace technique of spectral factorization was proposed by Van Over-

schee [75]. It assumed that the spectrum data can be decompoised as

$$S(\Omega_\ell) = G_0(e^{i\Omega_\ell})G_0^H(e^{i\Omega_\ell}) + \hat{S}_\ell \tag{4.6}$$

where $G_0(z)$ constitutes the finite-order rational discrete-time transfer function, and $\hat{S}_\ell$ is a sequence of uncorrelated noise terms. This non-iterative subspace technique is shown to be interpolative, i.e., when $\hat{S}_\ell = 0, \forall \ell$, the techniques factors $S(\Omega)$ with zero error, give a sufficient amount (N) of data. This technique also appeared to be consistent, i.e., even with the existence of $\hat{S}_\ell$, the asymptotic limit $\|G_0 G_0^H - S\|_\infty \to 0$ as $N \to \infty$, which was later shown by Akçay and Türkay that this was not the case [76]. In [77], Akçay improve the algorithm such that it is consistent as well as interpolative, by changing the way the Hankel matrix is constructed. The algorithm works well in most circumstances, but has a number of failure modes, especially for the spectrum data from some lightly damped systems.

In the problem of identifying the power spectrum for the stationary response of the heaving buoys excited by stochastic ocean waves, the use of such techniques without modifications can be challenging. In this case, the power spectrum of the buoys response is irrational and infinite-dimensional, which require the Hankel matrix in Akçay's algorithm to be fairly large. As such, we propose several modifications, one of which is a new way to assemble Hankel matrix without using the consecutive Markov coefficients. Additionally, we do not consider noise term $\hat{S}_\ell$ here since the inclusion of such noise is secondary to the analysis presently here.

4.2 Standard Algorithm

4.2.1 Assumptions

Because $S(\Omega)$ is assumed to be a valid power spectral density, it is the case that $S(\Omega) = S^H(\Omega) \geqslant 0, \ \forall \Omega \in [0, 2\pi)$. We further assume the stochastic process to have

64

finite variance, resulting in the assumption $\int_0^{2\pi} \|S(\Omega)\| d\Omega < \infty$. We further assume that there is no deterministic subspace of y; i.e., no vector $\eta \neq 0$ such that the signal $\eta^T y$ has zero variance. It is straight-forward to show that this is true if and only if $\int_0^{2\pi} S(\Omega) d\Omega > 0$. For convenience, let $S_\ell \triangleq S(\Omega_\ell)$. For the present analysis we strengthen the above conditions, such that they hold over the discrete S_ℓ data. This may be stated concisely by the following:

Assumption 4.2.1. *For each $\ell \in \{0, ..2N - 1\}$, we assume $S_\ell = S_\ell^H \geqslant 0$. Furthermore, we assume there exist $\{\kappa_1, \kappa_2\} \subset \mathbb{R}$ with $0 < \kappa_1 < \kappa_2 < \infty$, such that $\kappa_1 I < \sum_0^{2N-1} S_\ell < \kappa_2 I$.*

We seek to estimate $S(\Omega)$ by

$$\hat{S}(\Omega) = G(e^{j\Omega})G^H(e^{j\Omega}) \tag{4.7}$$

where $G(z)$ is a linear, time-invariant, finite-dimensional filter of order (i.e., MacMillian degree) equal to n. This implies a state space realization parametrized by matrices $A \in \mathbb{C}^{n \times n}$, $B \in \mathbb{C}^{n \times p}$, $C \in \mathbb{C}^{m \times n}$, and $D \in \mathbb{C}^{m \times p}$, such that

$$G(z) = D + C(zI - A)^{-1}B \tag{4.8}$$

Equivalently, we assume $\hat{S}(\Omega)$ is the power spectral density associated with the Gauss-Markov process

$$x_{k+1} = Ax_k + Bw_k \tag{4.9}$$

$$y_k = Cx_k + Dw_k \tag{4.10}$$

where w_k is an Independent, Identically-Distributed (IID) Gaussian sequence with $\mathcal{E} w_k w_\ell^H = \delta_{k\ell} I$. The existence of a power spectral density implies stationarity, thus requiring that the eigenvalues of A must have moduli strictly less than unity. Beyond

these requirements, we will place further restrictions on $G(z)$:

1. We restrict our attention to the case in which $G(z)$ is square; i.e,. $p = m$. Situations where $p > m$ can be reduced to the square case, by finding the equivalent innovations model. The case with $p < m$ corresponds to the case in which $\hat{S}(\Omega)$ is singular for each Ω, with a frequency-dependent null space equal to that of $G^H(e^{j\Omega})$. This problem has been investigated by other authors [78], but is not considered here.

2. For the assumption of $p = m$, we place the additional requirements that D be invertible, and that $G(z)$ be minimum-phase. Together these requirements are ensured by requiring that the eigenvalues of $A - BD^{-1}C$ have moduli less than or equal to unity. We note that this requirement does not preclude singularity of $\hat{S}(\Omega)$ at isolated frequencies, but does preclude singularity over any open interval.

3. Our development will require that A be invertible.

4.2.2 Interpolative Stochastic Realization Theory for Rational Spectra

We first consider the related problem in which a *rational* spectrum $S(\Omega_\ell)$ is given at $\Omega_\ell = e^{2\pi j\ell/2N}$, $\ell \in \{0, ..2N - 1\}$, and it is desired to extract the spectral factor $G(z)$ from this data. Although it is assumed that $S(\Omega) = G_0(e^{j\Omega})G_0^H(e^{j\Omega})$ for some $G_0(z) = D + C(zI - A)^{-1}B$, no specific model order n is assumed a priori. It is assumed that there is sufficient data (i.e., sufficiently large N) to determine all the system parameters $\{A, B, C, D\}$.

It is a classical result that $S(\Omega)$ can be factored into its spectral summands [74], as

$$S(\Omega) = C(e^{j\Omega}) + C^H(e^{j\Omega}) \tag{4.11}$$

where $C(z) = E + C(zI - A)^{-1}F$ is the so-called covariance model, with E and F

66

found as

$$E = \tfrac{1}{2} \left(DD^H + CPC^H \right) \tag{4.12}$$

$$F = APC^H + BD^H \tag{4.13}$$

and where $P > 0$ is the solution to Lyapunov equation

$$P = APA^H + BB^H \tag{4.14}$$

Let $S_\ell \triangleq S(\Omega_\ell)$. Its inverse Discrete Fourier Transform (DFT) is

$$s_k = \frac{1}{2N} \sum_{\ell=0}^{M-1} S_\ell e^{2\pi jk\ell/2N} \tag{4.15}$$

This evaluates to

$$s_k = \begin{cases} 2E + CA^{2N-1}(I - A^{2N})^{-1}F \\ \quad + F^H(I - A^{2N})^{-H}(A^H)^{2N-1}C^H \quad : \quad k = 0 \\ CA^{k-1}(I - A^{2N})^{-1}F \\ \quad + F^H(I - A^{2N})^{-H}(A^H)^{2N-k-1}C^H \quad : \quad k > 0 \end{cases} \tag{4.16}$$

Next, we construct a Hankel matrix from the s_k sequence, which is parametrized by two positive integers $\{p, q\}$. First, for $r = p + q - 1$, define the sequence h_k for $k \in \{1..r\}$ as

$$h_k = s_k + s_{2N-1-r+k} \tag{4.17}$$

It is straight-forward to verify that

$$h_k = CA^{k-1}\tilde{F} + \tilde{F}^H(A^H)^{r-k}C^H \tag{4.18}$$

where

$$\tilde{F} = (I + A^{2N-1-r})(I - A^{2N})^{-1}F. \tag{4.19}$$

Now, define the $p \times q$ block-Hankel matrix H_{pq} as

$$H_{pq} = \begin{bmatrix} h_1 & h_2 & \cdots & h_q \\ h_2 & \ddots & \ddots & h_{q+1} \\ \vdots & \ddots & \ddots & \vdots \\ h_p & h_{p+1} & \cdots & h_r \end{bmatrix} \tag{4.20}$$

Substituting (4.18) and factoring, we have that

$$H_{pq} = \mathcal{O}_p \mathcal{C}_q \tag{4.21}$$

where

$$\mathcal{O}_p = \begin{bmatrix} C & \tilde{F}^H (A^H)^{p-1} \\ CA & \tilde{F}^H (A^H)^{p-2} \\ \vdots & \vdots \\ CA^{p-1} & \tilde{F}^H \end{bmatrix} \tag{4.22}$$

$$\mathcal{C}_q = \begin{bmatrix} \tilde{F} & A\tilde{F} & \cdots & A^{q-1}\tilde{F} \\ (A^H)^{q-1}C^H & (A^H)^{q-2}C^H & \cdots & C^H \end{bmatrix} \tag{4.23}$$

It is straight-forward to show that if (A, B) is controllable and (A, C) observable, and if $p, q > 2n$, then the ranks of $\mathcal{O}_p$ and $\mathcal{C}_q$ are both $2n$.

Define

$$\mathcal{O}_{p2} = \{\mathcal{O}_p\}_{\text{rows } m+1:mp} \tag{4.24}$$

$$\mathcal{O}_{p1} = \{\mathcal{O}_p\}_{\text{rows } 1:(m-1)p} \tag{4.25}$$

68

and we note that

$$\mathcal{O}_{p2} = \mathcal{O}_{p1}\mathcal{A}, \tag{4.26}$$

where

$$\mathcal{A} = \begin{bmatrix} A & 0 \\ 0 & A^{-H} \end{bmatrix} \tag{4.27}$$

The singular value decomposition (SVD) of block-Hankel matrix is $H_{pq} = U\Sigma V^H$ where U and V have orthonormal columns and Σ is diagonal and contains the (nonzero) singular values. Then Σ has dimension $2n$, from which the order of $G_0(z)$ can be inferred. It must be the case that $U = \mathcal{O}_p M$ for some invertible $M \in \mathbb{C}^{2n \times 2n}$, because U and $\mathcal{O}_p$ share the same range space. It therefore follows that for $\mathcal{A}' = M\mathcal{A}M^{-1}$,

$$U_2 = U_1 \mathcal{A}', \tag{4.28}$$

with definitions for U_2 and U_1 analogous to those for $\mathcal{O}_{p2}$ and. $\mathcal{O}_{p1}$. The matrix $\mathcal{A}'$ can thus be found from the above overdetermined system as $\mathcal{A}' = (U_1^H U_1)^{-1} U_1^H U_2$. Factor $\mathcal{A}'$ into is Jordan form, or alternatively, any factorization that separates the stable and unstable eigenspaces, gives

$$\mathcal{A}' = M \begin{bmatrix} \Lambda_s & 0 \\ 0 & \Lambda_a \end{bmatrix} M^{-1} \tag{4.29}$$

where $\Lambda_s \in \mathbb{C}^{n \times n}$ and $\Lambda_a^{-1} \in \mathbb{C}^{n \times n}$ are both asymptotically stable. Recovering the stable eigenspace, we infer a realization for $G_0(z)$ in which $A = \Lambda_s$. For this same realization, C and $\tilde{F}$ can also be inferred from U, i.e.,

$$C = \left\{ UM^{-1} \right\}_{\text{row } 1:m, \text{ col } 1:n} \tag{4.30}$$

$$\tilde{F}^H = \left\{ UM^{-1} \right\}_{\text{row } m(p-1)+1:mp, \text{ col } n+1:2n} \tag{4.31}$$

From $\tilde{F}$ and A, F can be found via (4.19). With A, C, and F known, E can be recovered from s_0 via (4.16).

In terms of the covariance model parameters and (yet to be determined) P, B and D are

$$D = \left(2E - CPC^H\right)^{1/2} \tag{4.32}$$

$$B = \left(F - APC^H\right)D^{-1/2} \tag{4.33}$$

Substituting into (4.14) gives the Discrete-time Algebraic Riccati Equation (DARE)

$$P = APA^H + \left(F - APC^H\right)\left(2E - CPC^H\right)^{-1}\left(F - APC^H\right)^H \tag{4.34}$$

Due to (4.11), it is known that $C(z)$ is positive-real. It is a classical result that if $C(z)$ is positive real then (4.34) has multiple solutions P_i, one of which is minimal in the sense that $P_i < P_j$ for $i \neq j$. This minimal solution, when used to construct D and B via (4.32) and (4.33), results in $G(z)$ with the desired minimum-phase property.

4.2.3   Subspace Identification Algorithm

The idea is to use principles from the stochastic realization theory above, to identify an approximate spectral factor $G(z)$ from spectrum data S_ℓ, assumed only to adhere to Assumption 4.2.1. The fact that S_ℓ does not necessarily correspond to a rational spectrum implies that the resultant algorithm will no longer be interpolative, and requires the above technique to be adjusted to be reliable. As with the interpolative theory above, the algorithm requires a priori specification of $\{p, q\}$, in addition to the data S_ℓ. Our description below delineates the four steps described in the introduction, which can now be stated precisely.

1. For the data S_ℓ, find the inverse DFT s_k via (4.15), and find h_k from s_k via

(4.18). Construct H_{pq} from h_k, as in (4.20)

2. Perform a Singular Value Decomposition (SVD), to give

$$H_{pq} = \begin{bmatrix} U & U_r \end{bmatrix} \begin{bmatrix} \Sigma & 0 \\ 0 & \Sigma_r \end{bmatrix} \begin{bmatrix} V^H \\ V_r^H \end{bmatrix} \tag{4.35}$$

where Σ contains the $2n$ largest singular values of H_{pq} and Σ_r contains the rest. Truncate the residual singular values to give the the approximation $H_{pq} \approx U\Sigma V^H$, which has a $2n$-dimensional range space.

3. From U, extract matrices U_1 and U_2. Find $\mathcal{A}'$ such that $U_2 \approx U_1 \mathcal{A}'$ by finding $\min_{\mathcal{A}'} \|U_2 - U_1 \mathcal{A}'\|_F$. This is the pseudoinverse solution, i.e.,

$$\mathcal{A}' = \left(U_1^H U_1 \right)^{-1} U_1^H U_2 \tag{4.36}$$

Next, factor $\mathcal{A}'$ into stable and unstable eigenspaces, as in (4.29), where $\Lambda_s \in \mathbb{C}^{n_s \times n_s}$ and $\Lambda_a^{-1} \in \mathbb{C}^{(2n-n_s) \times (2n-n_s)}$ are both asymptotically stable. (Note that because the identified solution is not necessarily interpolative, it may be the case that the stable and unstable eigenspaces do not split evenly, and the resultant order of the stable eigenspace will be $n_s \neq n$. In this circumstance, the identified $G(z)$ will be of order n_s, not n.) Recovering the stable part, we take $A = \Lambda_s$. The corresponding estimate of C is

$$C = \left\{ U M^{-1} \right\}_{\text{row } 1:m,\ \text{col } 1:n_s} \tag{4.37}$$

4. With A and C found, the solution to E and F can be found to minimize the

least-squares spectral estimation error, i.e.,

$$\{E, F\} = \arg \min \sum_{\ell=0}^{M-1} \|2E + C(e^{j\Omega_\ell}I - A)^{-1}F$$

$$+ F^H(e^{j\Omega_\ell}I - A)^{-H}C^H - S_\ell\|_F^2 \quad (4.38)$$

which is a quadratic minimization with a closed-form solution. (Note that although $\tilde{F}$, and therefore F, could also be estimated from U analogously to (4.31) for the interpolative case, this is less robust than the above technique.) If the resultant $C(z)$ is not positive-real, then one of several methods must be used to enforce the positive-real constraint in the above minimization, such as those proposed by van Overschee et al [75], Hinnen et al [79], or Akçay and Türkay [80]. Alternatively, a simple approach to ensure $C(z)$ is positive-real (and the method used in the example for this paper) is to perform optimization (4.38) over the augmented domain $\{E, F, P\}$, where $P = P^H$ is an auxiliary variable, subject to the constraint

$$\begin{bmatrix} P - APA^H & F - APC^H \\ F^H - CPA^H & E - CPC^H \end{bmatrix} > 0 \quad (4.39)$$

With a positive-real $C(z)$ found, equation (4.14) is solved for the minimal solution $P > 0$, and then (4.32) and (4.33) are solved for B and D.

4.3 Modifications to Standard Algorithm

In the standard algorithm, the size of Hankel matrix H_{pq} (i.e., $m^2 \times p \times q$) should be made as large as possible, up to the computational constraints of the application. This is to ensure that the subset of consecutive Markov coefficients used, i.e., the first $r = p + q - 1$ parameters, are sufficient to characterize the salient aspects of the

full set. However, in practice, inaccurate inference of A and C can occur even if H_{pq} is quite large, especially for problems with large m. The reason for this is that for infinite-dimensional systems, the behavior of the Markov coefficients s_k for k large cannot be inferred from those for smaller k, but may nonetheless be of significance.

To remedy this, this section illustrates that another technique can be used to assemble a different matrix from which the parameters A and C can be inferred. Unlike the Hankel matrix in the standard algorithm, this matrix involves non-consecutive Markov coefficients.

4.3.1 Revised Interpolative Realization Theory

We first return to the interpolative realization theory discussed in Section 4.2.2, and re-frame this theory in a very particular way. Again starting from the definition of s_k in (4.15), we have that each of these Markov coefficients can be expressed in terms of the parameters $\{A, F, C, E\}$ as in (4.16). Let

$$\bar{F} \triangleq (1 - A^{2N})^{-1} F. \tag{4.40}$$

Then for $k \in \{1...2N - 1\}$ this equation can be stated compactly as

$$s_k = C A^{k-1} \bar{F} + \bar{F}^H \left(C A^{2N-k-1} \right) \tag{4.41}$$

Define the full block-Hankel matrix H as

$$H = \begin{bmatrix} s_1 & s_2 & \cdots & s_N \\ s_2 & \ddots & \ddots & s_{N+1} \\ \vdots & \ddots & \ddots & \vdots \\ s_N & s_{N+1} & \cdots & s_{2N-1} \end{bmatrix} \tag{4.42}$$

Then it is a straight-forward algebra exercise to verify that

$$H = \Theta J \Theta^H T_N \qquad (4.43)$$

where

$$J = \begin{bmatrix} 0 & I \\ I & 0 \end{bmatrix} \qquad (4.44)$$

$$\Theta = \begin{bmatrix} C & \bar{F}^H (A^H)^{N-1} \\ CA & \bar{F}^H (A^H)^{N-2} \\ \vdots & \vdots \\ CA^{N-1} & \bar{F}^H \end{bmatrix} \qquad (4.45)$$

$$T_N = \begin{bmatrix} & & & I \\ & & I & \\ & \iddots & & \\ I & & & \end{bmatrix} \qquad (4.46)$$

Note that H can be converted to a Hermitian matrix by reordering its columns:

$$K = H T_N = \Theta J \Theta^H \qquad (4.47)$$

Let index set $\mathcal{K}$ be a subset of $\{1, 2, ... N\}$, which has the following properties:

1. $\min(\mathcal{K}) = 1$

2. $\max(\mathcal{K}) = N$

3. For each $k \in \mathcal{K}$, $N - k + 1 \in \mathcal{K}$.

4. For each $k \in \mathcal{K}$, $\min \{|k - \ell| : \ell \in \{\mathcal{K} \setminus k\}\} = 1$.

For the remainder of this paper we will refer to the above as Rules 1-4. Let N' be the size of $\mathcal{K}$. We use the notation $\mathcal{K} = \{k_1, k_2, ...k_{N'}\}$ to imply that the components $k_i < k_j$ for $i < j$. (Thus, note that by our rules above, $k_1 = 1$ and $k_{N'} = N$.) Now, construct the matrix K' as only the block rows and columns of K which are included in $\mathcal{K}$. It follows that

$$
K' = \begin{bmatrix}
s_N & s_{N+1-k_2} & s_{N+1-k_3} & \cdots & s_{k_3} & s_{k_2} & s_1 \\
s_{N-1+k_2} & s_N & s_{N-k_3+k_2} & \cdots & s_{k_2+k_3-1} & s_{2k_2-1} & s_{k_2} \\
s_{N-1+k_3} & s_{N-k_2+k_3} & s_N & \cdots & s_{2k_3-1} & s_{k_2+k_3-1} & s_{k_3} \\
\vdots & \vdots & \vdots & \ddots & \vdots & \vdots & \vdots \\
s_{2N-k_3} & s_{2N+1-k_3-k_2} & s_{2N+1-2k_3} & \cdots & s_N & s_{N-k_3+k_2} & s_{N+1-k_3} \\
s_{2N-k_2} & s_{2N+1-2k_2} & s_{2N+1-k_2-k_3} & \cdots & s_{N-k_2+k_3} & s_N & s_{N+1-k_2} \\
s_{2N-1} & s_{2N-k_2} & s_{2N-k_3} & \cdots & s_{N-1+k_3} & s_{N-1+k_2} & s_N
\end{bmatrix}
$$

(4.48)

Because $s_{2N-k} = s_k^H$, and $s_N = s_N^H$, it follows that K' inherits the Hermitian property from K. In terms of the covariance model parameters $\{A, F, C, E\}$, K' is

$$
K' = \Theta' J (\Theta')^H \tag{4.49}
$$

where

$$
\Theta' = \begin{bmatrix} C & \bar{F}^H(A^H)^{N-1} \\ CA^{k_2-1} & \bar{F}^H(A^H)^{k_{N'-1}-1} \\ CA^{k_3-1} & \bar{F}^H(A^H)^{k_{N'-2}-1} \\ \vdots & \vdots \\ CA^{k_{N'-1}-1} & \bar{F}^H(A^H)^{k_2-1} \\ CA^{N-1} & \bar{F}^H \end{bmatrix} \tag{4.50}
$$

$$
= \begin{bmatrix} C & \bar{F}^H(A^H)^{N-1} \\ CA^{k_2-1} & \bar{F}^H(A^H)^{N-k_2} \\ CA^{k_3-1} & \bar{F}^H(A^H)^{N-k_3} \\ \vdots & \vdots \\ CA^{k_{N'-1}-1} & \bar{F}^H(A^H)^{N-k_{N'-1}} \\ CA^{N-1} & \bar{F}^H \end{bmatrix} \tag{4.51}
$$

where we have used Rule 3 to get the second line.

Due to the imposition of Rule 4 on the construction of set $\mathcal{K}$, it follows that there exist subsets $\mathcal{K}_1$ and $\mathcal{K}_2$ such that

$$
\mathcal{K} = \mathcal{K}_1 \cup \mathcal{K}_2 \tag{4.52}
$$

$$
\mathcal{K}_2 = \mathcal{K}_1 + 1 \tag{4.53}
$$

Let Θ'_1 and Θ'_2 be the corresponding sub-matrices of Θ' which contain the block rows corresponding to these indices. Then it follows that

$$
\Theta'_1 \mathcal{A} = \Theta'_2 \tag{4.54}
$$

Let the SVD of K' be $K' = U\Sigma V^H$. Then it follows that there exists a nonsingular

matrix M such that $U = \Theta'M$, because U and Θ' share the same range space. Consequently, if we define U_1 and U_2 to be the sub-matrices of U which contain the block rows for indices $\mathcal{K}_1$ and $\mathcal{K}_2$ respectively, then

$$U_1\mathcal{A}' = U_2 \tag{4.55}$$

where $\mathcal{A}'$ is

$$\mathcal{A}' = M \begin{bmatrix} \Lambda_s & 0 \\ 0 & \Lambda_a \end{bmatrix} M^{-1} \tag{4.56}$$

where $\Lambda_s \in \mathbb{C}^{n \times n}$ and $\Lambda_a^{-1} \in \mathbb{C}^{n \times n}$ are both asymptotically stable. Recovering the stable eigenspace, we infer a realization for $G(z)$ in which $A = \Lambda_s$. For this same realization, C and $\bar{F}$ can also be inferred from U, i.e.,

$$C = \left\{ UM^{-1} \right\}_{\text{row } 1:m,\ \text{col } 1:n} \tag{4.57}$$

$$\bar{F}^H = \left\{ UM^{-1} \right\}_{\text{row } m(p-1)+1:mp,\ \text{col } n+1:2n} \tag{4.58}$$

From $\bar{F}$ and A, F can be found via (4.40). With A, C, and F known, E can be recovered from s_0 via (4.16).

4.3.2 Modification to the Subspace Identification Algorithm

Based on the above observations regarding realization theory, we now reconsider the problem of identifying an approximate rational spectrum from non-parametric, infinite-dimensional spectrum $S(\Omega)$. To begin, we again calculate the inverse DFT of data S_ℓ as in the original algorithm, to get s_k, $k \in \{0, ...2N - 1\}$. However, from this data, instead of assembling a Hankel matrix as in the original algorithm, we wish to assemble a matrix K', as in (4.48). To do this, it is necessary to first determine the indices $\mathcal{K}$ from which this matrix is assembled from $\{s_1, ...s_{2N-1}\}$.

Suppose that it is desired to generate a matrix K' that contains a total of σ

entries. Then it follows that $\mathcal{K}$ should be chosen with length $N' = \sqrt{\sigma}/m$. Recalling the primary motivation for modifying the standard algorithm, we wish to choose the indices in $\mathcal{K}$ so as to be spread over the full range of k values for which $\|s_k\|$ is significant. We now propose a way to make this precise.

Let the coefficient ξ_k be defined as

$$\xi_k = \sum_{\ell=1}^{k} \|s_\ell\|_F^2 \tag{4.59}$$

and the associated normalized coefficient $\bar{\xi}_k$ be

$$\bar{\xi}_k = \frac{\xi_k}{\xi_N} \tag{4.60}$$

Then the sequence $\{\bar{\xi}_k, k \in \{1...N\}\}$ constitutes nondecreasing sequence with $\bar{\xi}_1 \geqslant 0$ and $\bar{\xi}_N = 1$. Suppose we wish to extract an N_0-component subsequence $\mathcal{K}_0$ of indices k for which their associated $\bar{\xi}_k$ values are approximately evenly-spaced. Then this can be done by defining the subsequence

$$\mathcal{K}_0 \triangleq \{\kappa_1, ...\kappa_{N_0}\} \tag{4.61}$$

where

$$\kappa_\ell = \min\left\{k \in \{1, ...N\} : \bar{\xi}_k \geqslant \frac{\ell-1}{N_0}\right\} \tag{4.62}$$

Then, we construct $\mathcal{K}$ as a sequence that contains the values in $\mathcal{K}_0$, as well as additional values so that it adheres to Rules 1-4. It is straight-forward to verify that this may always be done by constructing $\mathcal{K}$ as

$$\mathcal{K} = \mathcal{K}_0 \cup \{N - \mathcal{K}_0\} \cup \{\mathcal{K}_0 + 1\} \cup \{N + 1 - \mathcal{K}_0\} \tag{4.63}$$

Note that, so assembled, the maximum possible number of components of $\mathcal{K}$ is $N' =$

$4N_0$.

With this methodology for assembling $\mathcal{K}$, we can now state the modified algorithm. To state the algorithm, we first state that the target matrix size for K' is σ^2, where σ is some integer. Then the algorithm proceeds as follows.

1. From coefficients s_k find coefficients $\{\bar{\xi}_k, k \in \{1...N\}\}$ via (4.59) and (4.60). From these, generate an index set $\mathcal{K}_0$ of size $N_0 = \sqrt{\sigma}/4m$, using (4.61) and (4.62). From $\mathcal{K}_0$, generate the index set $\mathcal{K}$ from (4.63). Using these indices, construct K' by assembling the coefficients s_k as in (4.48).

2. Perform a SVD on K' to obtain

$$K' = \begin{bmatrix} U & U_r \end{bmatrix} \begin{bmatrix} \Sigma & 0 \\ 0 & \Sigma_r \end{bmatrix} \begin{bmatrix} V^H \\ V_r^H \end{bmatrix} \tag{4.64}$$

where Σ contains the $2n$ largest singular values of K' and Σ_r contains the rest. Truncate the smallest singular values to give the the approximation $K' \approx U\Sigma V^H$, which has a $2n$-dimensional range space.

3. Extract block rows from U corresponding to indices $\mathcal{K}_1$ and $\mathcal{K}_2$ respectively, where

$$\mathcal{K}_1 = \mathcal{K}_0 \cup \{N - \mathcal{K}_0\} \tag{4.65}$$

$$\mathcal{K}_2 = \{\mathcal{K}_0 + 1\} \cup \{N + 1 - \mathcal{K}_0\} \tag{4.66}$$

and call these two sub-matrices U_1 and U_2. Then find $\mathcal{A}'$ such solving $\min_{\mathcal{A}'} \|U_2 - U_1\mathcal{A}'\|_F$ via the pseudoinverse; i.e.,

$$\mathcal{A}' = \left(U_1^H U_1\right)^{-1} U_1^H U_2 \tag{4.67}$$

Next, factor $\mathcal{A}'$ into stable and unstable eigenspaces, as in (4.29), where $\Lambda_s \in$

$\mathbb{C}^{n_s \times n_s}$ and $\Lambda_a^{-1} \in \mathbb{C}^{(2n-n_s) \times (2n-n_s)}$ are both asymptotically stable. Recovering the stable part, we take $A = \Lambda_s$. The corresponding estimate of C is

$$C = \left\{ U M^{-1} \right\}_{\text{row } 1:m,\ \text{col } 1:n_s} \tag{4.68}$$

4. With A and C solved, the final step is identical to in the standard algorithm.

4.4   Numerical Example

In this section we consider the problem of factoring the wave force spectrum for an array of floating cylindrical buoys. The buoys have identical geometries as the one in Chapter 3, with radius 3m and draft 6m, and the depth of the water is 50m. The sea state is presumed to be a JONSWAP spectrum with $T_1 = 7$s and $H_{1/3} = 1$m. Figure 4.1 shows an m-buoy array, oriented at an angle of 45° relative to the propagatory direction of the waves. For this array, we consider the discrete-time velocity spectrum; i.e., $S(\Omega_\ell)$, where the sample time is assumed to be 1s. This spectrum is evaluated at $N = 8192$ evenly-spaced points over the domain $[0, \pi]$, to find the discrete values $S_0, ... S_N$. To assess the accuracy of the approximate spectral factorization, we will make use of the normalized error under the Frobenius norm; i.e.,

$$E\left(S, \hat{S} \right) = \frac{\displaystyle\sum_{k=0}^{2N-1} \| S_k - \hat{S}_k \|_F^2}{\displaystyle\sum_{k=0}^{2N-1} \| S_k \|_F^2} \tag{4.69}$$

where S_k and $\hat{S}_k$ are the original (infinite-dimensional) spectrum, and the approximate rational spectrum, respectively.

First, we consider a five buoys case and examine the manner how the size the Hankel matrix affect the accuracy of the algorithms. For the modified algorithm, we first find $\mathcal{K}_0$ and corresponding construct the Hankel matrix K'. For the standard
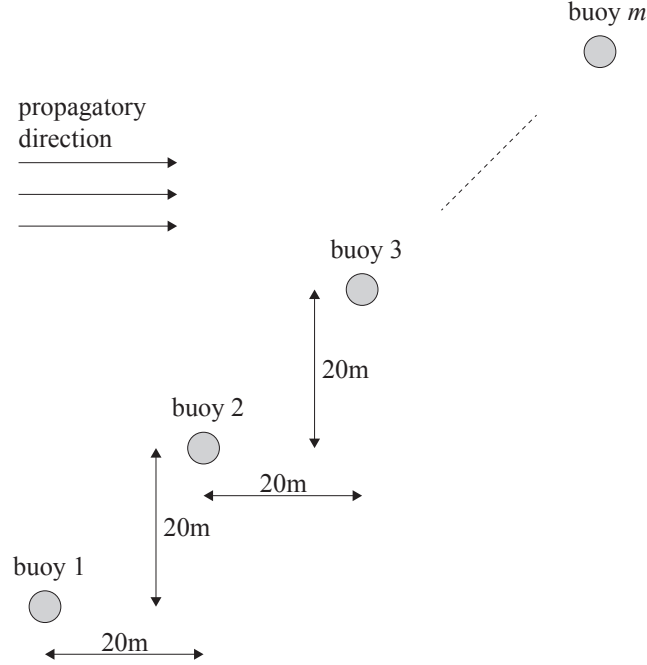
Figure 4.1: m-buoy array example

algorithm, we choose the Hankel matrix H_{pq} which has the same size as K' following step 1 of Section 4.2.3. Then for two matrices, the respective system identification methods were applied, assuming the model order n is equal to 30.

Figure 4.2 shows the resultant estimation error for this case. As shown, when the matrix size is sufficiently large, the two algorithms perform nearly identically. This is the circumstance in which the matrix size σ is sufficiently large such that both K' and H_{pq} include all Markov coefficients of significance. However, as the matrix size decreases, we see markedly more rapid degradation in the performance of the standard algorithm. If the Hankel matrix is small enough, there exists the case where the standard subspace algorithm fails to identify a state space model while the modified algorithm succeeds.

Constrained to a given matrix size, the modified algorithm allows for the more accurate spectral factorization of much larger buoy arrays, which is shown in Figure 4.3. To generate this data, the following procedure is following. For a give buoy array (the number of the buoys is m), we constrainted the Hankel matrix size σ to be 2^{30}
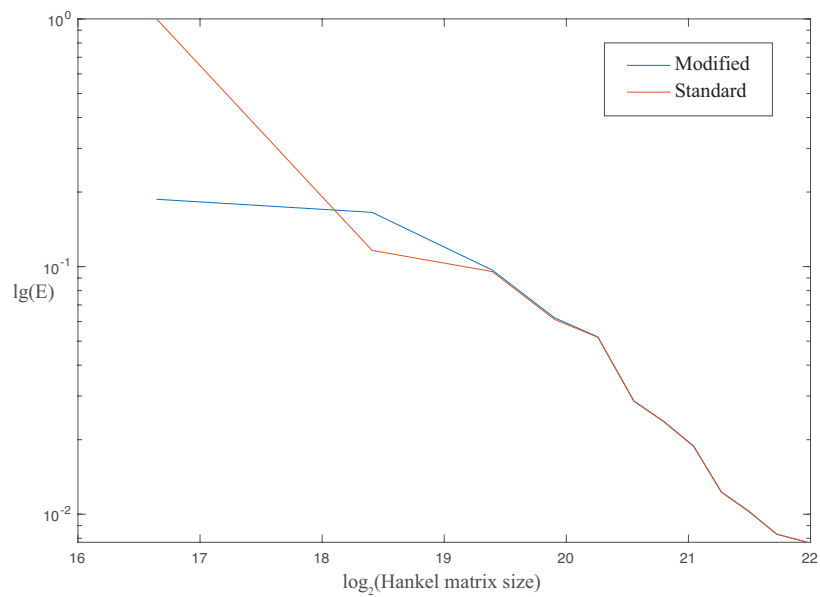
Figure 4.2: Estimation errors for 5 buoys example, as a function of matrix size, for the standard and modified algorithms
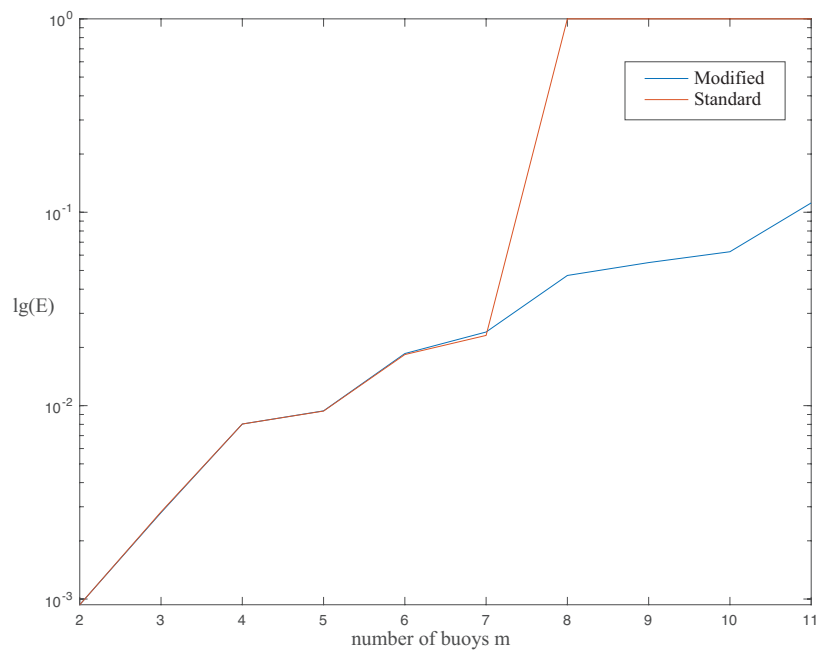
Figure 4.3: Estimation errors as a function of the number of buoys, for the standard and modified algorithms

and the moder order is $5m$. Given this, the index set $\mathcal{K}_0$ can be generated from the data, with the length $N_0 = \sqrt{2^{30}}/4m \approx 8190/m$. Following the step 1 of the modified algorithm, the Hankel matrix K' can be assembled. For the standard algorithm, the Hankel matrix H_{pq} can be generated with the same size as K'.

When the number of buoys is low (i.e., $\leqslant 5$) the performance of the standard and modified algorithms are the same, because for these low values of m, and for the matrix size of 2^{30}, it is possible to include all Markov coefficients of significance in H_{pq} and K'. However, clearly as the number of buoys grows larger the standard algorithm fails to accurately identify the spectrum. The modified algorithm, while giving less accuracy than in the case with m small, is orders of magnitude more accurate.

CHAPTER 5

Unconstrained Optimal Control

5.1   Optimal Anticausal Power Generation

From the discussion in Chapter 3, the dynamic of the WEC buoy in the stochastic ocean wave environment can be written in frequency domain.

$$\hat{v}(\omega) = G_{uv}(i\omega)\hat{u}(i\omega) + G_{wv}(i\omega)\hat{w}(\omega) \tag{5.1}$$

where the transfer functions G_{uv} and G_{wv} are defined as follows:

$$G_{uv}(i\omega) = \left(-i\omega(M + M_\infty) + \hat{H}_r(i\omega) + \frac{1}{i\omega}K\right)^{-1} \tag{5.2}$$

$$G_{wv}(i\omega) = -\left(-i\omega(M + M_\infty) + \hat{H}_r(i\omega) + \frac{1}{i\omega}K\right)^{-1} W(i\omega) \tag{5.3}$$

With the system model defined for the WEC buoy and a characterization for the stochastic ocean wave environment, the optimum power generation can be determined by the classical impedance matching. We assume that the power electronics are controlled by a linear controller, which establishes an effective admittance between u and v; e.g.,

$$\hat{u}(s) = -Y(s)\hat{v}(s) \tag{5.4}$$

The velocity v and the controller force u can be related to w in the frequency domain by:

$$\hat{v}(\omega) = [I + G_{uv}(i\omega)Y(i\omega)]^{-1}G_{wv}(i\omega)\hat{w}(\omega) \tag{5.5}$$

$$\hat{u}(\omega) = -Y(i\omega)[I + G_{uv}(i\omega)Y(i\omega)]^{-1}G_{wv}(i\omega)\hat{w}(\omega) \tag{5.6}$$

The objective is to maximize the average power generation, equal to the extracted power minus power loss; e.g.,

$$\bar{p} = \mathcal{E}\{-u^T v - u^T R_d u\} \tag{5.7}$$

$$= \frac{1}{2\pi}\int_{-\infty}^{\infty} S_p(\omega)d\omega \tag{5.8}$$

where $S_p(\omega)$ is the spectral density function of generated power in the frequency domain, found as:

$$S_p(\omega) = \mathrm{Tr}\{G_{wv}^H(i\omega)[I + G_{uv}(i\omega)Y(i\omega)]^{-H}[\mathrm{Re}\{Y(i\omega)\} - Y^H(i\omega)R_dY(i\omega)]$$
$$[I + G_{uv}(i\omega)Y(i\omega)]^{-1}G_{wv}(i\omega)\} \tag{5.9}$$

where $(\cdot)^H$ is the matrix conjugate transpose, and $\mathrm{Re}\{\cdot\}$ is the real component. We can find the optimal anticausal control law Y by maximizing the generated power spectral density function $S_p(\omega)$ in each frequency [81]. i.e.,

$$Y(i\omega) = [G_{uv}^T(-i\omega) + 2R_d]^{-1} \tag{5.10}$$

The resultant optimal anticausal power generation is:

$$\bar{p} = \frac{1}{2\pi}\int_{-\infty}^{\infty} \mathrm{Tr}\{G_{wv}^H(i\omega)G_{uv}^H(i\omega)[G_{uv}(i\omega) + G_{uv}^H(i\omega) + 2R_d]^{-1}G_{uv}(i\omega)G_{wv}(i\omega)\}d\omega \tag{5.11}$$

It has been shown in [82] that when G_{wv} and G_{uv} are finite-dimensional, and G_{uv} is

PR, the poles of $Y(s)$ are all in the right half plane and thus its dynamic is anticausal. As such, the controller makes decisions based on the future information of the wave. The infinite case is also discussed and the controller in this case is also noncausal [83].

5.2 Optimal Causal Power Generation

5.2.1 Causal Limit on Power Generation

The objective is to find a full state feedback law $x \mapsto u$ to maximize the power generation $\bar{p}$, or equivalently, minimizes $-\bar{p}$, where:

$$-\bar{p} = \mathcal{E}\{u^T v + u^T R_d u\} \tag{5.12}$$

$$= \frac{1}{2} \mathcal{E} \left\{ \begin{bmatrix} x \\ u \end{bmatrix}^T \begin{bmatrix} 0 & C_v^T \\ C_v & 2R_d \end{bmatrix} \begin{bmatrix} x \\ u \end{bmatrix} \right\} \tag{5.13}$$

This is can be regarded as a LQG problem, but it is non standard, since the performance function is sign-indefinite. We have the following theorem that gives an upper bound on the power generation.

Theorem 5.1. *For any causal feedback law $x \mapsto u$, the following equality holds:*

$$\bar{p} = -\operatorname{Tr}\{E^T P E\} - \mathcal{E} \|u - Kx\|_{R_d}^2 \tag{5.14}$$

where:

$$K = -R_d^{-1}(B_u^T P + \frac{1}{2}C_v) \tag{5.15}$$

and P can be solved in the following Continuous-time Algebraic Riccati Equation (CARE)

$$A^T P + PA - (B_u^T P + \frac{1}{2}C_v)^T R_d^{-1}(B_u^T P + \frac{1}{2}C_v) = 0 \tag{5.16}$$

Proof. It is a standard result from optimal control theory [84, 85] that the optimal

control feedback law, if exists, is:

$$K = -R_d^{-1}(B_u^T P + \frac{1}{2}C_v) \tag{5.17}$$

And P is the stabilizing solution to the CARE:

$$A^T P + PA - (B_u^T P + \frac{1}{2}C_v)^T R_d^{-1}(B_u^T P + \frac{1}{2}C_v) = 0 \tag{5.18}$$

It is also a standard result that the performance of any causal feedback law can be related to the optimal performance in equation (5.15) [86].

Since the $\bar{p}$ is sign-indefinite and the associated Riccati equation is non-standard, in [82] it is proven that equation (5.18) always has a solution and the resultant feedback law is stabilizing.

□

With the full state feedback law (5.15) implemented, the expression for the optimal causal power spectrum with full-state feedback is

$$S_p(\omega) = -2\,\mathrm{Re}\{G_i^H(i\omega)G_v(i\omega)\} - 2G_i^H(i\omega)R_d G_i(i\omega) \tag{5.19}$$

where

$$G_i(i\omega) = K[i\omega I - A - B_u K]^{-1} E \tag{5.20}$$

$$G_v(i\omega) = C_v[i\omega I - A - B_u K]^{-1} E \tag{5.21}$$

5.2.2 Optimal Power Generation with Velocity feedback

In practice, the state vector $x(t)$ needs to be estimated from sensor measurements, with the optimal estimates determined via kalman-bucy filter. Here, we only discuss the case where we can measure the WEC velocity $v(t)$. The dynamic of the estimate

states $\hat{x}(t)$ can be expressed as:

$$\dot{\hat{x}} = A\hat{x} + B_u u + L(C_v \hat{x} - v) \tag{5.22}$$

where L is the observer gain. The controller force u can be found through the certainty-equivalence principle, as:

$$u = K\hat{x} \tag{5.23}$$

where K is computed in the Theorem 5.1. Here, we also assume that the measurement noise is also white noise, with spectral intensity matrix Λ. The optimal estimator can be obtained via the standard Kalman filter design:

$$L = -SC_v^T \Lambda^{-1} \tag{5.24}$$

where S is the solution to the algebraic Riccati equation

$$AS + SA^T - SC_v^T \Lambda^{-1} C_v S + EE^T = 0 \tag{5.25}$$

The resultant optimal control law $Y : v \mapsto u$ can be formulated as:

$$Y(s) = K(sI - A - LC_v - B_u K)^{-1} L \tag{5.26}$$

The augmented close-loop system can be described by the augmented state $\xi(t) = \begin{bmatrix} x(t) & \hat{x}(t) \end{bmatrix}^T$, in which its dynamics governed by:

$$\begin{cases} d\xi = \bar{A}\xi dt + \bar{E} \begin{bmatrix} dw \\ dn \end{bmatrix} \\ v = \bar{C}_v \xi \end{cases} \tag{5.27}$$

where

$$\bar{A} = \begin{bmatrix} A & B_u K \\ -LC_v & A + LC_v + B_u K \end{bmatrix}, \bar{E} = \begin{bmatrix} E & 0 \\ 0 & -L \end{bmatrix} \tag{5.28}$$

$$\bar{C}_v = \begin{bmatrix} C_v & 0 \end{bmatrix} \tag{5.29}$$

the measurement noise with spectral intensity Λ is denoted as $\dot{n}$.

The causal optimal power generation spectrum is then

$$S_p(\omega) = -2\operatorname{Tr}\{\operatorname{Re}\{G_i^H(i\omega)G_v(i\omega)\} + G_i^H(i\omega)R_dG_i(i\omega)\} \tag{5.30}$$

where in this case the transfer function G_i and G_v are

$$G_i(i\omega) = \bar{K}[i\omega I - \bar{A}]^{-1}\bar{E} \tag{5.31}$$

$$G_v(i\omega) = \bar{C}_v[i\omega I - \bar{A}]^{-1}\bar{E} \tag{5.32}$$

and

$$\bar{K} = \begin{bmatrix} 0 & K \end{bmatrix} \tag{5.33}$$

The corresponding power generation performance is

$$\bar{p} = -\operatorname{Tr} E^T P E - \operatorname{Tr}\{KSK^T R_d\} \tag{5.34}$$

From the equation (5.34), we can see that the inabilitiy to accurately measure the velocity output can make the WEC generate less power. In [82], the asymptotic case as $\Lambda \to \mathbf{0}$ is investigated. Under certain condition, the asymptotic case can converge to the full state feedback. However, it can be proved that irrespective of the value of the Λ, or the particular parameters of the problem, (5.34) is always positive.

5.3 Numerical Examples

5.3.1 One Buoy Case
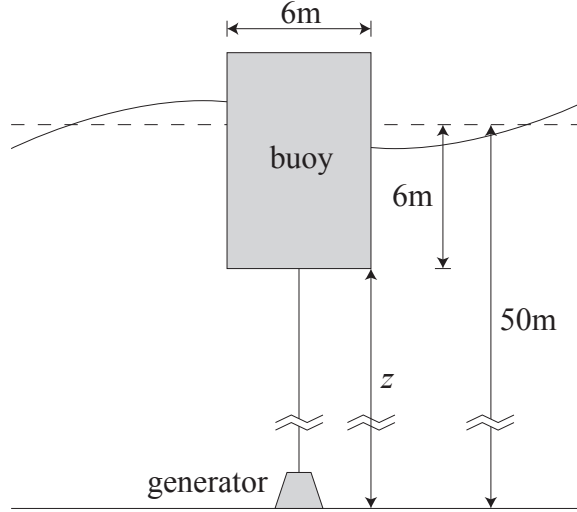
Figure 5.1: The same floating buoy as in the Chapter 3

We use the same floating buoy as the Chapter 3. We plan to compare the causal limit power generation with the anticausal limit in different loss models, in other words, different values of R_d. And we will also make a comparison among causal limit power generation, anticausal limit power generation and optimal power performance with velocity feedback in a certain range of mean wave periods and different sharpness factors. At last, the effect of different values of measurement noise on optimal power generation with velocity feedback will be examined.

Figure 5.2(a) and Figure 5.2(b) shows the comparison between anticausal limit power generation and causal limit power generation. As we can see in both case, the causal limit is very close to the anticausal limit, and as R_d becomes smaller, the difference between causal limit and anticausal limit becomes larger.

In Figure 5.3(a) and Figure 5.3(b), we plot the anticausal limit, causal limit and optimal performance with velocity feedback over different values of the sharpness factor γ. In all cases, these three performance are very close, which indicates that LQG

(a) Mean wave period $T1 = 7s$

(b) Mean wave period $T1 = 12s$
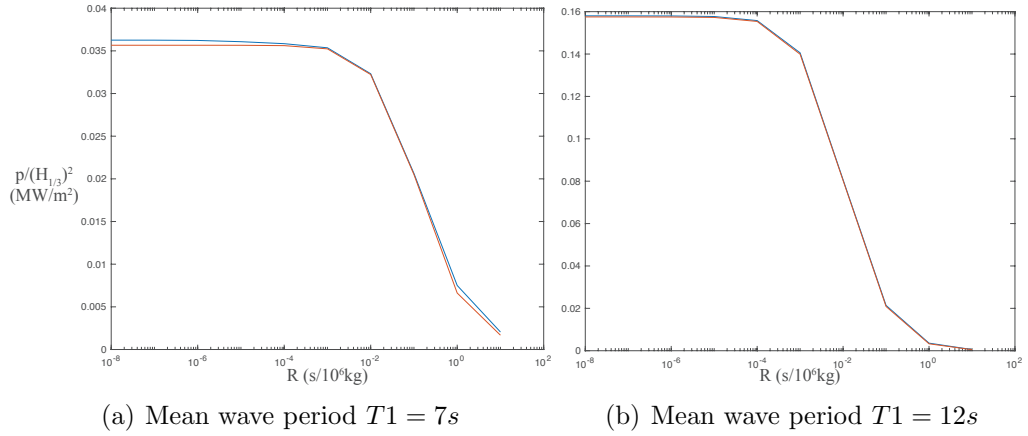
Figure 5.2: Anticausal limit power generation (blue line) and causal limit power generation(red line) over different values of R_d. Here, we choose the sharpness factor $\gamma = 1$

(a) Sharpness factor $\gamma = 1.0$

(b) Sharpness factor $\gamma = 3.3$
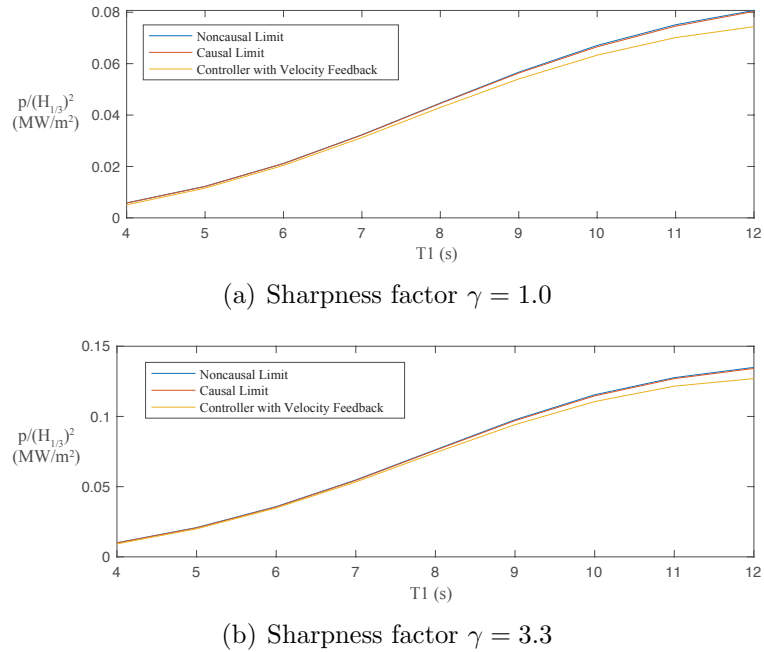
Figure 5.3: Anticausal power generation limit, casual power generation limit and optimal power generation with velocity feedback in a certain range of mean wave periods $T1$.
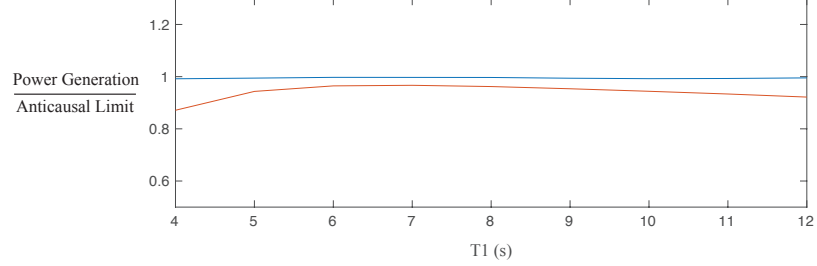
(a) Sharpness factor $\gamma = 1.0$
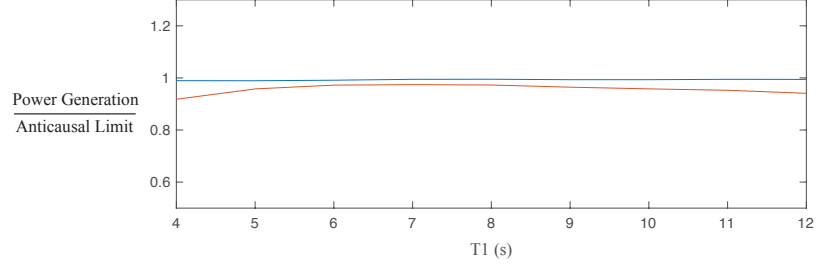
(b) Sharpness factor $\gamma = 3.3$

Figure 5.4: Ratio of optimal causal power generation (blue line) and optimal power generation with velocity feedback (red line) over optimal anticausal power generation in a certain range of mean wave periods T_1. We choose the loss model $R_d = 10^{-8}$s/kg and the measurement noise $\Lambda = 10^{-4}$.

framework is a very good approximation of the actual model and optimal controller with velocity feedback achieves a very high power extraction from waves. And we can also see that the influence the sharpness factor γ and the mean wave period T_1 have on the available power. Energy in sea states with higher sharpness factor and longer mean wave period is more concentrated near a single frequency, and consequently the WEC can generate more energy from them through exploitation of resonance. The Figure 5.4(a) and Figure 5.4(b) show the same result.

In Figure 5.5(a) and Figure 5.5(b), we compared the spectral density function $S_p(\omega)$ among anticausal limit, causal limit and optimal controller with velocity feedback. They are very close and as mean wave period increases, the difference between the first two cases and optimal controller with velocity feedback becomes larger, which is in accordance with Figure 5.3(a) and Figure 5.3(b). In Figure 5.6(a) and Figure 5.6(b), we show the optimal performance of the controller with velocity feedback over

(a) Mean wave period $T1 = 7s$ (b) Mean wave period $T1 = 12s$
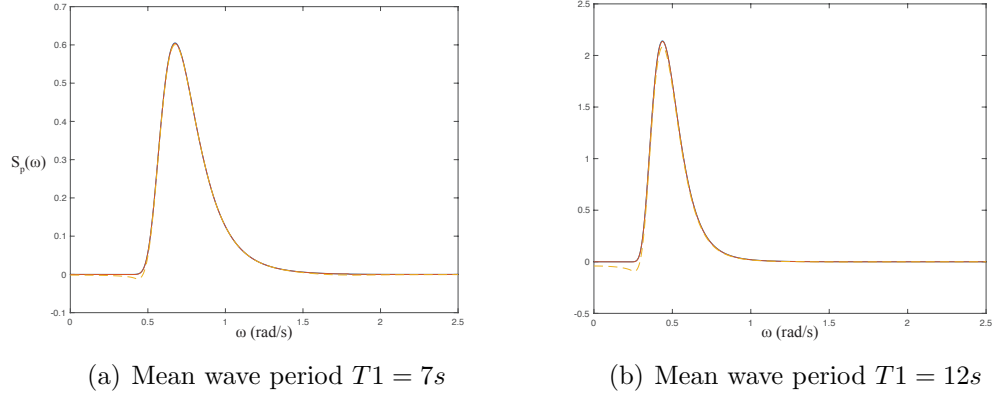
Figure 5.5: Spectral density function for anticausal limit (blue line), causal limit (red line) and optimal performance with velocity feedback (red dashed line). Here, we choose the sharpness factor $\gamma = 1$, the loss model $R_d = 10^{-8}$s/kg and the measurement noise $\Lambda = 10^{-4}$.

different value of measurement noises. The causal limit (or anticausal limit) is not changed as measurement noise changes, so it is a straight line. As we can see in the figure, as measurement noise increases, the optimal performance goes down but the close-loop becomes more robust. We will talk about it in the later section.

5.3.2   Distance Optimization in Two Buoy Case

For the two buoys case, one interesting discussion is about the optimal distance between each buoy. If we put two buoys far away from each other, the optimal causal power generation would be two times the single buoy optimal performance. If they are too close, the interaction of their movements would degrade the overall power generation. There must exist a sweet spot when the maximum power extraction can be larger than the two separated buoy case.

We fixed one buoy at the originial point $(0, 0)$, and change the location of the other buoy, while keeping the distance of two buoys larger than 6m. The Figure 5.7(a) shows the ratio of the causal optimal power generation of two buoys in different positions to the two independent buoys causal limits. As we can see in the Figure 5.7(a), if the two buoys are too close, the optimal performance is really low. And when the

(a) Mean wave period $T1 = 7s$

(b) Mean wave period $T1 = 12s$
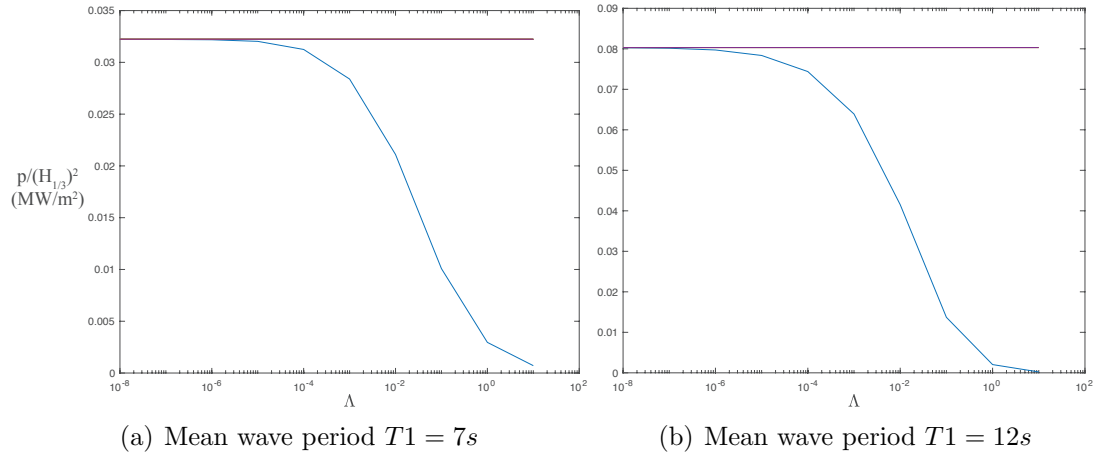
Figure 5.6: Causal limit (red line) and the optimal performace with velocity feedback (blue line) over different values of measurement noise Λ. Here, we choose the sharpness factor $\gamma = 1$ and the loss model $R_d = 10^{-8}$s/kg

(a) Optimal power generation in different positions

(b) General two buoys position diagram
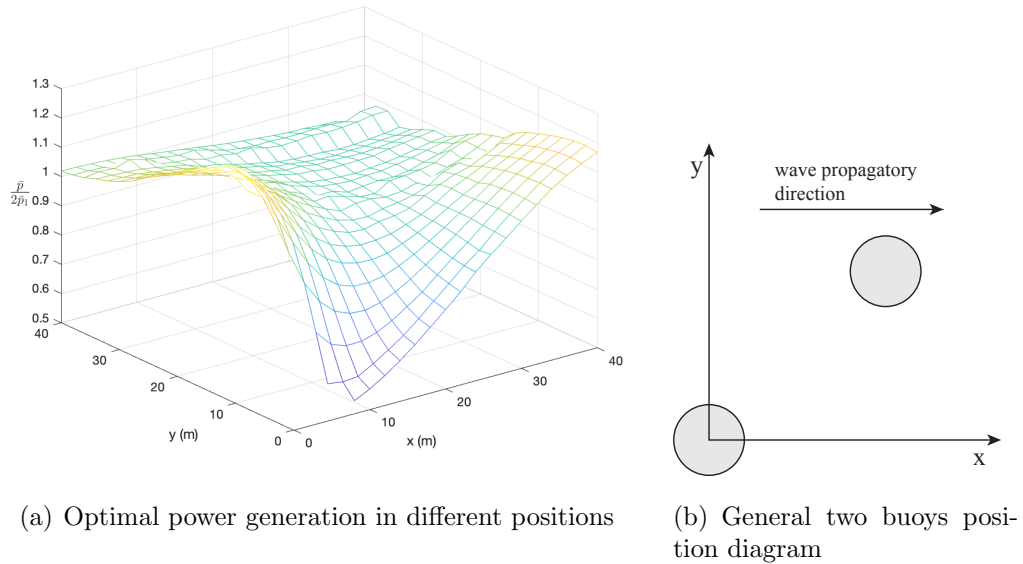
Figure 5.7: In Firgure 5.7(b), one buoy is fixed at $(0, 0)$ and the other buoy's coordinate (x, y) can be changed. The Figure 5.7(a) represents the power generation in different coordinate.

two buoys are distant, the optimal performance can be approximately equal to the independent case. The best performance can be achieved when placing the buoy at $(0, 14)$, and the corresponding power generation is 78.8 KW.

CHAPTER 6

Nonlinear Causal Control of Wave Energy Converters with Finite Stroke in Continuous Time Domain

6.1   Introduction

In order to be practical, the causal control techniques discussed in the Chapter 5 must be extended to accommodate more realistic models. One of the problems that is more challenging to address is that of enforcing PTO stroke constraints. This is made especially challenging due to the fact that the transfer function from PTO force to displacement is strictly proper, and consequently, non-anticipatory enforcement of stroke constraints would require $u(t)$ to be impulsive, which may result in hardware damages.

In this chapter, we will tackle the stroke saturation in these procedures.

1. First, a linear feedback law is designed with optimizes power generation subject to a competing objective that the mean-square stroke be maintained below a threshold. It was shown that this multi-objective optimal control design can be solved as a convex LMI optimization, without the introduction of any conservatism.

2. Next, the controller from the first step is augmented to include a second auxiliary input, u^n, which may be interpreted as a nonlinear restoring force used to constrain the PTO displacement. Critically, this augmentation must be done in such a way that the transfer function from u^n to the PTO velocity v is passive.

3. With this augmented controller in place, a nonlinear feedback law is designed which determines u^n from the PTO position, z, and its velocity, v. The feedback law is designed such that z is maintained below its maximum allowable stroke with probability 1. It is shown that by constraining the feedback law such that $v \mapsto u^n$ is passive, the closed-loop system is globally stable.

This methodolgy was first proposed by Scruggs [53], and later was improved in [87]. However, both papers did not provide the detailed proof about the global stability of the close-loop system. We will demonstrate the close-loop stability in this chapter and also discuss about how to design the variables in the augmented linear controller channel such that the power generation can still be maximized.

This chapter is organized as follows. First, the model assumptions and problem statement are given. Following this, the methodology for the linear multi-objective control design from Step 1 is introduced. Then, the main result is given, which describes the methodology for Step 2 and Step 3.

6.2 Problem Formulation

6.2.1 Addition Assumptions

We use the state-space model (3.45) to characterize the dynamic behavior of the WEC system. The assumptions from Chapter 3 are valid. In order to prove the global stability of the closed-loop system, we need to make two mild additional assumptions.

Assumption 6.2.1. *Driving point impedance $u \mapsto v$ is OSP, i.e., there exist $\beta \in \mathbb{R}_{>0}$*

such that:

$$\int_0^\infty (u(t) - \beta v(t))^T v(t) dt \geqslant 0 \quad \forall u \in \mathcal{L}_2 \tag{6.1}$$

Assumption 6.2.2. *Let $\{G_{uv}, G_{\dot{w}v}\}$ be the open-loop transfer functions from $\{u, \dot{w}\}$ to v; i.e.,*

$$\begin{bmatrix} G_{uv} & G_{\dot{w}v} \end{bmatrix} \sim \left[\begin{array}{c|cc} A & B_u & E \\ \hline C_v & 0 & 0 \end{array} \right] \tag{6.2}$$

Then there exists $U \in \mathcal{H}_\infty$ such that $G_{uv}U = G_{\dot{w}v}$.

The existence of $U \in \mathcal{H}_\infty$ satisfying Assumption 6.2.2 is rather mild, and is ensured in many cases by phyical constraints on the plant model. We will discuss more about the assumption 6.2.2 in the second design stage.

6.2.2 Optimization problem

The mean power generation $\bar{p}$ is defined in (3.36). We can formulate our control problem as an optimization problem.

$$\text{OP6.1}: \begin{cases} \text{Maximize:} & \bar{p} \\ \text{Domain:} & \text{causal } K : y \to u \\ \text{Constraint:} & \Pr[|z_i| > z_{mi}] = 0, \ i \in \{1..n_p\} \end{cases}$$

where $\Pr[\cdot]$ denotes the probability of occurrence for the stationary distribution.

6.3 Stage I: Multi-Objective Linear Feedback Control Design

In "Step 1" of the design process discussed in the introduction, we replace the constraint $\Pr[|z_i| > z_{mi}] = 0$ in OP6.1, with a mean-square constraint which is more amenable to linear control design. Specifically, we replace it with the constraint

$$\mathcal{E} \, z_i^2 < \tfrac{1}{4} z_{mi}^2 \ , \quad i \in \{1..n_p\} \tag{6.3}$$

The justification for the use of (6.3) to approximately constrain the peak values of $z_i(t)$ can be made as follows. Let ψ be a randomly-selected peak of the stationary response of $z_i(t)$, assuming a linear stochastic response. Then if $z_i(t)$ is sufficiently narrowband, then the distribution on ψ is Rayleigh-distributed, with cumulative distribution function

$$\Pr[\psi \leqslant \psi_0] = 1 - \exp\left\{-\psi_0^2/2\sigma_i^2\right\} \tag{6.4}$$

where $\sigma_z^2 = \mathcal{E}\, z_i^2$ [88]. It follows that enforcing (6.3) ensures that peaks violating constraint $\psi \leqslant z_{mi}$ occur with a probability of at most $e^{-2} \approx 0.14$. As such, designing a linear controller to adhere to (6.3) ensures that the peak stroke is safely within limits for the majority (e.g., 86%) of the peaks.

Enforcement of the equation 6.3 can be accommodated through multi-objective control techniques. The procedure is shown in the Theorem 6.1.

Theorem 6.1. *There exists an LTI feedback law $K : y \to u$ of order n, such that $\bar{p} > \gamma$ and (6.3) holds, if and only if there exist compatible matrices $X = X^T, Y =$*

$Y^T, W = W^T, \hat{A}, \hat{B}, \hat{C},$ and $\hat{D}$ such that

$$\text{He}\left\{\begin{bmatrix} AX + B_u\hat{C} & A + B_u\hat{D}C_y & E \\ \hat{A} & YA + \hat{B}C_y & YE \\ 0 & 0 & -\frac{1}{2}I \end{bmatrix}\right\} < 0 \tag{6.5}$$

$$\begin{bmatrix} W & \hat{C} - FX & -F + \hat{D}C_y \\ & X & I \\ (sym) & & Y \end{bmatrix} > 0 \tag{6.6}$$

$$i \in \{1...n_p\}, \quad \begin{bmatrix} \frac{1}{4}z_{mi}^2 & C_{zi}X & C_{zi} \\ & X & I \\ sym & & Y \end{bmatrix} > 0 \tag{6.7}$$

$$-\text{Tr}\{E^T Q E\} - \text{Tr}\{W R_d\} > \gamma \tag{6.8}$$

where $F = -R_d^{-1}[B_u^T Q + \frac{1}{2}C_v]$, and Q is the solution to Riccati equation

$$0 = A^T Q + QA - \left[QB_u + \frac{1}{2}C_v^T\right]R_d^{-1}\left[B_u^T Q + \frac{1}{2}C_v\right] \tag{6.9}$$

Furthermore, one such controller is $K(s) = D_K + C_K[sI - A_K]^{-1}B_K$, where $D_K = \hat{D}$,

$$C_K = \left(\hat{C} - D_K C_y X\right)M^{-T} \tag{6.10}$$

$$B_K = N^{-1}\left(\hat{B} - YB_u D_K\right) \tag{6.11}$$

$$A_K = N^{-1}\left(\hat{A} - YAX - \hat{B}C_y X - YB_u\hat{C}\right.$$
$$\left. + YB_u\hat{D}C_y X\right)M^{-T} \tag{6.12}$$

and where M and N are any matrices satisfying $NM^T = I - YX$.

Proof. Assuming there exists such a LTI and stabilizing controller that satisfies $\bar{p} > \gamma$

and (6.3). The controller can be represented by such state space model.

$$\begin{cases} \dot{x}_K = A_K x_K + B_K y \\ u = C_K x_k + D_K y \end{cases}$$ (6.13)

Combining the system (3.45) and (6.13), we can have the following augmented state space model.

$$\begin{cases} dx_t = A_t x_t dt + E_t dw \\ v = C_{vt} x_t \\ z = C_{zt} x_t \\ u = C_{ut} x_t \end{cases}$$ (6.14)

where the augmented state vector $x_t^T = \begin{bmatrix} x^T & x_K^T \end{bmatrix}$ and

$$A_t = \begin{bmatrix} A + B_u D_K C_y & B_u C_K \\ B_K C_y & A_K \end{bmatrix}, E_t = \begin{bmatrix} E \\ 0 \end{bmatrix}$$

$$C_{vt} = \begin{bmatrix} C_v & 0 \end{bmatrix}, C_{zt} = \begin{bmatrix} C_z & 0 \end{bmatrix}, C_{ut} = \begin{bmatrix} D_K C_y & C_K \end{bmatrix}$$

It has been shown in [89] that for some $\gamma \in \mathbb{R}$, we have the $\bar{p} > \gamma$ if and only if that there exist $P > 0$ and $W = W^T$ such that

$$\begin{bmatrix} A_t^T P + P A_t & P E_t \\ E_t^T P & -I \end{bmatrix} < 0$$ (6.15)

$$\begin{bmatrix} W & C_{ut} - F_1 \\ C_{ut}^T - F_1^T & P \end{bmatrix} > 0$$ (6.16)

$$i \in \{1...n_p\}, \begin{bmatrix} \frac{1}{4} z_{mi}^2 & C_{zti} \\ C_{zti}^T & P \end{bmatrix} > 0$$ (6.17)

101

$$\text{Tr}\{R_d W\} - \bar{p}_{\max} + \gamma > 0 \tag{6.18}$$

where $\bar{p}_{\max} = -\text{Tr}\{E^T Q E\}$ is the causal limit and

$$F_1 = \begin{bmatrix} F & 0 \end{bmatrix} \tag{6.19}$$

$$F = -R_d^{-1}(B_u Q + \frac{1}{2} C_v^T) \tag{6.20}$$

The positive definite matrix Q can be solved in the Riccati equation (6.9).

The matrix inequality (6.15) is not the LMI since P is unknown and A_t involves the unknown term. However, through the matrix transformation techniques in [90], we can shown that (6.15) is the LMI and the linear controller can be solved using *convex optimization.*

Without loss of generality, we partition P and its inverse as:

$$P = \begin{bmatrix} Y & N \\ N^T & \bullet \end{bmatrix}, \quad P^{-1} = \begin{bmatrix} X & M \\ M^T & \bullet \end{bmatrix} \tag{6.21}$$

where $\bullet$ is the matrix block does not need to be known and $Y = Y^T$, $X = X^T$. Next, define the transformation matrix

$$\Pi_1 = \begin{bmatrix} X & I \\ M^T & 0 \end{bmatrix} \tag{6.22}$$

and note that the following transformation occurs

$$\Pi_1^T P A_t \Pi_1 = \begin{bmatrix} AX + B_u \hat{C} & A + B_u \hat{D} C_y \\ \hat{A} & YA + \hat{B} C_y \end{bmatrix} \tag{6.23}$$

$$\Pi_1^T P E_t = \begin{bmatrix} E \\ YE \end{bmatrix} \tag{6.24}$$

$$C_{ut}\Pi_1 = \begin{bmatrix} \hat{C} & \hat{D}C_y \end{bmatrix} \tag{6.25}$$

$$i \in \{1...n_p\}, C_{zti}\Pi_1 = \begin{bmatrix} C_{zi}X & C_{zi} \end{bmatrix} \tag{6.26}$$

$$F_1\Pi_1 = \begin{bmatrix} FX & F \end{bmatrix} \tag{6.27}$$

$$\Pi_1^T P\Pi = \begin{bmatrix} X & I \\ I & Y \end{bmatrix} \tag{6.28}$$

where the transformed control variables $\{\hat{A}, \hat{B}, \hat{C}, \hat{D}\}$ are defined as

$$\begin{cases} \hat{D} = D_K \\ \hat{C} = D_K C_y X + C_K M^T \\ \hat{B} = Y B_u D_K + N B_K \\ \hat{A} = YAX + N B_K C_y X + Y B_u C_K M^T + Y B_u D_K C_y X + N A_K M^T \end{cases} \tag{6.29}$$

The reason that we do the transformation here is that it make the matrix inequalities (6.15), (6.16), (6.17) and (6.18) linear in the variables $\{\hat{A}, \hat{B}, \hat{C}, \hat{D}, X, Y, W, \gamma\}$. Respectively, they becomes the LMI (6.5), (6.6), (6.7) and (6.8).

To obtain the state space parameters $\{A_K, B_K, C_K, D_K\}$ for the optimal controller, we need to find the M and N. Obviously, there are infinite sets of M and N. and also the (6.21) shows that the feasible set of M and N needs to satisfy

$$XY + MN^T = I \tag{6.30}$$

By solving the $\{X, Y\}$, we can have find a pair of $\{M, N\}$ by performing the singular

value decomposition.

$$U\Sigma V^T = I - XY \tag{6.31}$$

$$N = U\Sigma^{\frac{1}{2}}, \quad M = V\Sigma^{\frac{1}{2}} \tag{6.32}$$

With these solved, we can find the set of the control variables $\{A_K, B_K, C_K, D_K\}$ by solving (6.10), (6.11) and (6.12).

□

This motivates the following convex optimization:

$$\text{OP6.2:} \begin{cases} \text{maximize:} & J \triangleq \bar{p}_{\max} - \text{Tr}\{WR_d\} \\ \text{Domain:} & X = X^T, Y = Y^T, Q = Q^T, \\ & \hat{A}, \hat{B}, \hat{C}, \hat{D} \\ \text{Constraints:} & (6.5), (6.6), (6.7) \end{cases}$$

Let the optimal variables be denoted by $X^\star, Y^\star$, etc. Then the resultant controller $K^\star$, synthesized via OP6.2, achieves power generation will be $\bar{p} = J^\star$.

Corollary 6.2. *OP6.2 always has a solution*

Proof. Since $u \mapsto v$ is OSP and in $\mathcal{H}_\infty$, it follows from the linear passivity theorem that any Strictly Positive Real (SPR) K will stabilize the close-loop system [91]. Let K_0 be one such SPR feedback law, then for $K = \beta K_0$ with the multiplier $\beta > 0$, it is straightforward to show that $\mathcal{E}\{z_i^2\} \to 0$ in stationary as $\beta \to \infty$. Consequently, it is known that there exists a close-loop stable feedback law K which achieves mean-square stroke constraint. This guarantees a feasible solution to the equation (6.5), (6.6) and (6.7). □

Consider a modification of our original optimization problem, OP6.1, in which its constraint is replaced with (6.3) . Then even though $K^\star$ is the synthesized feedback law for the optimum of OP6.2, it is in general a sub-optimal feasible design for this

modified version of OP6.1. This is due to the fact that in OP6.2 K is constrained to linearity, and to order n. It may be the case that better controllers can be found with higher order, or through the introduction of nonlinearity.

6.4 Stage II: Passivity-Based Nonlinear Control Design

6.4.1 Passivity-Based Design Strategy

The control design procedure described in Section 6.3 results in a linear $K^\star$ for which typical peak stroke values will be on the same order as (or less than) the maximum stroke limit. However, because only the mean-square stroke value was constrained, stroke saturation is not prohibited. To enforce a hard constraint on stroke saturation, we must introduce nonlinearity into the design. In this section we propose a technique of passivity-based nonlinear control design, with a structure illustrated in Figure 6.1. The technique is comprised of two design steps:

1. Extend the optimal linear feedback law $K^\star$ from OP6.2, to accept a second exogenous input u^n, resulting in an extended mapping $K : \{y, u^n\} \to u$ that preserves $K^\star$ with $u^n = 0$; i.e., $K(\cdot, 0) = K^\star$, and design this extension such that the mapping $u^n \mapsto v$ is output-strictly passive.

2. Design an outer nonlinear feedback law $Q : \{v, z\} \to u^n$ such that when $z(t) = \int_0^t v(\tau) d\tau$, the reduced feedback mapping $v \mapsto u^n$ is passive and prohibits $|z| \geqslant z_m$ with probability 1.

Because the mapping $u^n \mapsto v$ is OSP, it follows from the Passivity Theorem [56] that any nonlinear feedback law Q preserves stability as long as it is passive. Because there are many variations of this theorem, we give the following variant, below, in which we use the notation $G_{u^n v}(s)$ to refer to the transfer function for $u^n \mapsto v$ in Fig. 6.1. Similarly, $G_{\dot{w}v}(s)$ is the transfer function for $\dot{w} \mapsto v$. By way of clarification,
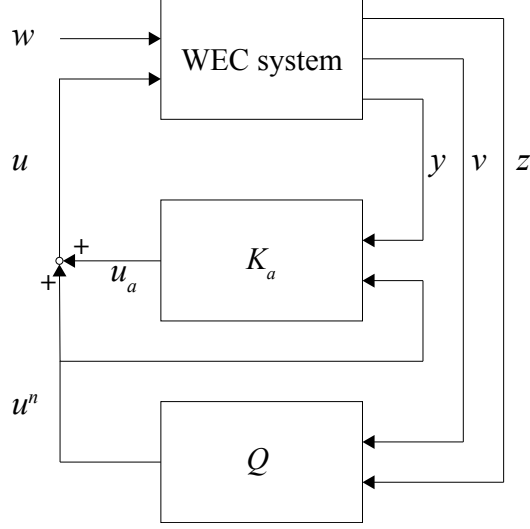
Figure 6.1: Stage-2 control system

we note that for the stochastic disturbances we consider here, $w(t)$ is a Wiener process, and therefore is not differentiable. Nonetheless, the above model reflects the mapping that would exist if $w(t)$ *were* differentiable and $\dot{w}(t)$ therefore existed. Equivalently, it may be viewed as the mapping for the case in which $\dot{w}(t)$ is modeled as unit-intensity white noise.

Theorem 6.3. *Suppose that $G_{u^n v} \in \mathcal{H}_\infty$ and is OSP that satisfies*

$$G_{u^n v}(j\omega) + G_{u^n v}^T(-j\omega) \geqslant \beta G_{u^n v}^T(j\omega) G_{u^n v}(j\omega) \quad , \quad \forall \omega \in \mathbb{R} \tag{6.33}$$

for some $\beta > 0$, and that there exists some transfer function $U \in \mathcal{H}_\infty$ such that

$$G_{\dot{w}v} = G_{u^n v} U \tag{6.34}$$

Further suppose an outer feedback loop $Q : \{v, z\} \to u^n$ is imposed, which satisfies

$$\int_0^t (u^n(\tau))^T v(\tau) d\tau \leqslant 0, \quad \forall t \in \mathbb{R}, \forall v \in \mathcal{L}_{2e} \tag{6.35}$$

Then with this feedback imposed, $v \in \mathcal{L}_{2e}$ with probability 1.

106

Proof. If (6.34) is true for some $U \in \mathcal{H}_\infty$ then $G_{\tilde{w}v}$ may be equivalently represented by eliminating the exogenous input channel w, and instead incorporating the effects of wave force f through the u^n input channel, via the substitution $u^n(t) \leftarrow u^n(t) + u^n_w(t)$, where $u^n_w(t)$ is a stochastic process with spectrum $U(j\omega)U^T(-j\omega)$. Requiring $U \in \mathcal{H}_\infty$ ensures that this spectrum has finite 2-norm and consequently that $u^n_w(t)$ has finite stationary covariance. As such, it ensures that $u^n_w \in \mathcal{L}_{2e}$ with probability 1. Meanwhile if (6.35) holds then the mapping $v \mapsto u^n$ is passive. If this is true and $u^n \mapsto v$ is OSP, the $\mathcal{L}_2$ gain of the closed-loop mapping $u^n_w \mapsto v$ is bounded from above by $\frac{1}{\beta}$ [91]. It follows that $v \in \mathcal{L}_{2e}$ with probability 1, because u^n_w is. $\qquad\square$

6.4.2 Parameterization of augmented linear controller K_a

Consider the augmentation

$$
K_a \sim \left[
\begin{array}{cc|cc}
A^\star_K & A_{12} & B^\star_K & B_{12} \\
0 & A_{22} & 0 & B_{22} \\
\hline
C^\star_K & C_2 & D^\star_K & I
\end{array}
\right]
\tag{6.36}
$$

where $\{A_{12}, B_{12}, A_{22}, B_{22}, C_2\}$ are new design variables, and where we note that the mapping $y \mapsto u$ remains the same $K^\star$ found from OP5.2. With the above controller imposed in closed-loop, the mapping $G \triangleq \{\dot{w}, u^n\} \mapsto \{v, z\}$ can be written as

$$
G \sim \left[
\begin{array}{cc|cc}
A^\star_{cl} & \begin{bmatrix} B_u C_2 \\ A_{12} \end{bmatrix} & B_{wcl} & \begin{bmatrix} B_u \\ B_{12} \end{bmatrix} \\
0 & A_{22} & 0 & B_{22} \\
\hline
C^\star_{vcl} & 0 & 0 & 0 \\
C_{zcl} & 0 & 0 & 0
\end{array}
\right]
\tag{6.37}
$$

where

$$A_{cl}^\star = \begin{bmatrix} A + B_u D_K^\star C_y & B_u C_K^\star \\ B_K^\star C_y & A_K^\star \end{bmatrix}, \quad B_{wcl} = \begin{bmatrix} E \\ 0 \end{bmatrix} \tag{6.38}$$

$$C_{vcl}^\star = \begin{bmatrix} C_v & 0 \end{bmatrix} \tag{6.39}$$

$$C_{zcl} = \begin{bmatrix} C_z & 0 \end{bmatrix} \tag{6.40}$$

To design $\{A_{12}, A_{22}, B_{12}, B_{22}, C_2\}$, we first prove that there exists at least one parameter sert which renders $G_{u^n v}$ output-strictly passive.

Theorem 6.4. *Let assumptions 6.2.1, 3.6.2, and 3.6.3 hold. Let L_2 is an arbitrary matrix of compatible dimension, and L_3 is a matrix of compatible dimension for which*

$$\left[\begin{array}{c|c} A + B_u L_3 & B_u \\ \hline C_v & 0 \end{array} \right] \tag{6.41}$$

is OSP. Then the following parameters result in OSP $G_{u^n v}$:

$$A_{22} = A + B_u L_3 \tag{6.42a}$$

$$A_{12} = L_2 A + L_2 B_u L_3 - A_K^\star L_2 - B_K^\star C_y \tag{6.42b}$$

$$B_{12} = L_2 B_u \tag{6.42c}$$

$$B_{22} = B_u \tag{6.42d}$$

$$C_2 = - C_K^\star L_2 - D_K^\star C + L_3 \tag{6.42e}$$

Proof. We first change the basis for the state space of $G_{u^n v}$, to bring about a simplified structure. If coordinates x characterize the state of the system in the basis as

originally expressed in (7.67), and x' are the new coordinates, then let

$$x = \begin{bmatrix} I & 0 & Z_1 \\ 0 & I & Z_2 \\ 0 & 0 & I \end{bmatrix} x' \tag{6.43}$$

where $\{Z_1, Z_2\} \subset \mathbb{R}^{n \times n}$ with Z_1 invertible. Now, consider the Sylvester equation

$$A_{cl}^\star \begin{bmatrix} Z_1 \\ Z_2 \end{bmatrix} + \begin{bmatrix} B_u C_2 \\ A_{12} \end{bmatrix} = \begin{bmatrix} Z_1 \\ Z_2 \end{bmatrix} A_{22} \tag{6.44}$$

For a given Z_1 and Z_2, the set of solutions $\{A_{12}, A_{22}, C_2\}$ which satisfies this equation is characterized by

$$A_{22} = Z_1^{-1} A Z_1 + Z_1^{-1} B_u Z_3 \tag{6.45}$$

$$C_2 = -C_K^\star Z_2 - D_K^\star C_y Z_1 + Z_3 \tag{6.46}$$

$$A_{12} = Z_2 A_{22} - A_K^\star Z_2 - B_K^\star C_y Z_1 \tag{6.47}$$

for any $Z_3 \in \mathbb{R}^{n \times n}$. Assuming the assignations (6.47), (6.45), and (6.46) to determine $\{A_{12}, A_{22}, C_2\}$ from $\{Z_1, Z_2\}$, the change of basis (6.43) produces the new realization

$$G_{u^n v} \sim \left[\begin{array}{cc|c} A_{cl}^\star & 0 & \begin{bmatrix} B_u - Z_1 B_{22} \\ B_{12} - Z_2 B_{22} \end{bmatrix} \\ 0 & Z_1^{-1} A Z_1 + Z_1^{-1} B_u Z_3 & B_{22} \\ \hline C_{vcl}^\star & C_v Z_1 & 0 \end{array} \right] \tag{6.48}$$

Now, suppose one chooses B_{22} and B_{12} as

$$B_{22} = Z_1^{-1} B_u, \qquad\qquad B_{12} = Z_2 B_{22} \tag{6.49}$$

Then the first $2n$ states are uncontrollable, and $G_{u^n v}$ has the minimal realization

$$G_{u^n v} \sim \left[\begin{array}{c|c} Z_1^{-1} A Z_1 + Z_1^{-1} B_u Z_3 & Z_1^{-1} B_u \\ \hline C_v Z_1 & 0 \end{array} \right] \qquad (6.50)$$

or, equivalently through a similarity transformation,

$$G_{u^n v} \sim \left[\begin{array}{c|c} A + B_u L_3 & B_u \\ \hline C_v & 0 \end{array} \right] \qquad (6.51)$$

where $L_3 \triangleq Z_3 Z_1^{-1}$. Now, we note that with $L_3 = 0$ (i.e., with $Z_3 = 0$), $G_{qv} = G_{uv}$, which is known to be output-strictly passive, thus proving that at least one feasible L_3 exists. $\qquad \square$

The above theorem proves that there always exists at least one K_a which renders $G_{u^n v}$ OSP. However, it does not ensure that, for this $G_{u^n v}$, there exists a $U \in \mathcal{H}_\infty$ such that (6.34) holds. With the help of the assumption 6.2.2, the following theorem shows the existence of $U \in \mathcal{H}_\infty$.

Theorem 6.5. *Let Assumptions 6.2.1, 3.6.2, 3.6.3, and 6.2.2 hold. Let augmented controller K_a be as in (6.36) with parameters $\{A_{12}, A_{22}, B_{12}, B_{22}, C_2\}$ determined by (6.4). Then there exists a $U \in \mathcal{H}_\infty$ satisfying (6.34).*

Proof. Let $G_{u^n v}$ have the form in (6.41). Since L_3 can be chosen such that $G_{u^n v}$ is OSP and it is known that $G_{u^n v} \in \mathcal{H}_\infty$. It can be shown that all its imaginary zeros are simple, and it is minimum phase, requires it to be shown that $G_{u^n v}(s)$ is nonsingular for almost all $s \in \mathbb{C}$. This can be established by noting that $G_{u^n v}$ has the same zeros as G_{uv} as well be shown below. From Assumption 3.6.3, $G_{uv}(s)$ is nonsingular for most $s \in \mathbb{C}$ and therefore so as $G_{u^n v}(s)$.

Let $u_w \triangleq V \dot{w}$. Then because $V \in \mathcal{H}_\infty$, the existence of $U \in \mathcal{H}_\infty$ satisfying (6.34) is guaranteed if there exists a $\bar{U} \in \mathcal{H}_\infty$ satisfying $G_{u_w v} = G_{u^n v} \bar{U}$. This can be

guaranteed if $G_{u_w v} \in \mathcal{H}_\infty$, if each imaginary zeros $i\omega_0$ of $G_{u^n v}$ is shared by $G_{u_w v}$ and $\mathcal{B}_{G_{u^n v}}(i\omega_0) \subseteq \mathcal{B}_{G_{u_w v}}(i\omega_0)$. In closed-loop, we have that $u_w \mapsto v$ is

$$
G_{u_w v} \sim
\left[
\begin{array}{cc|c}
A + B_u D_K^\star C_y & B_u C_K^\star & B_u \\
B_K^\star C_y & A_K^\star & 0 \\
\hline
C_v + D_{uv} D_K^\star C_y & D_{uv} C_K^\star & D_{uv}
\end{array}
\right]
\tag{6.52}
$$

That $G_{u_w v} \in \mathcal{H}_\infty$ is guaranteed by the prior design $K^\star$.

Let $i\omega_0$ be an imaginary zero of $G_{u^n v}$ with associate nonzero blocking vector $\eta \in \mathbb{C}^{n_p}$. There exists a vector $\xi \in \mathbb{C}^n$ s.t.

$$
\begin{bmatrix} \xi \\ \eta \end{bmatrix}^H
\begin{bmatrix} A - i\omega_0 I & B_u \\ C_v & 0 \end{bmatrix}
\begin{bmatrix} I & 0 \\ L & I \end{bmatrix} = 0
\tag{6.53}
$$

It follows that $\eta \in \mathcal{B}_{G_{u^n v}}(i\omega_0) = \mathcal{B}_{G_{uv}}(i\omega_0)$ Now, consider that for this imaginary zero $i\omega_0$ and vectors $\{\xi, \eta\}$ as in (6.53),

$$
\begin{bmatrix} \xi \\ 0 \\ \eta \end{bmatrix}^T
\begin{bmatrix} (A + B_u D_K^\star C_y) - i\omega_0 I & B_u C_K^\star & B_u \\ B_K^\star C_y & A_K^\star & 0 \\ C_v & 0 & 0 \end{bmatrix}
$$

$$
= \begin{bmatrix} \xi \\ \eta \end{bmatrix}^T
\begin{bmatrix} (A + B_u D_K^\star C_y) - i\omega_0 I & B_u C_K^\star & B_u \\ C_v & 0 & 0 \end{bmatrix}
\tag{6.54}
$$

$$
= \begin{bmatrix} \xi \\ \eta \end{bmatrix}^T
\begin{bmatrix} A - i\omega_0 I & B_u \\ C_v & 0 \end{bmatrix}
\begin{bmatrix} I & 0 & 0 \\ D_K^\star C_y & C_K^\star & I \end{bmatrix}
\tag{6.55}
$$

As such, we conclude that if $G_{u^n v}$ has ann imaginery zero $i\omega_0$ with blocking vector η, then so must $G_{u_w v}$. We conclude that $\mathcal{B}_{G_{u^n v}}(i\omega_0) \subseteq \mathcal{B}_{G_{u_w v}}(i\omega_0)$ $\qquad\square$

6.4.3 Designing Augmented Linear Controller K_a

With the knowledge there there exists at least one feasible design for K_a (i.e., a design that renders $G_{u^n v}$ OSP), it remains to determine the best feasible design via optimization. There does not appear to be an obvious way to transform the output-strict passivity constraint into a convex constraint on parameters $\{A_{12}, A_{22}, B_{12}, B_{22}, C_2\}$, without the introduction of conservatism. As such, the theorem below characterizes a convex subdomain which contains, in its closure, the known feasibility point found in Theorem 6.4

Theorem 6.6. *Let assumptions 6.2.1, 3.6.2, and 3.6.3 hold. Let $S_1 = S_1^T \in \mathbb{R}^{2n \times 2n}$, $S_2 = S_2^T \in \mathbb{R}^{n \times n}$, $\tilde{B}_{12}, \in \mathbb{R}^{n \times n_p}$, $B_{22} \in \mathbb{R}^{n \times n_p}$, $\tilde{L}_3 \in \mathbb{R}^{n_p \times n}$, and $\beta \in \mathbb{R}_{>0}$ be such that*

$$\mathrm{He}\,\{\Xi\} \leqslant 0 \tag{6.56}$$

$$S_1 > 0, \quad S_2 > 0 \tag{6.57}$$

where

$$\Xi \triangleq \begin{bmatrix} A_{cl}^\star S_1 & 0 & \begin{bmatrix} B_u - B_{22} \\ \tilde{B}_{12} \end{bmatrix} & 0 \\ 0 & AS_2 + B_u \tilde{L}_3 & B_{22} & 0 \\ -C_{vcl}^\star S_1 & -C_v S_2 - D_{uv} \tilde{L}_3 & -D_{uv} & 0 \\ -C_{vcl}^\star S_1 & -C_v S_2 - D_{uv} \tilde{L}_3 & -D_{uv} & -\frac{1}{2\beta} I \end{bmatrix}, \tag{6.58}$$

Let the mapping $q \mapsto v$ be parametrized by $\{A_{12}, A_{22}, B_{12}, B_{22}, C_2\}$ as in (7.67), with

$$A_{12} = L_2 A_{22} - A_K^\star L_2 - B_K^\star C_y \tag{6.59}$$

$$A_{22} = A + B_u \tilde{L}_3 S_2^{-1} \tag{6.60}$$

$$B_{12} = \tilde{B}_{12} + L_2 B_{22} \tag{6.61}$$

$$C_2 = -C_K^\star L_2 - D_K^\star C_y + \tilde{L}_3 S_2^{-1}. \tag{6.62}$$

where L_2 is an arbitrary matrix of compatible dimension. Then the mapping $u^n \mapsto v$ is OSP.

Proof. From Theorem 6.4 we have that the with A_{22}, A_{12}, and C_2 defined as in (6.45), (6.47), (6.46) respectively, $G_{u^n v}$ is

$$G_{u^n v} \sim \left[\begin{array}{cc|c} A_{cl}^\star & 0 & \begin{bmatrix} B_u - B_{22} \\ B_{12} - L_2 B_{22} \end{bmatrix} \\ 0 & A + B_u L_3 & B_{22} \\ \hline C_{vcl}^\star & C_v + D_{uv} L_3 & D_{uv} \end{array} \right] \tag{6.63}$$

We then have that $G_{u^n v}$ is OSPR if and only if there exists $S = S^T$ and a $\beta > 0$ such that

$$\mathrm{He}\left\{ \left[\begin{bmatrix} A_{cl}^\star & 0 \\ 0 & A + B_u L_3 \end{bmatrix} S \\ - \begin{bmatrix} C_{vcl}^\star & C_v + D_{uv} L_3 \end{bmatrix} S \quad \begin{bmatrix} B_u - B_{22} \\ B_{12} - L_2 B_{22} \end{bmatrix} \\ -D_{uv} \end{bmatrix} \right\}$$

$$+ \beta \left[\begin{matrix} S \begin{bmatrix} C_{vcl}^\star & C_v + D_{uv} L_3 \end{bmatrix}^T \\ D_{uv}^T \end{matrix} \right] \left[\begin{matrix} S \begin{bmatrix} C_{vcl}^\star & C_v + D_{uv} L_3 \end{bmatrix}^T \\ D_{uv}^T \end{matrix} \right]^T$$

$$\leqslant 0 \quad (6.64)$$

as well as

$$E_c^T S E_c > 0, \tag{6.65}$$

where E_c is a full-column-rank matrix spanning the controllable subspace of the state space realization for $H_{u^n v}$. Assuming $E_c = I$ is therefore sufficient to guarantee this condition. □

Theorem 6.6 provides conditions guaranteeing that $u^n \mapsto v$ is OSP, but in order

for Theorem 6.3 to hold, it must also be shown that there exists $U \in \mathcal{H}_\infty$ satisfying (6.34). To present the condition guaranteeing this, first let $\{\omega_1, ...\omega_p\}$ be the set of all solutions to the eigenvalue problem

$$\begin{bmatrix} A - i\omega I & B_u \\ C_v & 0 \end{bmatrix}^H \eta = 0 \ , \eta \neq 0, \quad \omega \in \mathbb{R} \tag{6.66}$$

and

$$\begin{bmatrix} I & 0 \\ 0 & 0 \end{bmatrix}^H \eta = 0 \ , \eta \neq 0, \quad \omega = \infty \tag{6.67}$$

where $p \in \mathbb{Z}$ is the number of imaginary-axis zeros of G_{uv} (counting multiplicity). Define $N \triangleq \begin{bmatrix} \eta_1 & \cdots & \eta_p \end{bmatrix}$ as the corresponding (linearly independent) set of eigenvectors. Define $N_\perp$ as a full-column-rank matrix such that $\begin{bmatrix} N & N_\perp \end{bmatrix}$ is square and $N^H N_\perp = 0$. Then we have the following lemma, which will be useful in the theorem to follow.

Lemma 6.7. *Let* $\{A, B_u, C_v, 0\}$ *be OSP, and* $\{\eta_1, \ldots \eta_p\}$ *be defined above. There must exist some* $S \geq 0$ *and* $\beta > 0$, *such that*

$$\text{span}\{\eta_1, \ldots \eta_p\} \subseteq \text{null}\left\{ \begin{bmatrix} AS + SA^T & B_u - SC_v^T \\ B_u^T - C_v S & 0 \end{bmatrix} \right\} \tag{6.68}$$

Proof. Consider that for each $i \in \{i, \ldots p\}$, for $\omega_i \in \mathbb{R}$

$$
\eta_i^H \begin{bmatrix} AS + SA^T & B_u - SC_v^T \\ B_u^T - C_v S & 0 \end{bmatrix} \eta_i
$$

$$
= \eta_i^H \operatorname{He} \left\{ \begin{bmatrix} A - i\omega & B_u \\ C_v & 0 \end{bmatrix} \begin{bmatrix} S & 0 \\ 0 & I \end{bmatrix} \right\} \eta_i
$$

$$
= 0 \tag{6.69}
$$

Similarly for $\omega = \infty$

$$
\eta_i^H \begin{bmatrix} AS + SA^T & B_u - SC_v^T \\ B_u^T - C_v S & 0 \end{bmatrix} \eta_i = 0 \tag{6.70}
$$

implying that the first p diagonal terms of the matrix

$$
\begin{bmatrix} N^H \\ N_\perp^H \end{bmatrix} \eta_i^H \begin{bmatrix} AS + SA^T & B_u - SC_v^T \\ B_u^T - C_v S & 0 \end{bmatrix} \begin{bmatrix} N^H \\ N_\perp^H \end{bmatrix}^H \tag{6.71}
$$

must be zero. Since the $G_{u^n v}$ is OSP, so the above the matrix is negative semidefinite. In order for this to be true, the first p rows and p columns must be identically zero. This is equivalent to the statement (6.68) □

Furthermore, partition $N_\perp$ as

$$
N_\perp = \begin{bmatrix} N_{\perp 1} \\ N_{\perp 2} \end{bmatrix}, \quad N_{\perp 1} \in \mathbb{C}^{n \times p} \tag{6.72}
$$

Then in terms of $\{N_{\perp 1}, N_{\perp 2}\}$, we have the following theorem:

Theorem 6.8. *In Theorem 6.6, let Assumption 6.2.2 hold. Let parameters*

$\{S_1, S_2, \tilde{B}_{12}, B_{22}, \tilde{L}_3, \beta\}$ *satisfy* (6.56), (6.57), *and let* K_a *be as in in* (6.36). *Let*

$$\Upsilon_\perp \triangleq \begin{bmatrix} I & 0 & N_{\perp 1} \\ 0 & I & 0 \\ 0 & 0 & N_\perp \\ 0 & 0 & 0 \end{bmatrix} \tag{6.73}$$

Then if (6.56) *is strengthened to require that*

$$\mathrm{He}\left\{\Upsilon_\perp^H \Xi \Upsilon_\perp\right\} < 0 \tag{6.74}$$

then there exists $U \in \mathcal{H}_\infty$ *satisfying* (6.34).

Proof. From Lemma 6.7 it is known that if (6.56) holds with S_2 nonsingular, then the space of all $\eta = \begin{bmatrix} \eta_1^H & \eta_2^H \end{bmatrix}$ satisfying

$$\begin{bmatrix} \eta_1 \\ \eta_2 \end{bmatrix}^H \mathrm{He}\left\{ \begin{bmatrix} AS_2 & B_u \\ C_v S_2 & 0 \end{bmatrix} \right\} = 0 \tag{6.75}$$

has a basis $\{\eta_1, ... \eta_p\}$ where each η_i has associated with it an ω_i such that

$$\begin{bmatrix} \eta_{i1} \\ \eta_{i2} \end{bmatrix}^H \begin{bmatrix} A - j\omega_i & B_u \\ C_v & 0 \end{bmatrix} = 0 \tag{6.76}$$

or else $\omega_i = \infty$ and

$$\eta_{i1} = 0 \tag{6.77}$$

For $\omega_i \in \mathbb{R}$, let $\tilde{\Xi}(\omega_i)$ be defined as

$$\tilde{\Xi}(\omega_i) = \begin{bmatrix} A_{cl}^{\star} S_1 - j\omega_i S_1 & 0 & \begin{bmatrix} B_u - B_{22} \\ \tilde{B}_{12} \end{bmatrix} \\ 0 & AS_2 + B_u \tilde{L}_3 - j\omega_i S_2 & B_{22} \\ C_{vcl}^{\star} S_1 & C_v S_2 & 0 \end{bmatrix} \qquad (6.78)$$

Then we note that for each η_i,

$$\begin{bmatrix} \eta_{i1}^H & 0 & \eta_{i1}^H & \eta_{i2}^H \end{bmatrix} \tilde{\Xi}(\omega_i)$$

$$= \eta_{i1}^H \begin{bmatrix} (A_{cl}^{\star} - j\omega_i I)S_1 & (A - j\omega_i I + B_u L_3)S_2 & B_u \end{bmatrix}$$

$$+ \eta_{i2}^H \begin{bmatrix} C_{vcl}^{\star} S_1 & (C_v + D_{uv} L_3)S_2 & D_{uv} \end{bmatrix} \qquad (6.79)$$

$$= \begin{bmatrix} \eta_{i1} \\ \eta_{i2} \end{bmatrix}^H \begin{bmatrix} A - j\omega_i I & B_u \\ C_v & D_{uv} \end{bmatrix} \begin{bmatrix} \begin{bmatrix} I & 0 \\ D_K^{\star} C_y & C_K^{\star} \end{bmatrix} S_1 & \begin{bmatrix} S_2 & 0 \\ \tilde{L}_3 & I \end{bmatrix} \end{bmatrix} \qquad (6.80)$$

$$= 0 \qquad (6.81)$$

Meanwhile if $\omega_i = \infty$ then

$$\begin{bmatrix} \eta_{i1}^H & 0 & \eta_{i1}^H & \eta_{i2}^H \end{bmatrix} \mathrm{He}\{\tilde{\Xi}(\omega_i)\} \begin{bmatrix} \eta_{i1}^H & 0 & \eta_{i1}^H & \eta_{i2}^H \end{bmatrix}^H = 0 \qquad (6.82)$$

for any $\omega \in \mathbb{R}$, which together with (6.56) implies that

$$\begin{bmatrix} \eta_{i1}^H & 0 & \eta_{i1}^H & \eta_{i2}^H \end{bmatrix} \in \mathrm{null}\left\{\mathrm{He}\{\tilde{\Xi}\}\right\} \qquad (6.83)$$

117

Consequently, the null space of $\text{He}\{\tilde{\Xi}(\omega)\}$ contains the subspace

$$\tilde{\mathcal{N}} \triangleq \text{span} \left\{ \begin{bmatrix} \eta_{11} \\ 0 \\ \eta_{11} \\ \eta_{12} \end{bmatrix}, \dots \begin{bmatrix} \eta_{p1} \\ 0 \\ \eta_{p1} \\ \eta_{p2} \end{bmatrix} \right\} \tag{6.84}$$

As such, any $G_{u^n v}$ adhering to (6.56) and (6.57) with S_2 nonsingular, will be such that it inherits the zeros $\{j\omega_1, \dots j\omega_p\}$ of plant G_{uv}. Moreover, if $\eta_{i2}^H G_{uv}(j\omega_i) = 0$ then $\eta_{i2}^H G_{u^n v}(j\omega_i) = 0$. If it is the case that $\text{He}\{\tilde{\Xi}(\omega)\}$ is negative definite in the subspace orthogonal to $\tilde{\mathcal{N}}$ then by Lemma 6.7 it follows that these zeros are the only zeros of $G_{u^n v}$. This negative definiteness condition is equivalent to requiring (6.74).

Analogously to the proof for Theorem 6.5, it is known that the finite imaginary-axis zeros and corresponding adjoint blocking spaces of $G_{u_w v}$ includes all those of G_{uv}. Satisfaction of (6.74) implies that the same is true of $G_{u^n v}$ and that these are its only imaginary-axis zeros. We can conclude that $G_{u^n v}^{-1} G_{u_w v} \in \mathcal{H}_\infty$ and therefore that there exists a $U \in \mathcal{H}_\infty$ such that $G_{wv} = G_{u^n v} U$. $\quad\square$

Theorem 6.6 and Theorem 6.8 provides a parametric domain over which to optimize K parameters $\{A_{12}, A_{22}, B_{12}, B_{22}, C_2\}$ which is convex, and the closure of which is guaranteed to contain a feasible point. Given this, it remains to determine a suitable metric under which to optimize these parameters, which is also convex in the $\{S_1, S_2, \tilde{B}_{12}, B_{22}, \tilde{L}_3, \beta\}$ domain.

To do this, consider that $G_{u^n v}$ can be written as:

$$G_{u^n v} = G_0 + G_1 \tag{6.85}$$

118

where

$$
G_0 \sim \left[\begin{array}{c|c} A_{cl}^{\star} & \left[\begin{array}{c} B_u \\ 0 \end{array} \right] \\ \hline C_{vcl}^{\star} & 0 \end{array} \right] \tag{6.86}
$$

$$
G_1 \sim \left[\begin{array}{cc|c} A_{cl}^{\star} & \left[\begin{array}{c} B_u C_2 \\ A_{12} \end{array} \right] & \left[\begin{array}{c} 0 \\ B_{12} \end{array} \right] \\ 0 & A_{22} & B_{22} \\ \hline C_{vcl}^{\star} & 0 & 0 \end{array} \right] \tag{6.87}
$$

As such, G_0 is the transfer function from q to v without the control augmentation, while G_1 is the adjustment to this transfer function that is necessary to make $G_{u^n v}$ OSP. We wish to choose $\{S_1, S_2, \tilde{B}_{12}, B_{22}, \tilde{L}_3, \beta\}$ to minimize the gain G_1, subject to constraints 6.6 and 6.8. To do this, a norm must be chosen for the gain to be minimized, and here we choose the $\mathcal{H}_2$ norm. The following theorem establishes a way of accomplishing this.

Theorem 6.9. $\|G_1\|_{\mathcal{H}_2}^2 < \gamma$ if there exists $S_3 = S_3^T > 0$ and $\alpha > 0$ such that

$$
\left[\begin{array}{ccc} \mathrm{He}\{A_{cl}^{\star} S_3\} & 0 & \cdot \left[\begin{array}{c} -B_{22} \\ \tilde{B}_{12} \end{array} \right] \\ & \mathrm{He}\{A S_2 + B_u \tilde{L}_3\} & B_{22} \\ (sym) & & -\frac{1}{\alpha} I \end{array} \right] \leqslant 0 \tag{6.88}
$$

$$
\left[\begin{array}{ccc} \alpha \gamma & C_{vcl}^{\star} S_3 & C_v S_2 + D_{uv} \tilde{L}_3 \\ & S_3 & 0 \\ (sym) & & S_2 \end{array} \right] > 0 \tag{6.89}
$$

where $\{S_2, \tilde{B}_{12}, B_{22}, \tilde{L}_3 \beta\}$ are the same as in (6.56).

Proof. From the proof to Theorem 6.6, it follows that

$$G_1 \sim \left[\begin{array}{c|c} A_0 & B_0 \\ \hline C_0 & 0 \end{array} \right] \tag{6.90}$$

where

$$A_0 = \begin{bmatrix} A_{cl}^{\star} & 0 \\ A + B_u L_3 \end{bmatrix} \qquad B_0 = \begin{bmatrix} -B_{22} \\ \tilde{B}_{12} \\ B_{22} \end{bmatrix} \tag{6.91}$$

$$C_0 = \begin{bmatrix} C_{vcl}^{\star} & C_v + D_{uv} L_3 \end{bmatrix} \tag{6.92}$$

It is a standard result that $\|G_1\|_{\mathcal{H}_2}^2 < \gamma$ if and only if there exists a matrix $S = S^T > 0$, such that

$$A_0 S + S A_0^T + B_0 B_0^T < 0 \tag{6.93}$$

$$\mathrm{Tr}\{C_0 S C_0^T\} < \gamma \tag{6.94}$$

Conservatively choosing

$$S = \frac{1}{\alpha} \begin{bmatrix} S_3 & 0 \\ 0 & S_2 \end{bmatrix}, \tag{6.95}$$

and performing Schur complements on both inequalities, gives (6.88) and (6.89). $\square$

We therefore arrive at an optimization problem to determine parameters $\{S_1, S_2, S_3, \tilde{B}_{12}, B_{22}, \tilde{L}_3, \alpha\}$:

$$\text{OP3}: \begin{cases} \text{Minimize:} & \gamma \\ \text{Domain:} & S_1, S_2, S_3, \tilde{B}_{12}, B_{22}, \tilde{L}_3, \alpha \\ \text{Constraints:} & (6.56), (6.57), (6.88), (6.89). \end{cases} \tag{6.96}$$

6.4.4 Designing Nonlinear Feedback Loop Q

We now consider the design of Q, the nonlinear component of the control law. We propose a formulation of Q in which each PTO $i \in \{1...n_p\}$ has a decentralized law Q_i, which is a static function of $v_i(t)$ and $z_i(t)$. Specifically, for a differentiable, scalar function V_i, we assume

$$Q_i(v_i, z_i) = -\left.\frac{\partial V_i}{\partial q}\right|_{q=z_i+\alpha v_i} \tag{6.97}$$

where $\alpha \geqslant 0$ is a design parameter. With $\alpha = 0$, we can think of $V_i(\cdot)$ as the stored energy for a (potentially nonlinear) spring. The presence of $\alpha > 0$ introduces dissipation into this elastic model.

Lemma 6.10. *Let $V_i : \mathbb{R} \to \mathbb{R}_{\geqslant 0}$ be a differentiable, semiconvex function with $V_i(0) = 0$. Let $Q_i : \mathbb{R}^2 \to \mathbb{R}$ be defined as in (6.97), for $\alpha \geqslant 0$. Then for any $v_i(t) \in \mathcal{L}_{2e}$ with $z_i(t) = \int_0^t v_i(\tau)d\tau$,*

$$\int_0^t v_i(\tau)Q_i(v_i(\tau), z_i(\tau))d\tau \leqslant -V_i(z_i(t)), \quad \forall t \in \mathbb{R}_{>0} \tag{6.98}$$

Proof. For any $\alpha \geqslant 0$, semiconvexity of V_i implies that

$$v_i \geqslant 0 \quad \Rightarrow \quad \left.\frac{\partial V_i}{\partial q}\right|_{q=z_i+\alpha v_i} \geqslant \left.\frac{\partial V_i}{\partial q}\right|_{q=z_i} \tag{6.99}$$

$$v_i \leqslant 0 \quad \Rightarrow \quad \left.\frac{\partial V_i}{\partial q}\right|_{q=z_i+\alpha v_i} \leqslant \left.\frac{\partial V_i}{\partial q}\right|_{q=z_i} \tag{6.100}$$

Consequently, for any $\alpha \geqslant 0$,

$$v_i(\tau)Q_i\left(v_i(\tau), z_i(\tau)\right) = -v_i(\tau)\left.\frac{\partial V_i}{\partial q}\right|_{q=z_i(\tau)+\alpha v_i(\tau)} \tag{6.101}$$

$$\leqslant -v_i(\tau)\left.\frac{\partial V_i}{\partial q}\right|_{q=z_i(\tau)} \tag{6.102}$$

121

Consequently

$$\int_0^t v_i(\tau)Q_i(v_i(\tau), z_i(\tau))d\tau \leqslant -\int_0^t v_i(\tau) \left.\frac{\partial V_i}{\partial q}\right|_{q=z_i(\tau)} d\tau \qquad (6.103)$$

$$= -\int_0^t \frac{d}{d\tau}V_i(z_i(\tau))d\tau \qquad (6.104)$$

$$= -V_i(z_i(t)) - V_i(z_i(0)) \qquad (6.105)$$

which, together with the conditions that $V_i(0) = 0$ and $z_i(t) = \int_0^t v_i(\tau)d\tau$, completes the proof. $\qquad\square$

Our approach will be to resort to this physical intuition to design $V_i(\cdot)$. Specifically, we formulate $V_i(\cdot)$ as the potential function

$$V_i(q_i) = \Gamma_i \max\left\{0, -\ln\left(\frac{z_{mi} - |q_i|}{\delta_i}\right) + \frac{z_{mi} - |q_i|}{\delta_i} - 1\right\} \qquad (6.106)$$

where $\Gamma_i > 0$ and $\delta_i \in (0, z_{mi})$ are design parameters that, along with α_i and z_{mi}, fully characterize Q_i. This is illustrated in Figure 6.2. For the $\alpha = 0$ case, it corresponds to a hardening spring with asymptotic potential barriers at $q_i = \pm z_{mi}$, and a dead zone for all $|q_i| < z_{mi} - \delta_i$. As such, the effect is to apply a nonlinear restoring force when $|q_i|$ is close to z_{mi}.

Theorem 6.11. *Assume B_q has been designed such that (6.33) holds for some $\beta > 0$, and that there exists $U \in \mathcal{H}_\infty$ such that (6.34) holds. For each $i \in \{1..n_p\}$, let nonlinear controllers $Q_i : \{v_i, z_i\} \to q_i$ be as in (6.97), and with $V_i(q_i)$ characterized as in (6.106) for $\Gamma_i > 0$, $\alpha_i \geqslant 0$, and $\delta_i \in (0, z_{mi})$. Then for the stochastically-excited closed-loop system,*

- *$v \in \mathcal{L}_{2e}$ with probability 1.*

- *Over any finite interval $t \in [t_1, t_2]$, $\max_{t \in [t_1, t_2]} |z_i(t)| < z_{mi}$, for all $i \in \{1...n_p\}$, with probability 1.*

Proof. The first claim follows directly from the combination of Theorem 6.3 with Lemma 6.10. To show the second claim, let $G_{u^n v}$ have some minimal realization

$$G_{u^n v} \sim \left[\begin{array}{c|c} A_{u^n v} & B_{u^n v} \\ \hline C_{u^n v} & D_{u^n v} \end{array} \right] \tag{6.107}$$

Then because $G_{u^n v}$ satisfies (6.33), from the PR Lemma there exists a matrix $P = P^T > 0$, and compatible matrices L and W such that

$$\begin{bmatrix} A_{u^n v}^T P + P A_{u^n v} & P B_{u^n v} - C_{u^n v}^T \\ B_{u^n v}^T P - C_{u^n v} & -D_{u^n v} - D_{u^n v}^T \end{bmatrix} = - \begin{bmatrix} L \\ W \end{bmatrix} \begin{bmatrix} L \\ W \end{bmatrix}^T \tag{6.108}$$

with the requirement that (6.33) holds with $\beta > 0$ implying that the above must be satisfied for $(A_{u^n v}, L^T)$ observable. Because it is assumed (6.34) exists for $U \in \mathcal{H}_2$, define u_w^n as in the proof for Theorem 6.3, and it follows that for all $u_w^n \in \mathcal{L}_{2e}$ and all $t > 0$,

$$\int_0^t (u_w^n(\tau) + u^n(\tau))^T v(\tau) d\tau \geqslant \frac{1}{2} x_{u^n v}^T(t) P x_{u^n v}(t) \tag{6.109}$$

where $x_{u^n v}$ is the state coordinate vector for realization (6.107). Due to Lemma 6.10, this implies that

$$\int_0^t (u_w^n(\tau))^T v(\tau) d\tau \geqslant \frac{1}{2} x_{u^n v}^T(t) P x_{u^n v}(t) + \sum_{i=1}^{n_p} V_i(z_i(t)) \tag{6.110}$$

It follows that if u_w^n and v are in $\mathcal{L}_{2e}$, then over any finite amount of time, $t \in [t_1, t_2]$, $V_i(z_i(t))$ is bounded from above, and consequently $|z_i(t) < z_{mi}$. Because u_w^n and v are in $\mathcal{L}_{2e}$ with probability 1, this bound also follows with probability 1. $\square$

It was found that potentials of the form (6.106) perform well for the purpose of stroke saturation prevention. All three parameters $\{\alpha_i, \delta_i, \Gamma_i\}$ need to be tuned for a given application. A positive value of α_i is not strictly necessary (i.e., it can be set to
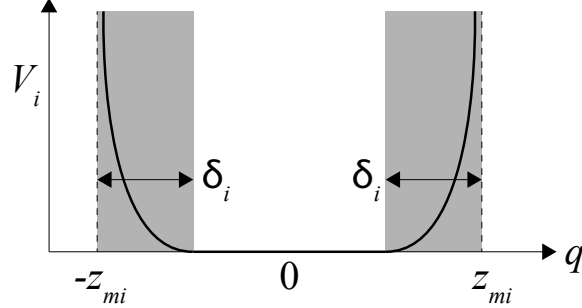
Figure 6.2: Potential function V_i

zero) although it was found to be advantageous to have a positive value. Meanwhile, as Γ_i and δ_i are reduced in magnitude, $u(t)$ will exhibit increasingly exaggerated impulsive phenomena. On the other hand, increasing their magnitudes depreciates the stationary value of $\bar{p}$, relative to the optimized Stage 1 design.

6.5 Numerical Example

We use the same single-degree-of-freedom WEC shown in Figure 6.3 as the one buoy case in Section 5. For more details on the modeling of the system in Fig.6.3, and in particular of its finite-dimensional state space model formulation, we refer the readers to the one buoy case in Section 5. For our purpose here, we assume the stroke limit $z_m = 3$m.

6.5.1 Design Stage I

Executing the linear feedback design in Section 6.3, the performance at the optimized solution is $\bar{p} = 25.5$kW, while the causal limit on power generation is $\bar{p}_0 = 29.7$kW. Figure 6.4 shows one hour of simulated transsient response data for the closed-loop system implementing $K^\star$, the optimized linear controller. The root-mean-square stroke in steady-state is equal 1.5m; i.e., the upper constraint specified by (6.3). However, as is clear from the transient plot, the stroke regularly exceeds its maximum allowable value of 3m.
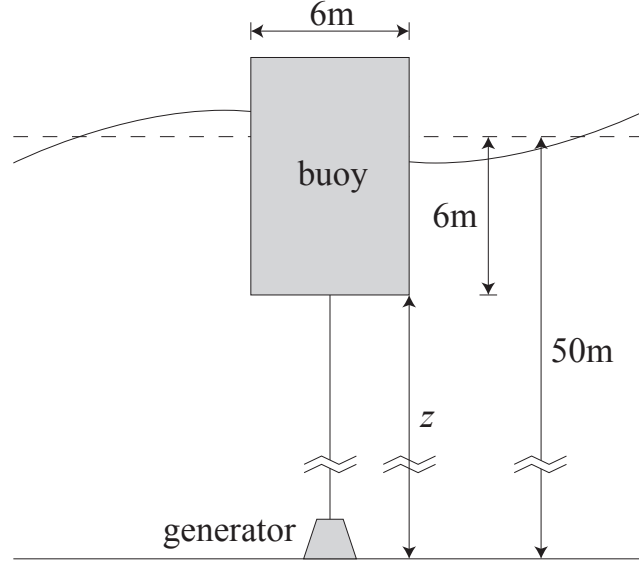
Figure 6.3: Diagram of example WEC

We compare the performance reduction under different sea states and stroke constraints in Figure 6.5(a) and 6.5(b). As we can see in both figures, as we relax the mean-square stroke constraint, the performance reduction will become smaller. For a fixed stroke constraint, the performance reduction would increase if we choose the higher mean wave period. This is because the dynamic response of the WEC system increases in the low-frequency waves. In accordance with the results in Chapter 5, there exists a positive relationship with the dynamic response and the sharpness factor γ.

6.5.2 Design Stage II

For the optimized $K^\star$, the design procedure outlined in Section 6.4 was followed, to arrive at a design for K_a. With $B_{12} = 0$ and $B_{22} = 0$, the transfer function $u^n \mapsto v$ is shown in Figure 6.6, illustrating that it is clearly not positive real. Meanwhile, with the optimized K_a, the transfer function becomes that in Figure 6.7, which clearly is positive real.

Regarding the nonlinear controller Q, the described technique was implemented,
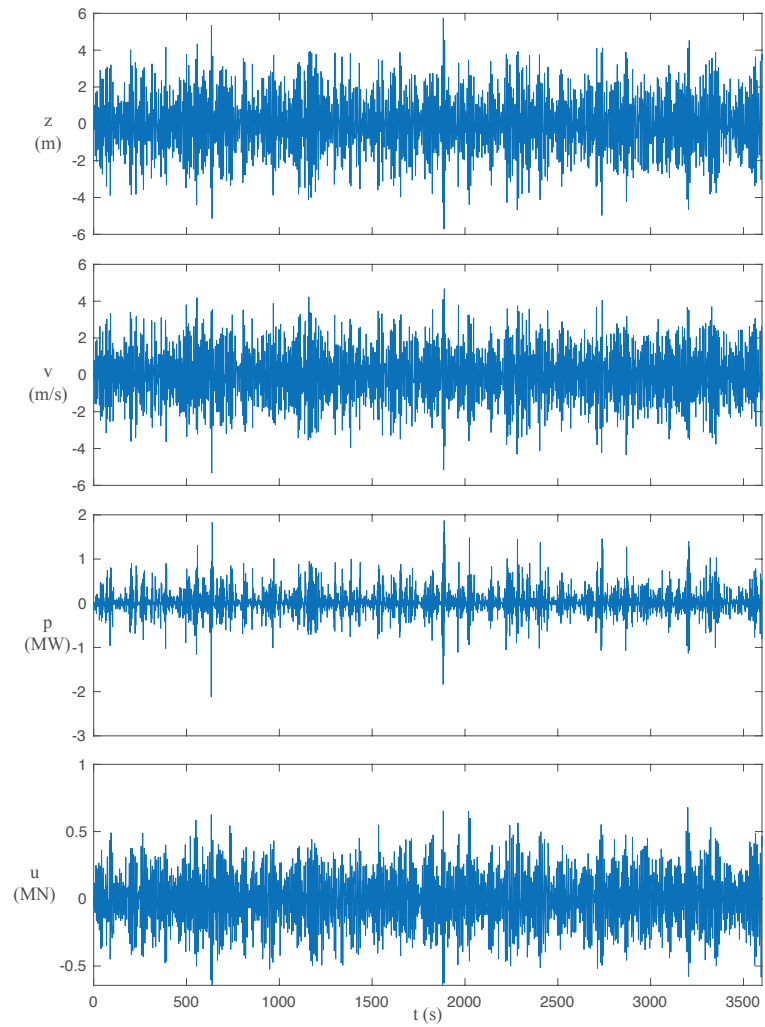
Figure 6.4: Transient response of optimized linear controller for Design Stage 1
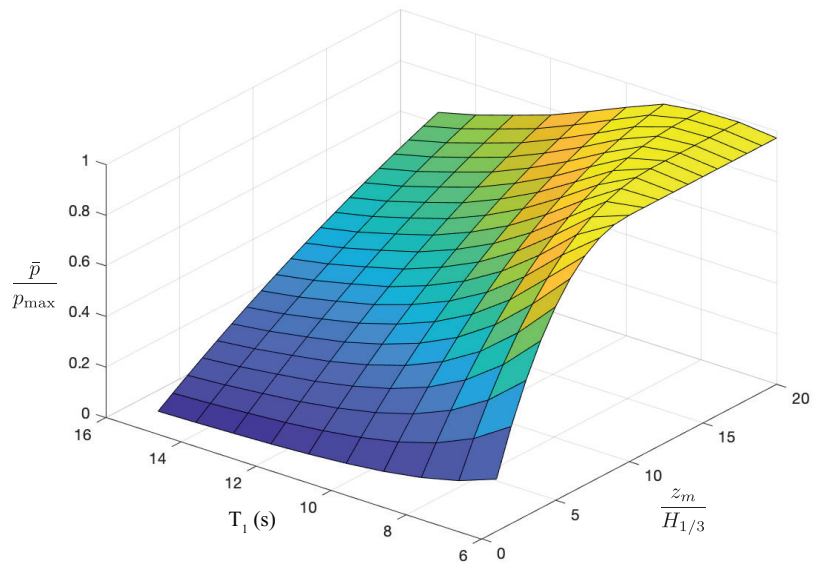
(a) $\gamma = 1$
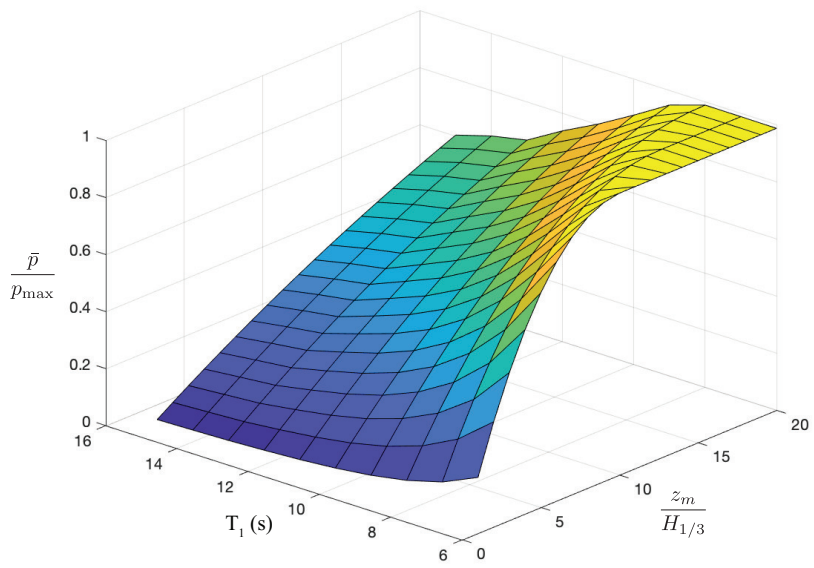
(b) $\gamma = 3.3$

Figure 6.5: Performance reduction in different mean wave periods and stroke constraints
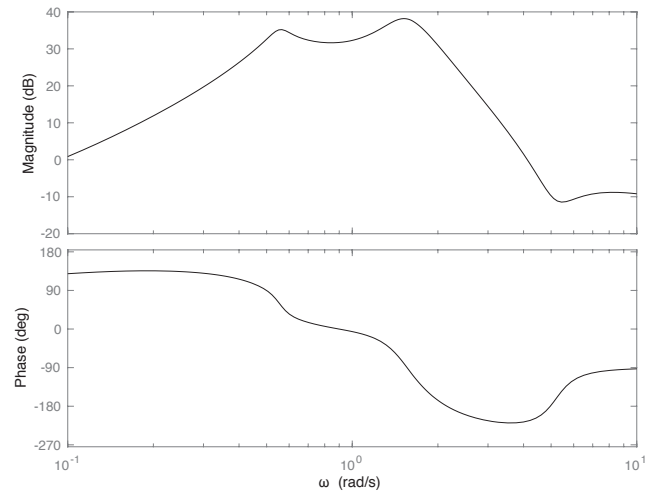
Figure 6.6: Mapping $u^n \mapsto v$ with K as in (6.36), with $B_{12} = 0$ and $B_{22} = 0$
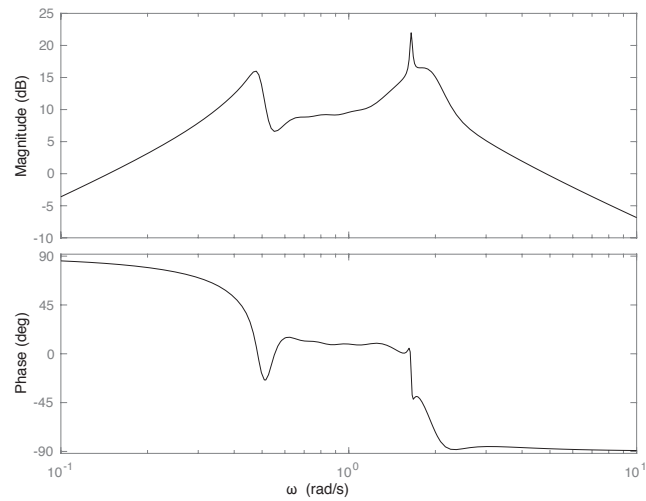
Figure 6.7: Mapping $u^n \mapsto v$ with K as in (6.36), with K_a optimized
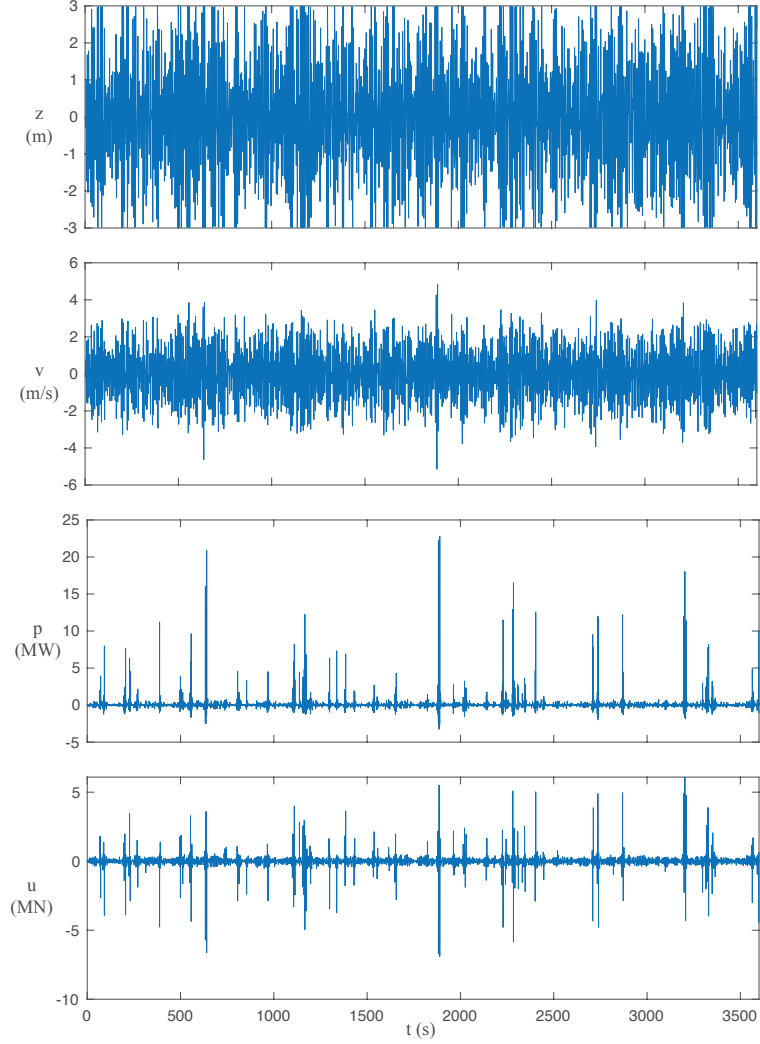
Figure 6.8: Transient response of optimized linear controller for Design Stage 2

with parameters $\{\alpha, \delta, \Gamma\}$ tuned for favorable performance. Via a parameter search, the values $\alpha = 0.1$s, $\delta = 1$m, and $\Gamma = 1$kN/m were found to perform well. For these responses, the mean power generation (found through simulation) for the closed-loop nonlinear system was $\bar{p} = 23.8$kW, which is a mere 6.7% drop from the linear Stage-1 design. Figure 6.8 shows the transient response for this case. Comparison with Figure 6.4 clearly illustrates the effect of the nonlinearity. The stroke is successfully maintained below 3m at all times, but this clearly comes at a price, in the form of the higher PTO forces needed for deceleration. These higher forces stand out in the transient plot, but they are infrequent in the dynamic response. This can be seen

129

by comparing the mean force magnitudes for the simulations of Stage-1 and Stage-2, which are, respectively, 0.154MN and 0.171MN. As such, we see that although high pulsating PTO forces are necessary to maintain the stroke limit, the mean-square force is increased from Stage-1 by less than 15%.

Figure 6.9(a) and Figure 6.9(b) show the dependency of both the mean power generation and mean square controller force on the nonlinear controller parameter α and Γ, for $\delta = 1m$. As we can see in the figure, there is a trade off in the figure, because lower mean-square forces are favorable, as are high values of $\bar{p}$. The plot clearly demonstrate that α plays an important role in the performance of nonlinear controller and it can be tuned to satisfy the certain requirements, as well as some constraints.
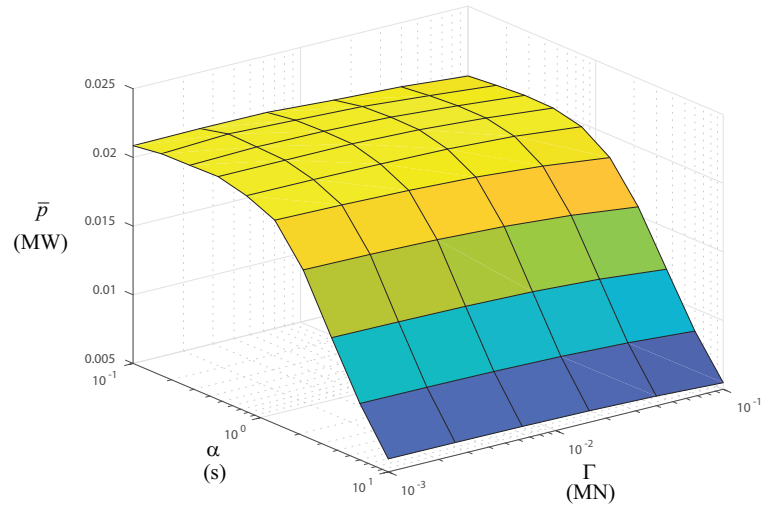
(a) Mean power generation $\bar{p}$
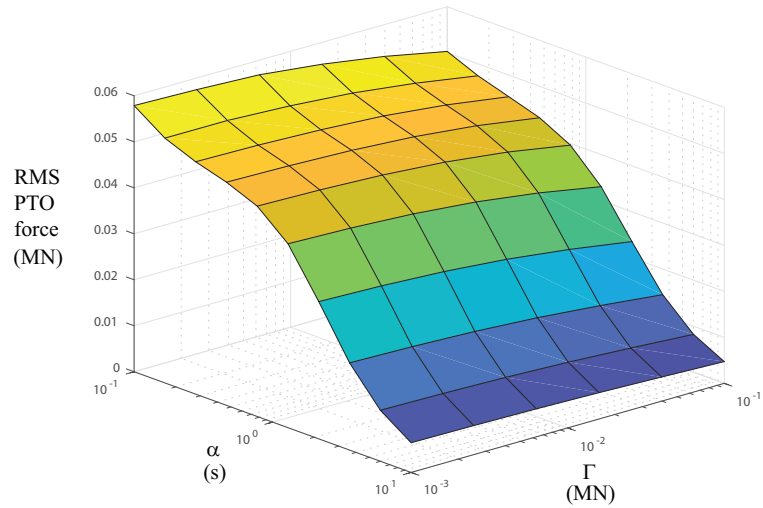
(b) Mean square controller force $\mathcal{E}\{u^2\}$

Figure 6.9: Mean power generation $\bar{p}$ and $\mathcal{E}\{u^2\}$ on the nonlinear controller parameter α and Γ, where δ is fixed at $1m$

CHAPTER 7

Nonlinear Causal Control of Wave Energy Converters with Finite Stroke in Discrete Time Domain

7.1 Introduction

We present a technique for discrete-time control of WECs with finite stroke, which is based on multi-objective optimal control, as well as passivity theory. The design technique shares many similarities with the continuous time controller designed in Chapter 6 and is comprised of three analogous design steps:

1. First, an optimal linear LQG controller is designed which accommodates a weakened, time-averaged version of the stroke limit constraint. This first design component makes use of multi-objective optimal control theory, and is cast in the context of a semidefinite program.

2. Second, this linear controller is augmented to include an extra input channel $u_k^n, k \in \{0, 1, \dots\}$, which can be interpreted as a nonlinear force that constraint the PTO displacement. In particular, the design of this augmentation should follow such a way that the mapping: $u_k^n \mapsto q_k$ is OSPR.

132
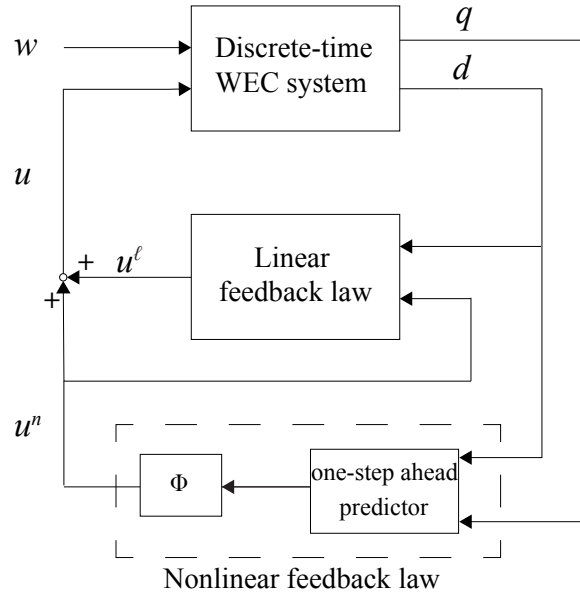
Figure 7.1: Block diagram of the WEC system under stroke constraint

3. Third, a nonlinear controller should contain two parts: one-step-ahead predictor and nonlinear control law. One-step-ahead predictor forecasts the displacement variable d_k only considering the effect of linear controller. Nonlinear feedback law Φ is designed to protect the stroke from saturation. It is shown that the close-loop system is stable by constraining the mapping $q_k \mapsto u_k^n$ mean-square passive.

In Chapter 6, we apply a variant of this general technique to continuous time systems. In this Chapter, the first two design steps of this technique is similar to the continuous case. The last step, which involves the design of nonlinear feedback law, is more complex than Chapter 6.

7.2 Problem Formulation

7.2.1 Discrete-Time Dynamic Model

We assume that $u(t)$ is controlled in discrete-time, via a zero-order-hold convention; i.e.,

$$u(t) = u_k, \quad t \in [kT, (k+1)T) \tag{7.1}$$

where T is the sample time and k is the discrete time index. We similarly refer to other output signals sampled at time $t = kT$ with a subscript k; i.e., $v_k = v(kT)$, $d_k = d(kT)$, etc.

The dissipation in the power train of the WEC can be adequately modeled as a quadratic function of the PTO force. Let p_k be the average power generation over interval $t \in [kT, (k+1)T)$. Then due to the zero-order-hold convention, we have that

$$p_k = \frac{1}{T} \int_{kT}^{(k+1)T} \left[-u^T(t)v(t) - p_{diss}(t) \right] dt \tag{7.2}$$

$$= -\frac{1}{T} u_k^T R_d u_k - u_k^T \frac{1}{T} \int_{kT}^{(k+1)T} v(t)dt \tag{7.3}$$

$$= -u_k^T R_d u_k - u_k^T \frac{1}{T} \left(z_{k+1} - z_k \right) \tag{7.4}$$

Letting

$$q_k \triangleq \frac{1}{T} \left(d_{k+1} - d_k \right), \tag{7.5}$$

we have that

$$p_k = -u_k^T R_d u_k - u_k^T q_k \tag{7.6}$$

Let the z-transforms of the discrete-time sampled variables be denoted by overbar; i.e., for discrete-time signal q_k,

$$\bar{q}(z) = \sum_{k=-\infty}^{\infty} z^{-k} q_k \tag{7.7}$$

134

Then following the methodology outlined in [49], the linear dynamics of the WEC as described in Section 3 are equivalent to the discrete time system

$$\bar{q}(z) = Z_{wq}(z)\bar{w}(z) + Z_{uq}(z)\bar{u}(z) \tag{7.8}$$

where $\{w_k, k \in \mathbb{Z}\}$ is an independent, identically distributed Gaussian stochastic sequence with $\mathcal{E}\, w_k = 0$ and $\mathcal{E}\, w_k w_k^T = I$. Transfer function $Z_{uq}(z)$ is solved in the frequency domain (i.e., for $z = e^{j\Omega}$, $\Omega \in [-\pi, \pi]$) via

$$Z_{uq}(e^{j\Omega}) = G_{uv}\left(i\frac{2}{T}\tan(\Omega/2)\right) \tag{7.9}$$

with the transfer function $Z_{uq}(z)$ obtained from the frequency-domain solution as the analytic continuation for all $|z| > 1$. Meanwhile, transfer function $Z_{wq}(z)$ is found by first finding the discrete-time power spectral density

$$\Sigma_{wq}(\Omega) = \frac{1}{T}G_{fv}\left(i\frac{2}{T}\tan(\Omega/2)\right) S_a\left(\frac{2}{T}\tan(\Omega/2)\right) G_{fv}^T\left(-i\frac{2}{T}\tan(\Omega/2)\right) \tag{7.10}$$

Then, from Σ_{wq}, transfer function $Z_{wq}(z)$ is its unique minimum-phase spectral factorization, found as the solution to

$$\Sigma_{wq}(\Omega) = Z_{wq}(e^{j\Omega})Z_{wq}(e^{-j\Omega})^T \tag{7.11}$$

7.2.2 Finite-Dimensional Discrete-Time Model

We assume that Z_{uq} and Z_{wq} have been approximated as finite-dimensional linear discrete-time systems, using a system identification technique. For example, in [47] subspace techniques are used to identify Z_{uq}. In [49], Z_{wq} is identified using the subspace spectral factorization technique described in [77]. The same procedures are used in the present paper, resulting in the discrete-time model we shall use for the

135

remainder of the paper:

$$x_{k+1} = Ax_k + B_w w_k + B_u u_k \tag{7.12}$$

$$q_k = C_q x_k + D_{wq} w_k + D_{uq} u_k \tag{7.13}$$

We assume that the identified realization is minimal; i.e., that all uncontrollable or unobservable modes have been eliminated. We assume that in approximating the system via a finite dimensional state space, the identification of the model parameters has been constrained such that the properties inherited from Assumptions 3.6.1, 3.6.2 and 3.6.3 still hold for finite-dimensional approximations.

$$Z_{uq}(z) \approx C_q [zI - A]^{-1} B_q + D_{uq} \tag{7.14}$$

$$Z_{wq}(z) \approx C_q [zI - A]^{-1} B_w + D_{wq} \tag{7.15}$$

The discrete time transfer function $Z_{uq}(z)$ and $Z_{wq}(z)$ have zeros at $z = 1$, implying that

$$D_{uq} + C_q [I - A]^{-1} B_u = 0 \tag{7.16}$$

$$D_{wq} + C_q [I - A]^{-1} B_w = 0 \tag{7.17}$$

Note that for this model, it is the case that

$$d_{k+1} = d_0 + T \sum_{i=0}^{k} q_i \tag{7.18}$$

$$= d_0 + T \sum_{i=0}^{k} C_q x_i + D_w w_i + D_q u_i \tag{7.19}$$

which, using the consequence of assumption A3 above, implies

$$d_{k+1} = d_0 + TC_q[I - A]^{-1} \sum_{i=0}^{k} (x_i - Ax_i - B_w w_i - B_u u_i) \tag{7.20}$$

$$= d_0 + TC_q[I - A]^{-1} \sum_{i=0}^{k} (x_i - x_{i+1}) \tag{7.21}$$

$$= d_0 + TC_q[I - A]^{-1} x_0 - TC_q[I - A]^{-1} x_{k+1} \tag{7.22}$$

Assuming the system is initiated at a zero initial state at $k = 0$, then it follows that

$$d_k = C_d x_k \tag{7.23}$$

where $C_d \triangleq -TC_q[I - A]^{-1}$.

7.2.3 Assumptions

We note that for the discrete-time system model, four assumptions will be made here which are the discrete time version of the assumptions in continuous case:

Assumption 7.2.1. *$Z_{uq}(z)$ is OSPR in discrete-time; i.e., it is analytic in the open region of the complex plane exterior to the unit disk, and there exist a $\beta \in \mathbb{R}_{>0}$*

$$Z_{uq}(\alpha e^{j\Omega}) + Z_{uq}^H(\alpha e^{-j\Omega}) \geqslant \beta Z_{uq}^H(\alpha e^{-j\Omega}) Z(\alpha e^{j\Omega}) \tag{7.24}$$

for all $\Omega \in [0, 2\pi)$ and $\beta \in \mathbb{R}_{>0}$ with $|\alpha| \geqslant 1$.

Assumption 7.2.2. *$\{u, w\} \rightarrow \{q, d\}$ has ℓ_2 bounded gain;*

Assumption 7.2.3. *The discrete time system which mapping $\{u, w\} \rightarrow \{q, d\}$ is the minimal realization.*

This is the assumption we made when constructing state space model.

Assumption 7.2.4. *Let* $\{Z_{uq}, Z_{wq}\}$ *be the discrete time open loop transfer function from* $\{u, w\}$ *to* q; *i.e.,*

$$[Z_{uq} \quad Z_{wq}] \sim \left[\begin{array}{c|cc} A & B_u & B_w \\ \hline C_q & D_{uq} & D_{wq} \end{array}\right]$$

Then there exists $U \in \mathcal{H}_\infty$ *such that* $Z_{uq}U = Z_{wq}$

7.3 Optimal Linear Control Design with Mean-Square Stroke Constraints

We wish to design a feedback law $\mathcal{K} : d \mapsto u$ which maximizes the mean power generation $\bar{p} \triangleq \mathcal{E} p$, with the expectation evaluated in stationary response. In this section we begin with the design of a linear controller, which while not explicitly enforcing the stroke constraints at every time, enforces them in a mean-square sense. In the next section we will then design a nonlinear controller, based on this linear design, which does enforce the stroke constraints at every time, explicitly.

To be more specific, suppose that the true stroke limit of the PTO is d_m; i.e., the condition $|d_i(t)| \leqslant d_{mi}, i \in \{1..n_p\}$ must be enforced. In order to enforce this explicitly, nonlinear control is required. In this section, we replace this condition with a more relaxed one, which places a constraint on the mean-square value of the stroke; i.e., on the quantity

$$s_{di} \triangleq \mathcal{E} d_i{}^2, \quad i \in \{1..n_p\} \tag{7.25}$$

with the expectation taken in stationarity.

Specifically, our constraint will be of the form

$$s_{di} \leqslant \tfrac{1}{4}d_{mi}^2, \quad i \in \{1..n_p\} \tag{7.26}$$

The reason that we choose the $\frac{1}{4}d_m$ value here is the same as the one in Chapter 6. As such, it ensures that the linear controller will render most peaks within the stroke limit, with only the outliers needing to be dealt with via nonlinear control.

For the linear control design, we consider finite-dimensional time-invariant controllers, which can be parametrized by matrices $\{A_K, B_K, C_K\}$ in the feedback form

$$\xi_{k+1} = A_K\xi_k + B_Kd_k \tag{7.27}$$

$$u_k = C_K\xi_k \tag{7.28}$$

This results in an augmented closed-loop system

$$\chi_{k+1} = A_{cl}\chi_k + B_{wcl}w_k \tag{7.29}$$

$$q_k = C_{qcl}\chi_k + D_{qcl}w_k \tag{7.30}$$

$$d_k = C_{dcl}\chi_k \tag{7.31}$$

$$u_k = C_{ucl}\chi_k \tag{7.32}$$

where

$$A_{cl} = \begin{bmatrix} A & B_uC_K \\ B_KC_d & A_K \end{bmatrix} \tag{7.33}$$

$$B_{wcl} = \begin{bmatrix} B_w \\ 0 \end{bmatrix} \tag{7.34}$$

$$C_{qcl} = \begin{bmatrix} C_q & D_{uq}C_K \end{bmatrix} \tag{7.35}$$

$$D_{qcl} = D_{wq} \tag{7.36}$$

$$C_{dcl} = \begin{bmatrix} C_d & 0 \end{bmatrix} \tag{7.37}$$

$$C_{ucl} = \begin{bmatrix} 0 & C_K \end{bmatrix} \tag{7.38}$$

We then consider the following optimization problem:

$$
\begin{aligned}
\text{Given:} &\quad A, B_w, B_u, C_q, D_{wq}, D_{uq}, C_d \\
\text{Maximize:} &\quad \bar{p} \triangleq \mathcal{E}\, p \\
\text{Constraint:} &\quad s_{di} < \tfrac{1}{4} d_{mi}^2,\, i \in \{1..n_p\} \\
\text{Over:} &\quad A_K, B_K, C_K
\end{aligned}
\tag{7.39}
$$

where in the above problem, the expectations are taken in stationarity.

To perform this optimization, we need the following theorem:

Theorem 7.1. *For any linear feedback parameters $\{A_K, B_K, C_K\}$ which stabilize the closed-loop system,*

$$
\bar{p} = \bar{p}_0 - \mathcal{E}\left\{ (u - Fx)^T \Delta\, (u - Fx) \right\}
\tag{7.40}
$$

where we define $\tilde{R} \triangleq R_d + \tfrac{1}{2} D_{uq} + \tfrac{1}{2} D_{uq}^T$, and

$$
F \triangleq -(\tilde{R} - B_u^T W B_u)^{-1}(\tfrac{1}{2} C_q^T - A^T W B_u)^T
\tag{7.41}
$$

with W is the solution to the DARE

$$
W = A^T W A + (\tfrac{1}{2} C_q^T - A^T W B_u)(\tilde{R} - B_u^T W B_u)^{-1}(\tfrac{1}{2} C_q^T - A^T W B_u)^T
\tag{7.42}
$$

The causal power generation limit p_0 on discrete time system is defined as:

$$
\bar{p}_0 \triangleq \mathrm{Tr}\{B_w^T W B_w\}
\tag{7.43}
$$

and $\Delta \triangleq \tilde{R} - B_u^T W B_u$.

Proof. The proof here can be found analogous to Theorem 5.1 in Chapter 5 with only superficial differences. □

Theorem 7.1 implies that the maximization of average generated power is equiv-

alent to the minimization of the second term on the right-hand side of (7.40), which is positive semidefinite. In particular, it leads to the following result:

Theorem 7.2. *Control parameters $\{A_K, B_K, C_K\}$ result in the mean power generation bound $\bar{p} > \gamma$ and mean-square stroke bound $s_{di} < \frac{1}{4}d_{mi}^2, i \in \{1..n_p\}$, for some $\gamma \in \mathbb{R}$, if and only if there exists a matrix $S = S^T > 0$ such that*

$$S - A_{cl}SA_{cl}^T - B_{wcl}B_{wcl}^T > 0 \tag{7.44}$$

$$(F_{cl} - C_{ucl}) S (F_{cl} - C_{ucl})^T < \bar{p}_0 - \gamma \tag{7.45}$$

$$i \in \{1..n_p\}, \quad C_{dicl}SC_{dicl}^T < \frac{1}{4}d_{mi}^2 \tag{7.46}$$

Proof. Let $\Sigma = \mathcal{E}\,\chi\chi^T$. Then Σ is the solution to Lyapunov equation

$$A_{cl}\Sigma A_{cl}^T - \Sigma + B_{wcl}B_{wcl}^T = 0 \tag{7.47}$$

and the existence of closed-loop stationarity implies that $\Sigma \geqslant 0$ and that A_{cl} is asymptotically stable in discrete-time. The corresponding power generation performance is then as in (7.40), i.e.,

$$\bar{p} = \bar{p}_0 - (F_{cl} - C_{ucl}) \Sigma (F_{cl} - C_{ucl})^T \tag{7.48}$$

Now, let S be the solution to

$$A_{cl}SA_{cl}^T - S + B_{wcl}B_{wcl}^T = -\epsilon I \tag{7.49}$$

for some $\epsilon > 0$. It follows that

$$A_{cl}(S - \Sigma)A_{cl}^T - (S - \Sigma) = -\epsilon I \tag{7.50}$$

141

which, due to the asymptotic stability of A_{cl} implies that $S - \Sigma > 0$. As a result, we have that

$$\gamma \triangleq \bar{p}_0 - (F_{cl} - C_{ucl}) S (F_{cl} - C_{ucl})^T \tag{7.51}$$

$$= \bar{p} - \delta \tag{7.52}$$

where

$$\delta = (F_{cl} - C_{ucl}) (S - \Sigma) (F_{cl} - C_{ucl})^T \tag{7.53}$$

By making ϵ arbitrarily small, δ can be made arbitrarily small and consequently γ can be made to approach $\bar{p}$ from below. A similar argument can be made for the constraint on s_{di}, and noting that

$$s_{di} = C_{dicl} \Sigma C_{dicl}^T \tag{7.54}$$

This proves necessity.

To prove sufficiency, we note that if $S = S^T > 0$ satisfies (7.44) then A_{cl} must be asymptotically stable, implying the existence of a stationary solution to $\Sigma = \mathcal{E} \chi \chi^T > 0$ satisfying (7.47). We then have that $S - \Sigma$ satisfies

$$A_{cl}(S - \Sigma)A_{cl}^T - (S - \Sigma) < 0 \tag{7.55}$$

which, due to the asymptotic stability of A_{cl} implies that $S - \Sigma > 0$. This guarantees that $\delta > 0$ and thus that $\bar{p} < \gamma$. It similarly guarantees that $C_{dicl}(S - \Sigma)C_{dicl}^T > 0$, and consequently that $\frac{1}{4}d_{mi}^2 > s_{di}$. $\qquad \square$

Theorem 7.3. *There exists a set of control parameters $\{A_K, B_K, C_K\}$ resulting in mean power generation bound $\bar{p} > \gamma$ and mean-square stroke bound $s_{di} < \frac{1}{4}d_{mi}^2, i \in \{1..n_p\}$, for some $\gamma \in \mathbb{R}$, if and only if there exist matrices $X = X^T > 0, Y = Y^T > 0$*

$\hat{A}$, $\hat{B}$, and $\hat{C}$ such that

$$
\begin{bmatrix}
X & I & AX + B_u\hat{C} & A & B_w \\
I & Y & \hat{A} & YA + \hat{B}C_d & YB_w \\
XA^T + \hat{C}^T B_u^T & \hat{A}^T & X & I & 0 \\
A^T & A^T Y + C_d^T \hat{B}^T & I & Y & 0 \\
B_w^T & B_w^T Y & 0 & 0 & I
\end{bmatrix} > 0 \qquad (7.56)
$$

$$
\begin{bmatrix}
p_0 - \gamma & FX - \hat{C} & F \\
XF^T - \hat{C}^T & X & I \\
F^T & I & Y
\end{bmatrix} > 0 \qquad (7.57)
$$

$$
i \in \{1..n_p\}, \qquad
\begin{bmatrix}
\frac{1}{4}d_{mi}^2 & C_{di}X & C_{di} \\
XC_{di}^T & X & I \\
C_{di}^T & I & Y
\end{bmatrix} > 0 \qquad (7.58)
$$

One such controller can be found as

$$
A_K = N^{-1}\left(\hat{A} - \hat{B}C_dX - YB_u\hat{C} - YAX\right)M^{-T} \qquad (7.59)
$$

$$
B_K = N^{-1}\hat{B} \qquad (7.60)
$$

$$
C_K = \hat{C}M^{-T} \qquad (7.61)
$$

where M and N are any matrices such that $MN^T = I - XY$.

Proof. The proof follows in a manner entirely analogous to the Theorem 6.1 in Chapter 6, with only superficial differences. □

The above theorem provides a convex domain over which to optimize a linear con-
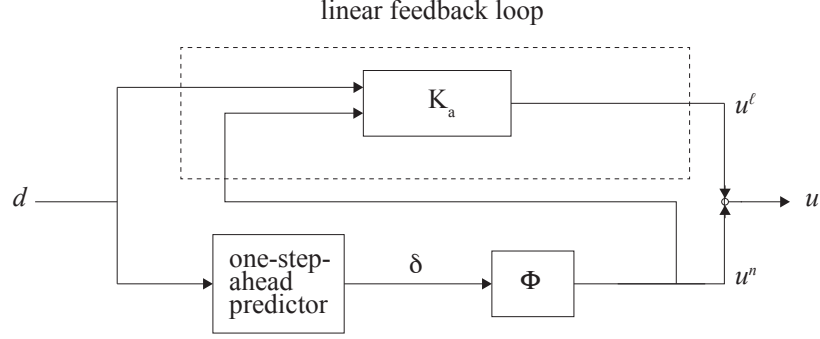
Figure 7.2: Design of augmented linear feedback law K_a and nonlinear feedback law Φ

troller. Specifically, the optimal control problem from (7.39) becomes, equivalently,

$$
\begin{array}{ll}
\text{Given:} & A, B_w, B_u, C_q, D_{wq}, D_{uq}, C_d, d_m \\
\text{Maximize:} & \gamma \\
\text{Constraints:} & (7.56), (7.57), (7.58) \\
\text{Over:} & X = X^T, Y = Y^T, \hat{A}, \hat{B}, \hat{C}, \gamma
\end{array}
\tag{7.62}
$$

7.4 Passivity-based Linear Control Redesgin

7.4.1 Passivity-Based Design Strategy

In section 7.3, we propose a linear $K^\star$ to make sure mean-square stroke value below safety limit. However, this is not enough to meet stroke saturation requirement. We need to put a strict constraint on stroke value, i.e., $d_{ki} \leqslant d_{mi}, i \in \{1..n_p\}$. By doing this, nonlinearity was introduced into the controller design. In this paper, we apply a new technique of passivity-based linear controller design. The technique can be described as follows:

Extend the optimal linear controller $K^\star$ from (7.62), add another exogenous input u^n, making the new control law: $K_a : \{d, u^n\} \to u^l$ that preserves $K^\star$ when $u^n = 0$; i.e $K(\cdot, 0) = K^\star$, and also design mapping: $u^n \to q$ is OSP. And nonlinear feedback law $\Phi : d \to u^n$ will be designed in next section. Since it is in discrete time domain,

it is not quite same as continuous time case. Moreover, feedback function $\Phi(\cdot)$ need to be mean-square passive with respect to q to satisfy close-loop system stability.

Since the mapping: $u^n \to q$ is OSP, and nonlinear feedback law $\Phi(\cdot)$ is mean-square passive, close-loop system is stable according to the following Theorem. Note, notation Z_{nq} refer to the discrete time transfer function from u^n to q. Similarly, Z_{wq} is the discrete time transfer function for $w \to q$

Theorem 7.4. *Suppose that $Z_{nq} \in \mathcal{H}_\infty$ is OSPR; i.e.,*

$$\sum_{k=0}^{\infty}(u_k^n - \beta_1 q_k)^T q_k \geq 0 \tag{7.63}$$

for some $\beta_1 > 0$, and that there exists some transfer function $U \in \mathcal{H}_\infty$ such that

$$Z_{wq} = Z_{nq} U \tag{7.64}$$

Further suppose an outer feedback loop $Q : \{q, d\} \to u^n$ is imposed, which has the property that it is mean-square passive with respect to q, i.e., for all $N \geq 0$, and with $d_0 = 0$, there exists a constant β_2 such that:

$$\mathcal{E}\{\frac{1}{N}\sum_{k=0}^{N} u_k^n q_k\} \leq \beta_2 \tag{7.65}$$

Then with this feedback law imposed, whole feedback system is mean-square stable.

Proof. If (7.64) is true for some $U \in \mathcal{H}_\infty$ then Z_{wq} may be equivalently represented by eliminating the explicit input channel w, and instead incorporating the effects of w through the q input channel, via the substitution $u^n \leftarrow u^n + u^w$, where $\{u_k^w\}$ is a stochastic process with spectrum $U(e^{j\theta})U^T(e^{-j\theta})$. Requiring $U \in \mathcal{H}_\infty$ ensures that that $\{u_k^w\}$ has finite stationary covariance. From Z_{nq} is OSPR, we know that

$$\langle u, q \rangle_N \geq \beta_1 \|q\|_N^2$$

145

Since u^n is mwan-square passive with respect to q, we can write it in the form of inner product:

$$\langle u^n, q \rangle_N \leq \beta_2$$

Based on the figure, we know that

$$\langle u^w, q \rangle_N = \langle u, q \rangle_N - \langle u^n, q \rangle_N \geq \beta_1 \|q\|_N^2 - \beta_2$$

But by the Cauchy-Schwartz inequality, $\langle u^w, q \rangle_N \leq \|u^w\|_N \|q\|_N$, so

$$\|u^w\|_N \|q\|_N \geq \beta_1 \|q\|_N^2 - \beta_2$$

And consequently, we have that :

$$\|q\|_N \leq \frac{\|u^w\|_N}{2\beta_1} + \sqrt{\left(\frac{\|u^w\|_N}{2\beta_1}\right)^2 + \frac{\beta_2}{\beta_1}}$$

It follows that if $\|u_w\|_N$ is bounded as $N \to \infty$, $\|q\|_N$ should also be bounded. The mapping: $u_f \to q$ is mean-square stable. $\qquad\square$

7.4.2 Finite-Dimensional Augmentation of K_a

$$K_a \sim \left[\begin{array}{cc|cc} A_K^\star & A_{12} & B_K^\star & B_{12} \\ 0 & A_{22} & 0 & B_{22} \\ \hline C_K^\star & C_2 & 0 & 0 \end{array} \right] \tag{7.66}$$

where $\{A_{12}, B_{12}, A_{22}, B_{22}, C_2\}$ are new design variables, and where we note that the mapping $d \mapsto u$ remains the same $K^\star$ found from (7.62). With the above controller

146

imposed in closed-loop, the mapping $Z \triangleq \{w, u^n\} \mapsto \{q, d\}$ can be written as

$$
Z \sim \left[
\begin{array}{cc|cc}
A_{cl}^\star & \begin{bmatrix} B_u C_2 \\ A_{12} \end{bmatrix} & B_{wcl} & \begin{bmatrix} B_u \\ B_{12} \end{bmatrix} \\
0 & A_{22} & 0 & B_{22} \\
\hline
C_{qcl}^\star & D_{uq} C_2 & D_{wq} & D_{uq} \\
C_{dcl} & 0 & 0 & 0
\end{array}
\right]
\tag{7.67}
$$

where

$$
A_{cl}^\star = \begin{bmatrix} A & B_u C_K^\star \\ B_K^\star C_d & A_K^\star \end{bmatrix}, \quad B_{wcl} = \begin{bmatrix} B_w \\ 0 \end{bmatrix}
\tag{7.68}
$$

$$
C_{qcl}^\star = \begin{bmatrix} C_q & D_{uq} C_K^\star \end{bmatrix}, \quad C_{dcl} = \begin{bmatrix} C_d & 0 \end{bmatrix}
\tag{7.69}
$$

To design $\{A_{12}, A_{22}, B_{12}, B_{22}, C_2\}$, we first prove that there exists at least one parameter sert which renders Z_{nq} OSP.

Theorem 7.5. *Let assumptions 7.2.1, 7.2.2 and 7.2.3 hold. Let L_2 be an arbitrary matrix of compatible dimension, and L_3 be a matrix of compatible dimension for which*

$$
\left[
\begin{array}{c|c}
A + B_u L_3 & B_u \\
\hline
C_q + D_{uq} L_3 & D_{uq}
\end{array}
\right]
$$

is OSP. Then the following parameters result in OSP Z_{nq}:

$$A_{22} = A + B_u L_3 \tag{7.70a}$$

$$A_{12} = L_2 A + L_2 B_u L_3 - A_K L_2 - B_K C_d \tag{7.70b}$$

$$B_{12} = L_2 B_u \tag{7.70c}$$

$$B_{22} = B_u \tag{7.70d}$$

$$C_2 = -C_K L_2 + L_3 \tag{7.70e}$$

Proof. The proof is completely parallel to the one in continuous time case. The detailed proof can refer to the Theorem 6.4 in the Chapter 6. $\square$

The above theorem proves that there always exists at least one K_a which renders Z_{nq} OSP. However, it does not ensure that, for this Z_{nq}, there exists a $U \in \mathcal{H}_\infty$ such that (7.64) holds. For this, we require an additional assumption 7.2.4.

Theorem 7.6. *Let Assumptions 7.2.1, 7.2.2, 7.2.3, and 7.2.4 hold. Let augmented controller K_a be as in (7.66) with parameters $\{A_{12}, A_{22}, B_{12}, B_{22}, C_2\}$ determined by (7.70). Then there exists a $U \in \mathcal{H}_\infty$ satisfying (7.64).*

Proof. The proof is completely parallel to the one in continuous time case. The detailed proof can refer to the Theorem 6.5 in the Chapter 6 $\square$

7.4.3 Designing K_a Augmentation Parameters

Wth the knowledge there there exists at least one feasible design for K_a (i.e., a design that renders Z_{nq} OSP), it remains to determine the best feasible design via optimization. There does not appear to be an obvious way to transform the output-strict passivity constraint into a convex constraint on parameters $\{A_{12}, A_{22}, B_{12}, B_{22}, C_2\}$, without the introduction of conservatism. As such, the theorem below characterizes

a convex subdomain which contains, in its closure, the known feasibility point found in Theorem 7.5.

Theorem 7.7. *Let assumptions 7.2.1, 7.2.2, and 7.2.3 hold. Let $S_1 = S_1^T \in \mathbb{R}^{2n \times 2n}$, $S_2 = S_2^T \in \mathbb{R}^{n \times n}$, $\tilde{B}_{12}, \in \mathbb{R}^{n \times n_p}$, $B_{22} \in \mathbb{R}^{n \times n_p}$, $\tilde{L}_3 \in \mathbb{R}^{n_p \times n}$, and $\beta \in \mathbb{R}_{>0}$ be such that*

$$\text{He}\{\Xi\} \leqslant 0 \tag{7.71}$$

$$S_1 > 0, \quad S_2 > 0 \tag{7.72}$$

where

$$
\Xi \triangleq \left\{
\begin{array}{cc}
\frac{1}{2}(A_{cl}^\star S_1 A_{cl}^{\star\,T} - S_1) & 0 \\[2mm]
0 & \frac{1}{2}\{\Gamma_1 - S_2\} \\[2mm]
C_{qcl}^\star S_1 A_{cl}^{\star\,T} & \Gamma_2 \\[2mm]
\begin{bmatrix} B_u^T - B_{22}^T & B_{12}^T - B_{22}^T L_2^T \end{bmatrix} & B_{22}^T \\[2mm]
0 & 0
\end{array}
\right.
$$
$$
\left.
\begin{array}{ccc}
-\begin{bmatrix} B_u - B_{22} \\ B_{12} - L_2 B_{22} \end{bmatrix} & 0 & 0 \\[4mm]
-B_{22} & 0 & B_u \tilde{L}_3 \\[2mm]
-D_{uq} + \frac{1}{2}\{C_{qcl}^\star S_1 C_{qcl}^{\star\,T} + \Gamma_3\} & 0 & D_{uq}\tilde{L}_3 \\[2mm]
D_{uq}^T & -\frac{1}{2\beta}I & 0 \\[2mm]
0 & 0 & -\frac{1}{2}S_2
\end{array}
\right\} \tag{7.73}
$$

$$\Gamma_1 \triangleq AS_2 A^T + A\tilde{L}_3^T B_u^T + B_u \tilde{L}_3 A^T \tag{7.74}$$

$$\Gamma_2 \triangleq C_q S_2 A^T + D_{uq}\tilde{L}_3 A^T + C_q \tilde{L}_3 B_u^T \tag{7.75}$$

$$\Gamma_3 \triangleq C_q S_2 C_q^T + D_{uq}\tilde{L}_3 C_q^T + C_q \tilde{L}_3^T D_{uq}^T \tag{7.76}$$

Let the mapping $u^n \mapsto q$ be parametrized by $\{A_{12}, A_{22}, B_{12}, B_{22}, C_2\}$ as in (7.67),

149

with

$$A_{12} = L_2 A_{22} - A_K L_2 - B_k C_d \tag{7.77}$$

$$A_{22} = A + B_u \tilde{L}_3 S_2^{-1} \tag{7.78}$$

$$B_{12} = \tilde{B}_{12} + L_2 B_{22} \tag{7.79}$$

$$C_2 = -C_k L_2 + \tilde{L}_3 S_2^{-1}. \tag{7.80}$$

where L_2 is an arbitrary matrix of compatible dimension. Then the mapping $u^n \mapsto q$ is OSP.

Proof. From Theorem 7.5 we have that the with A_{22}, A_{12}, and C_2 defined as in (7.70a), (7.70b), (7.70e) respectively, Z_{nq} is

$$Z_{nq} \sim \left[\begin{array}{cc|c} \begin{matrix} A_{cl}^{\star} & 0 \\ \\ 0 & A + B_u L_3 \end{matrix} & \begin{bmatrix} B_u - B_{22} \\ B_{12} - L_2 B_{22} \end{bmatrix} \\ & B_{22} \\ \hline C_{qcl}^{\star} \quad C_q + D_{uq} L_3 & D_{uq} \end{array} \right] \tag{7.81}$$

We then have that Z_{nq} is OSPR if and only if there exists $S = S^T$ and a $\beta > 0$ such

that

$$\text{He}\left\{\begin{bmatrix} \frac{1}{2}(A^\star S A^{\star T} - S) & -\begin{bmatrix} B_u - B_{22} \\ B_{12} - L_2 B_{22} \end{bmatrix} \\ & -B_{22} \\ -C_q^\star S A^{\star T} & -D_{uq} + \frac{1}{2} C_q^\star S C_q^{\star T} \end{bmatrix}\right\}$$

$$+ \beta \begin{bmatrix} \begin{bmatrix} B_u - B_{22} \\ B_{12} - L_2 B_{22} \end{bmatrix} \\ B_{22} \\ D_{uq} \end{bmatrix} \begin{bmatrix} \begin{bmatrix} B_u - B_{22} \\ B_{12} - L_2 B_{22} \end{bmatrix} \\ B_{22} \\ D_{uq} \end{bmatrix}^T \leqslant 0 \quad (7.82)$$

as well as

$$E_c^T S E_c > 0, \tag{7.83}$$

where we denote that

$$A^\star \triangleq \begin{bmatrix} A_{cl}^\star & 0 \\ 0 & A + B_u L_3 \end{bmatrix} \tag{7.84}$$

$$C_q^\star \triangleq \begin{bmatrix} C_{qcl}^\star & C_q + D_{uq} L_3 \end{bmatrix} \tag{7.85}$$

E_c is a full-column-rank matrix spanning the controllable subspace of the state space realization for Z_{nq}. Assuming $E_c = I$ is therefore sufficient to guarantee this condition.

□

Theorem 7.7 provides conditions guaranteeing that $u^n \mapsto q$ is OSP, but in order for Theorem 7.4 to hold, it must also be shown that there exists $U \in \mathcal{H}_\infty$ satisfying (7.64). To present the condition guaranteeing this, first let $\{\theta_1, ...\theta_p\}$ be the set of all

solutions to the eigenvalue problem

$$
\begin{bmatrix} A - e^{j\theta}I & B_u \\ C_q & D_{uq} \end{bmatrix}^H \eta = 0 \quad , \eta \neq 0, \quad \theta \in [0, 2\pi) \tag{7.86}
$$

where $p \in \mathbb{Z}$ is the number of imaginary-axis zeros of Z_{uv} (counting multiplicity). Define $N \triangleq \begin{bmatrix} \eta_1 & \cdots & \eta_p \end{bmatrix}$ as the corresponding (linearly independent) set of eigenvectors. Define $N_\perp$ as a full-column-rank matrix such that $\begin{bmatrix} N & N_\perp \end{bmatrix}$ is square and $N^H N_\perp = 0$.

Lemma 7.8. *Let* $\{A, B_u, C_q, D_{uq}\}$ *satisfy positive real constraint for some* $S \geqslant 0$ *and* $\beta > 0$, *and let* N *and* $N_\perp$ *defined as above. Then*

$$
N_\perp^H \begin{bmatrix} ASA^T - S & ASC_q^T - B_u \\ C_q SA^T - B_u^T & -D_{uq} - D_{uq}^T + C_q SC_q^T \end{bmatrix} N_\perp \leqslant 0 \tag{7.87}
$$

Proof. Consider that for each $i \in \{1...p\}$, for $\theta_i \in [0, 2\pi)$,

$$
\begin{aligned}
&\eta_i^H \begin{bmatrix} ASA^T - S & ASC_q^T - B_u \\ C_q SA^T - B_u^T & -D_{uq} - D_{uq}^T + C_q SC_q^T \end{bmatrix} \eta_i \\
&= \eta_i^H \operatorname{He} \left\{ \begin{bmatrix} A - e^{j\theta}I & B_u \\ C_q & D_{uq} \end{bmatrix} \begin{bmatrix} S & 0 \\ 0 & I \end{bmatrix} \begin{bmatrix} A^H + e^{-j\theta}I & C_q^H \\ 0 & -I \end{bmatrix} \right\} \eta_i \\
&= 0
\end{aligned} \tag{7.88}
$$

implying that the first p diagonal terms of the matrix

$$
\begin{bmatrix} N^H \\ N_\perp^H \end{bmatrix} \begin{bmatrix} ASA^T - S & ASC^T - B_u \\ CSA^T - B_u^T & -D_{uq} - D_{uq}^T + CSC^T \end{bmatrix} \begin{bmatrix} N^H \\ N_\perp^H \end{bmatrix}^H \tag{7.89}
$$

must be zero. Now if passivity holds then implys that matrix above is negative

semidefinite. In order for this to be truesimultaneously with the first p diagnoal terms being zero, the first p rows and columns should also be zero. In order to keep negative semidefinite of matrix, equation (7.87) should be valid. □

Furthermore, partition $N_\perp$ as

$$N_\perp = \begin{bmatrix} N_{\perp 1} \\ N_{\perp 2} \end{bmatrix}, \quad N_{\perp 1} \in \mathbb{C}^{n \times p} \tag{7.90}$$

Then in terms of $\{N_{\perp 1}, N_{\perp 2}\}$, we have the following theorem:

Theorem 7.9. *In Theorem 7.7, let Assumption 7.2.4 hold. Let parameters $\{S_1, S_2, \tilde{B}_{12}, B_{22}, \tilde{L}_3, \beta\}$ satisfy (7.71), (7.72), and let K_a be as in in (7.66). Let*

$$\Upsilon_\perp \triangleq \begin{bmatrix} I & 0 & N_{\perp 1} & 0 \\ 0 & I & 0 & 0 \\ 0 & 0 & N_\perp & 0 \\ 0 & 0 & 0 & 0 \\ 0 & 0 & 0 & I \end{bmatrix} \tag{7.91}$$

Then if (7.71) *is strengthened to require that*

$$\Upsilon_\perp^H \Xi \Upsilon_\perp < 0 \tag{7.92}$$

then there exists $U \in \mathcal{H}_\infty$ satisfying (7.64).

Proof. The proof is completely parallel to the one in continuous time case. The detailed proof can refer to the Theorem 6.8 at the Chapter 6 □

Theorem 7.7 provides a parametric domain over which to optimize K parameters $\{A_{12}, A_{22}, B_{12}, B_{22}, C_2\}$ which is convex, and the closure of which is guaranteed to contain a feasible point. Given this, it remains to determine a suitable metric under which

to optimize these parameters, which is also convex in the $\{S_1, S_2, \tilde{B}_{12}, B_{22}, \tilde{L}_3, \beta\}$ domain.

To do this, consider that Z_{nq} can be written as

$$Z_{nq} = Z_0 + Z_1 \tag{7.93}$$

where

$$Z_0 \sim \left[\begin{array}{c|c} A_{cl}^{\star} & \begin{bmatrix} B_u \\ 0 \end{bmatrix} \\ \hline C_{qcl}^{\star} & D_{uq} \end{array} \right] \tag{7.94}$$

$$Z_1 \sim \left[\begin{array}{cc|c} A_{cl}^{\star} & \begin{bmatrix} B_u C_2 \\ A_{12} \end{bmatrix} & \begin{bmatrix} 0 \\ B_{12} \end{bmatrix} \\ 0 & A_{22} & B_{22} \\ \hline C_{qcl}^{\star} & D_{uq} C_2 & 0 \end{array} \right] \tag{7.95}$$

As such, Z_0 is the transfer function from u^n to q without control augmentation, while Z_1 is the adjustment to this transfer function to make Z_{nq} OSP. We wish to choose $\{S_1, S_2, \tilde{B}_{12}, B_{22}, \tilde{L}_3\}$ to minimize the gain Z_1, subject to constraints (7.71) and (7.72). To do this, a norm must be chosen for the gain to be minimized, and here we choose the $\mathcal{H}_2$ norm. The following theorem establishes a means of accomplishing this.

Theorem 7.10. $\|T_1\|_{\mathcal{H}_2}^2 < \lambda$ *if there exists* $S_3 = S_3^T > 0$ *and* $\alpha > 0$ *such that*

$$
\begin{bmatrix}
A_{cl}^\star S_3 (A_{cl}^\star)^T - S_3 & 0 & \cdot \begin{bmatrix} -B_{22} \\ \tilde{B}_{12} \end{bmatrix} & 0 \\
 & \Gamma_1 - S_2 & B_{22} & B_u \tilde{L}_3 \\
 & & -\frac{1}{\alpha} I & 0 \\
(sym) & & & -S_2
\end{bmatrix} \leqslant 0
\tag{7.96}
$$

$$
\begin{bmatrix}
\alpha \lambda & C_{qcl}^\star S_3 & C_q S_2 + D_{uq} \tilde{L}_3 \\
 & S_3 & 0 \\
(sym) & & S_2
\end{bmatrix} > 0
\tag{7.97}
$$

where $\{S_2, \Gamma_1, \tilde{B}_{12}, B_{22}, \tilde{L}_3\,\beta\}$ *are the same as in* (7.71).

Proof. From the proof to Theorem 7.7, it follows that

$$
T_1 \sim \left[\begin{array}{c|c} A^\star & B_u^\star \\ \hline C_q^\star & 0 \end{array} \right]
\tag{7.98}
$$

where

$$
B_u^\star = \begin{bmatrix} -B_{22} \\ \tilde{B}_{12} \\ B_{22} \end{bmatrix}
\tag{7.99}
$$

It is a standard result that $\|T_1\|_{\mathcal{H}_2}^2 < \lambda$ if and only if there exists a matrix $S = S^T > 0$, such that

$$
A^\star S A^{\star T} - S + B_u^\star B_u^{\star T} < 0
\tag{7.100}
$$

$$
\mathrm{Tr}\{C_q^\star S C_q^\star\} < \lambda
\tag{7.101}
$$

155

Conservatively choosing

$$S = \frac{1}{\alpha} \begin{bmatrix} S_3 & 0 \\ 0 & S_2 \end{bmatrix}, \tag{7.102}$$

and performing Schur complements on both inequalities, gives (7.96) and (7.97). $\quad\square$

We therefore arrive at an optimization problem to determine parameters $\{S_1, S_2, S_3, \tilde{B}_{12}, B_{22}, \tilde{L}_3\}$:

$$\text{OP3}: \begin{cases} \text{Minimize:} & \lambda \\ \text{Domain:} & S_1, S_2, S_3, \tilde{B}_{12}, B_{22}, \tilde{L}_3 \\ \text{Constraints:} & (7.71), (7.72), (7.92), (7.96), (7.97). \end{cases} \tag{7.103}$$

7.5 Nonlinear Stroke Protection Loop

Consider the strong stroke limitation, i.e., $|d_i| \leq d_{mi}, i \in \{1..n_p\}$, linear controller K_a from previous section should be augmented with nonlinear feedback. The consequence of this is a total PTO force at time k which is a summation of the linear and nonlinear parts; i.e.,

$$u_k = u_k^\ell + u_k^n \tag{7.104}$$

where the linear control force u_k^ℓ is designed as in the section 5.4; i.e.,

$$u_k^\ell = C_K \xi_k \tag{7.105}$$

We may therefore view the nonlinear control loop as introducing a supplemental restoring force u_k^n which modifies the optimized linear feedback, when necessary, to prevent stroke saturation.

As shown in Figure 7.3, this nonlinear control loop consists of two components. The first of these is a one-step-ahead predictor, which forecasts the displacement that will result at discrete time $k+1$ (i.e., d_{k+1}) assuming only the linear control force is
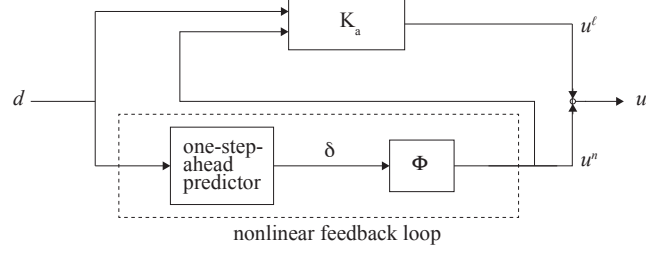
Figure 7.3: Design of linear and nonlinear feedback loops

applied; i.e., assuming $u_k = u_k^\ell$. This forecast is made using the values of y and u up to and including discrete-time k. We denote this forecast as δ_k.

The second part of the nonlinear control loop is the nonlinear function $u_k^n = \Phi(\delta_k)$, which acts as a kind of discrete-time "hard spring," producing a significant decelerating force when necessary. To illustrate the qualitative manner in which this is done, consider Figure 7.4, which shows a hypothetical time history for several discrete time steps over which d_k approaches its maximum allowable stroke d_m. As shown, the one-step-ahead predictor produces a forecast, at time k, of where d_{k+1} will be if u_k^n is made equal to 0. When this forecast has a magnitude well below d_m, the PTO stroke is deemed to be within its "safe zone" and $u_k^n = 0$. However, when the forecast has a magnitude above some threshold βd_m, for $\beta < 1$ equal to some safety factor (say, 0.9), the PTO stroke is deemed to be exiting its safe zone, triggering the nonlinear control loop to issue a corrective force to reverse its direction.

7.5.1 One-Step-Ahead Predictor Design

First note that

$$d_{k+1} = d_k + Tq_k \tag{7.106}$$

$$= d_k + T\left(C_q x_k + D_{uq} u_k + D_{wq} w_k\right) \tag{7.107}$$

157
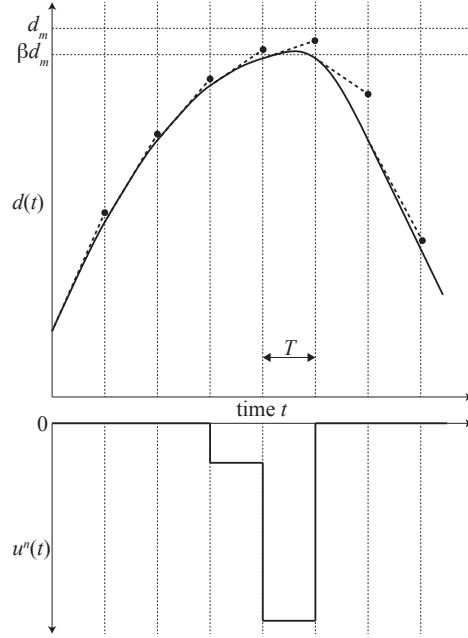
Figure 7.4: Upper plot: Trajectory for d (solid) with one-step-ahead prediction trajectories (dashed). Lower plot: Corresponding trajectory for nonlinear force u^n

We assume that at time k, the information that is known to the controller is comprised of

$$\mathcal{I}_k = \{d_k, u_k, d_{k-1}, u_{k-1}, d_{k-2}, u_{k-2}, ...\} \tag{7.108}$$

Let the conditional expectation for x_k, given this information, be denoted $\hat{x}_k$; i.e.,

$$\hat{x}_k \triangleq \mathcal{E}\left\{x_k | \mathcal{I}_k\right\} \tag{7.109}$$

Then we have the theorem 7.11 shows how to find $\hat{x}_k$ recursively.

Theorem 7.11. *Assuming we have the information of $\mathcal{I}_k$, $\hat{x}_k$ can be found as:*

$$\hat{x}_{k+1} = [A + LC_q]\,\hat{x}_k - Lq_k + B_u u_k \tag{7.110}$$

where the Kalman gain L is

$$L = -ASC_q^T\left[C_q S C_q^T + D_{wq} D_{wq}^T\right]^{-1} \tag{7.111}$$

and where the matrix $S = S^T$ is the solution to DARE

$$S = ASA^T + B_w B_w^T - ASC_q^T \left[C_q SC_q^T + D_{wq} D_{wq}^T \right]^{-1} C_q SA^T \tag{7.112}$$

Proof. The above theorem is mainly about the use of discrete time Kalman filter, the detailed derivation can be found in [92]. □

The forecasted displacement δ_k is the expected value of d_{k+1} for the specific case where the control input u_k is chosen as the linear control input only; i.e., $u_k = C_K \xi_k$, so

$$\delta_k = d_k + T \left(C_q \hat{x}_k + D_{uq} C_K \xi_k \right) \tag{7.113}$$

Consequently, the expectation of the true displacement and the forecast can be related via

$$\mathcal{E} \left\{ d_{k+1} | \mathcal{I}_k \right\} = \delta_k + T D_{uq} u_k^n \tag{7.114}$$

7.5.2 Nonlinearity Design

The nonlinear function $\Phi(\cdot)$ is designed to bring about a direction reversal of the one-step-ahead forecast δ_k, such that it remains inside the safe zone. To do this we note that if $\Phi(\delta_{ki}) \neq 0$ then this implies that $|\delta_{ki}| > \beta d_{mi}$. We seek the nonlinear control force u_{ki}^n which will result in

$$\left| \mathcal{E} \left\{ d_{(k+1)i} | \mathcal{I}_k \right\} \right| = \beta d_{mi}, \quad i \in \{1..n_p\} \tag{7.115}$$

In other words, we require that

$$\delta_{ki} + T D_{uq} u_{ki}^n = \beta d_{mi} \, \mathrm{sgn}(\delta_{ki}), \quad i \in \{1..n_p\} \tag{7.116}$$

resulting in the nonlinear feedback law $\Phi(\cdot)$ as

$$
\Phi(\delta_{ki}) = \begin{cases} 0 & : \quad |\delta_{ki}| < \beta d_{mi} \\ \Gamma\left(\beta d_{mi} - |\delta_{ki}|\right) \operatorname{sgn}(\delta_{ki}) & : \quad |\delta_{ki}| \geqslant \beta d_{mi} \end{cases} \qquad i \in \{1..n_p\} \qquad (7.117)
$$

where

$$
\Gamma = \frac{1}{TD_{uq}} \qquad (7.118)
$$

7.5.3   Mean-Square Passivity

The nonlinear control loop shown in Figure 7.3 has the advantage of being heuristic and therefore straight-forward to conceptualize, but in general it cannot be implemented without modification. This is because in many situations (including the example in this paper) the nonlinear feedback loop interacts with the linear controller in such a way as to destabilize the closed-loop system. In order to implement the technique, stability must be recovered.

To do this, we first note that the nature of the feedback function $\Phi(\cdot)$, as formulated here, has the special property of passivity, as illustrated in the lemma below. The proof of this lemma is lengthy, and consequently is omitted here in the interest of brevity.

Lemma 7.12. *The feedback function $\Phi(\delta_{ki})$ in (7.117) has the property that it is mean-square passive with respect to the q; i.e., for all $N \geqslant 0$, and with $d_0 = 0$, there exists a constant β such that*

$$
\mathcal{E}\left\{ \frac{1}{N} \sum_{k=0}^{N} \Phi(\delta_{ki}) q_{ki} \right\} \leqslant \beta, \quad i \in \{1..n_p\} \qquad (7.119)
$$

for any Γ in the range

$$
\Gamma \in \left[0, \frac{1}{TD_{uq}} \right] \qquad (7.120)
$$

160

Proof. Let $\hat{d}_{k+1} \triangleq \mathcal{E}\left\{d_{k+1}|\mathcal{I}_k\right\}$. Then

$$\hat{d}_{k+1} = \delta_k + TD_{uq}u_k^n \tag{7.121}$$

and consequently u_k^n can be expressed in terms of $\hat{d}_{k+1}$ as

$$u_k^n = \Gamma\left(\beta d_m - \left|\hat{d}_{k+1} - TD_{uq}u_k^n\right|\right)\mathrm{sgn}\left(\hat{d}_{k+1} - TD_{uq}u_k^n\right) \tag{7.122}$$

$$= \Gamma\beta d_m\,\mathrm{sgn}\left(\hat{d}_{k+1} - TD_{uq}u_k^n\right) - \Gamma\left(\hat{d}_{k+1} - TD_{uq}u_k^n\right) \tag{7.123}$$

$$= \frac{\Gamma}{1 - \Gamma TD_{uq}}\left(\beta d_m\,\mathrm{sgn}\left(\hat{d}_{k+1} - TD_{uq}u_k^n\right) - \hat{d}_{k+1}\right) \tag{7.124}$$

Next, we recognize that if $TD_{uq}\Gamma \leqslant 1$, then it follows that $\mathrm{sgn}\left(\hat{d}_{k+1}\right) = \mathrm{sgn}\left(\delta_k\right)$, and consequently

$$u_k^n = \frac{\Gamma}{1 - \Gamma TD_{uq}}\left(\beta d_m\,\mathrm{sgn}\left(\hat{d}_{k+1}\right) - \hat{d}_{k+1}\right) \tag{7.125}$$

$$= \frac{\Gamma}{1 - \Gamma TD_{uq}}\left(\beta d_m - \left|\hat{d}_{k+1}\right|\right)\mathrm{sgn}\left(\hat{d}_{k+1}\right) \tag{7.126}$$

$$= -\frac{\Gamma}{1 - \Gamma TD_{uq}}\frac{\partial V(d)}{\partial d}\bigg|_{d=\hat{d}_{k+1}} \tag{7.127}$$

where

$$V(d) \triangleq \begin{cases} 0 & : \ |d| < \beta d_m \\ \frac{1}{2}\frac{\Gamma}{1-\Gamma TD_{uq}}\left(\beta d_m - |d|\right)^2 & : \ |d| \geqslant \beta d_m \end{cases} \tag{7.128}$$

But V is semiconvex so it follows that

$$V\left(d_k\right) \geqslant V\left(\hat{d}_{k+1}\right) + \frac{\partial V}{\partial d}\bigg|_{d=\hat{d}_{k+1}}\left(d_k - \hat{d}_{k+1}\right) \tag{7.129}$$

and consequently

$$u_k^n \, \mathcal{E} \left\{ q_k | \mathcal{I}_k \right\} = u_k^n \tfrac{1}{T} \left(\hat{d}_{k+1} - d_k \right) \tag{7.130}$$

$$\leqslant \frac{\Gamma}{1 - \Gamma T D_{uq}} \tfrac{1}{T} \left(V(d_k) - V(\hat{d}_{k+1}) \right) \tag{7.131}$$

So

$$T \sum_{k=0}^{N} u_k^n \, \mathcal{E} \left\{ q_k | \mathcal{I}_k \right\}$$

$$\leqslant \frac{\Gamma}{1 - \Gamma T D_{uq}} \left\{ \sum_{k=0}^{N} \left(V(d_k) - V(\hat{d}_{k+1}) \right) \right\} \tag{7.132}$$

$$= \frac{\Gamma}{1 - \Gamma T D_{uq}} \left\{ V(d_0) - V(\hat{d}_{N+1}) + \sum_{k=1}^{N} \left(V(d_k) - V(\hat{d}_k) \right) \right\} \tag{7.133}$$

But $d_0 = 0$ and $V(0) = 0$ so

$$\sum_{k=0}^{N} u_k^n \, \mathcal{E} \left\{ q_k | \mathcal{I}_k \right\}$$

$$\leqslant \frac{\Gamma}{1 - \Gamma T D_{uq}} \left\{ -\tfrac{1}{T} V(\hat{d}_{N+1}) + \tfrac{1}{T} \sum_{k=1}^{N} \left(V(d_k) - V(\hat{d}_k) \right) \right\} \tag{7.134}$$

162

Now, consider that

$$
2V(d_k) = \begin{cases} 0 & : \ |d_k| < \beta d_m \\ (\beta d_m - |d_k|)^2 & : \ |d_k| \geqslant \beta d_m \end{cases} \tag{7.135}
$$

$$
= \begin{cases} \left(\beta d_m - \hat{d}_k - r_k\right)^2 & : \ r_k \geqslant \beta d_m - \hat{d}_k \\ \left(\beta d_m + \hat{d}_k + r_k\right)^2 & : \ r_k \leqslant -\beta d_m - \hat{d}_k \\ 0 & : \ \text{otherwise} \end{cases} \tag{7.136}
$$

$$
= \begin{cases} \left(\beta d_m - \hat{d}_k\right)^2 - 2r_k\left(\beta d_m - \hat{d}_k\right) + r_k^2 & : \ r_k \geqslant \beta d_m - \hat{d}_k \\ \left(\beta d_m + \hat{d}_k\right)^2 + 2r_k\left(\beta d_m + \hat{d}_k\right) + r_k^2 & : \ r_k \leqslant -\beta d_m - \hat{d}_k \\ 0 & : \ \text{otherwise} \end{cases} \tag{7.137}
$$

$$
\leqslant r_k^2 + \begin{cases} \left(\beta d_m - \hat{d}_k\right)^2 - 2r_k\left(\beta d_m - \hat{d}_k\right) & : \ r_k \geqslant \beta d_m - \hat{d}_k \\ \left(\beta d_m + \hat{d}_k\right)^2 + 2r_k\left(\beta d_m + \hat{d}_k\right) & : \ r_k \leqslant -\beta d_m - \hat{d}_k \\ 0 & : \ \text{otherwise} \end{cases} \tag{7.138}
$$

where r_k is the zero-mean Gaussian innovations process $d_k - \hat{d}_k$. Let the CDF of the r_k be $F_k(r_k)$, and the variance of r_k be S_k. Because $\hat{d}_k$ is estimated via a Kalman filter, r_k is independent of $\hat{d}_k$. Consequently

$$
\begin{aligned}
2\mathcal{E}\left\{V(d_k)|\hat{d}_k\right\} \leqslant &\ S_k + \left(\beta d_m - \hat{d}_k\right)^2 \left[1 - F_k(\beta d_m - \hat{d}_k)\right] + \left(\beta d_m + \hat{d}_k\right)^2 F_k \\
&\ (-\beta d_m - \hat{d}_k) - 2\sqrt{\frac{S_k}{2\pi}} e^{-(\beta d_m - \hat{d}_k)^2/2S_k} \left(\beta d_m - \hat{d}_k\right) \\
&\ + 2\sqrt{\frac{S_k}{2\pi}} e^{-(\beta d_m + \hat{d}_k)^2/2S_k} \left(\beta d_m + \hat{d}_k\right)
\end{aligned} \tag{7.139}
$$

Meanwhile, we may express

$$
2V(\hat{d}_k) = \left(\beta d_m - \hat{d}_k\right)^2 H(\hat{d}_k - \beta d_m) + \left(\beta d_m + \hat{d}_k\right)^2 H(-\hat{d}_k - \beta d_m) \tag{7.140}
$$

where $H(\cdot)$ is the Heaviside step function. So

$$
\begin{aligned}
2\,\mathcal{E}\left\{V(d_k)|\hat{d}_k\right\} - V(\hat{d}_k) &\leqslant S_k \\
&+ \left(\beta d_m - \hat{d}_k\right)^2 \left[H(\beta d_m - \hat{d}_k) - F_k(\beta d_m - \hat{d}_k)\right] - 2\sqrt{\frac{S_k}{2\pi}} e^{-(\beta d_m - \hat{d}_k)^2/2S_k}\left(\beta d_m - \hat{d}_k\right) \\
&+ \left(\beta d_m + \hat{d}_k\right)^2 \left[F_k(-\beta d_m - \hat{d}_k) - H(-\hat{d}_k - \beta d_m)\right] + 2\sqrt{\frac{S_k}{2\pi}} e^{-(\beta d_m + \hat{d}_k)^2/2S_k}\left(\beta d_m + \hat{d}_k\right)
\end{aligned}
$$
(7.141)

Now consider that because $F(r_k)$ is a Gaussian CDF with zero mean and finite covariance S_k, it follows that

$$
\Sigma_k \triangleq \sup_{r \in \mathbb{R}} r^2 \left(H(r) - F_k(r)\right) < \infty
$$
(7.142)

$$
\Sigma'_k \triangleq \sup_{r \in \mathbb{R}} r^2 \left(F_k(r) - H(r)\right) < \infty
$$
(7.143)

$$
\Lambda_k \triangleq 2\sqrt{\frac{S_k}{2\pi}} \sup_{r \in \mathbb{R}} r e^{-r^2/2S_k} < \infty
$$
(7.144)

$$
\Lambda'_k \triangleq 2\sqrt{\frac{S_k}{2\pi}} \sup_{r \in \mathbb{R}} -r e^{-r^2/2S_k} < \infty
$$
(7.145)

Therefore we have that

$$
2\,\mathcal{E}\left\{V(d_k)|\hat{d}_k\right\} - V(\hat{d}_k) \leqslant S_k + \Sigma_k + \Sigma'_k + \Lambda_k + \Lambda'_k
$$
(7.146)

Returning to (7.134), and taking an unconditional expectation, we therefore have

that

$$\mathcal{E}\left\{\sum_{k=0}^{N} u_k^n \, \mathcal{E}\left\{q_k | \mathcal{I}_k\right\}\right\}$$

$$= \mathcal{E}\left\{\sum_{k=0}^{N} u_k^n q_k\right\}$$

$$\leqslant \frac{\Gamma}{1 - \Gamma T D_{uq}} \frac{1}{T} \mathcal{E}\left\{\sum_{k=1}^{N} \left(V(d_k) - V(\hat{d}_k)\right)\right\}$$

$$\leqslant \frac{\Gamma}{1 - \Gamma T D_{uq}} \frac{1}{T} \mathcal{E}\left\{\sum_{k=1}^{N} \mathcal{E}\left(V(d_k) - V(\hat{d}_k) | \hat{d}_k\right)\right\}$$

$$\leqslant \frac{\Gamma}{1 - \Gamma T D_{uq}} \frac{1}{2T} \left(S_k + \Sigma_k + \Sigma_k' + \Lambda_k + \Lambda_k'\right) \tag{7.147}$$

$\square$

The above lemma is important because of the Theorem 7.4, which is a standard result from robust control.

7.5.4 Generalizing Nonlinearity

The formulation of nonlinear feedback law $\Phi(\cdot)$, as in (7.117), has the advantage of being heuristic. It is reasonably straight-forward to understand how the feedback law makes use of a one-step-ahead forecast in order to facilitate stroke protection. However, there are certain advantages to generalizing the nonlinear feedback law beyond that shown in (7.117).

Specifically, it is straight-forward to show that all the results on stability in Section 7.5.3 still hold if $\Phi(\cdot)$ is generalized by still implementing equation (7.117), but redefining δ_k from (7.113), to

$$\delta_k = d_k + (T + \tau)\left(C_q \hat{x}_k + D_{uq} C_K \xi_k\right) \tag{7.148}$$

where $\tau > 0$ can be chosen as any nonnegative value. Indeed, this makes the stroke

protection algorithm more cautious. More importantly, though, raising the value of τ reduces the magnitude of the nonlinear forces u_k^n. As we shall see in the example in the next section, this comes at the expense of lower power generation with higher τ.

With δ_k redefined as in (7.148), the value of Γ in (7.117) must also be changed to assure stability. In this case, (7.117) is guaranteed to be passive with respect to q, for Γ in the range

$$\Gamma \in \left[0, \frac{1}{D_{uq}(T + \tau)}\right] \tag{7.149}$$

Although the value in (7.118) at the upper end of this range works very effectively in theory, in practice the implementation of this value may result in instability due to uncertainty in D_{uq} or T. As such, a value should be chosen which is the maximal value such that (7.149) can be assured, even in the presence of uncertainty.

7.6 Numerical Example

To demonstrate the control methodology described in the previous sections, we consider the cylindrical buoy-type WEC shown in Figure 7.5, which is the same device as in the Chapter 5 and Chapter 6. For consistency, the parameters of the WEC model and JONSWAP spectrum are the same as before. The maximum stroke of this WEC is assumed to be 3m. To characterize the loss model, we choose the parameter R_d in loss model (7.6) as 10^8kg/s. We assume the sampling time T is 0.1s. For this case, Figure 7.6 shows the original infinite-dimensional discrete-time transfer function $Z_{uq}(e^{j\Omega})$ (as derived in (7.9)), as well as its finite-dimensional approximation (as in (7.14)). Figure 7.7 shows the original infinite-dimensional discrete-time spectrum for $\Sigma_{wq}(j\Omega)$ (as in (7.10)), as well as its finite-dimensional approximation (as in (7.11) and (7.15)). We note that the total dimension of the discrete-time state space used to model these dynamics was 18.

For this case, the causal limit on the power that can be generated at this sample
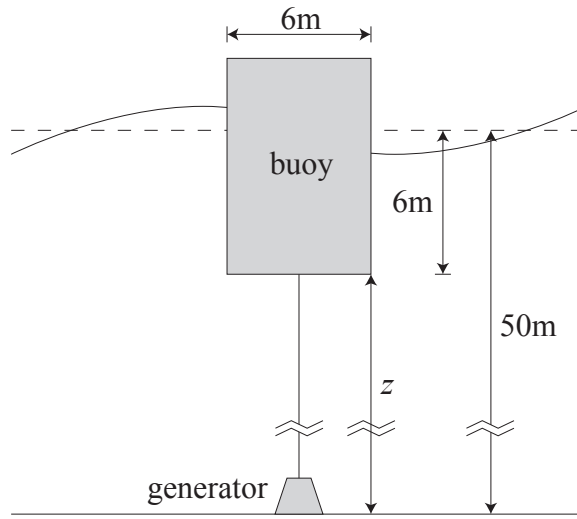
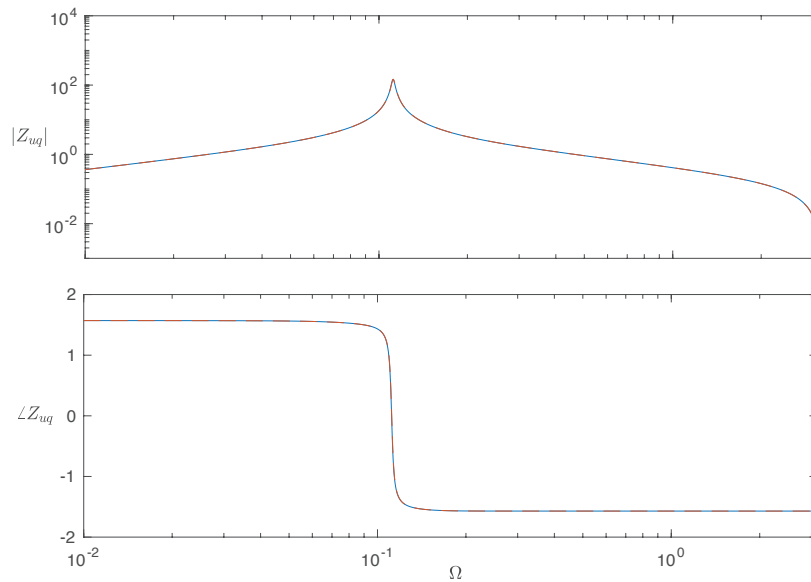Figure 7.5: Buoy-type WEC considered in the example

Figure 7.6: Bode diagrams for infinite-dimensional Z_{uq} (solid), as well as its finite-dimensional approximation (dash)
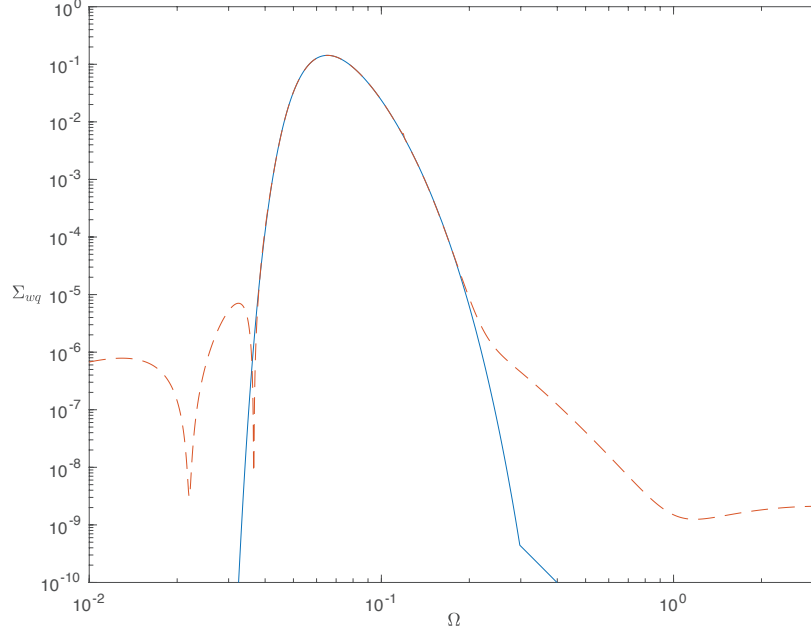
Figure 7.7: Infinite-dimensional discrete-time force spectrum $\Sigma_{wq}(j\Omega)$ (solid), as well as the spectrum for its finite-dimensional approximation (dash)

rate can be found via (7.43) to be 59.1kW. However, this causal limit does not take the stroke limit into consideration, and is therefore considerably higher than the power that can be generated by the system under stroke constraints.

7.6.1   Performance of Optimized Linear Controller

First we consider the linear control design described in Section 7.3. In this case, we have an optimal linear performance (i.e., the maximized value of γ in optimization (7.62)) is 33.1kW. At this performance, the stroke covariance is equal to its constrained upper limit of $\frac{1}{4}d_m^2$. It is also interesting to note that the optimal linear feedback controller in this case is open-loop unstable.

Figure 7.8 shows transient plots for the stroke, force, and power, for one hour of data. Note that to achieve the optimal average power generation requires that the PTO be capable of bidirectional power flow. Also note that the relaxed stroke constraint has accomplished its desired goal, with the majority (but not all) of the displacement peaks occurring at displacements less than 3m.
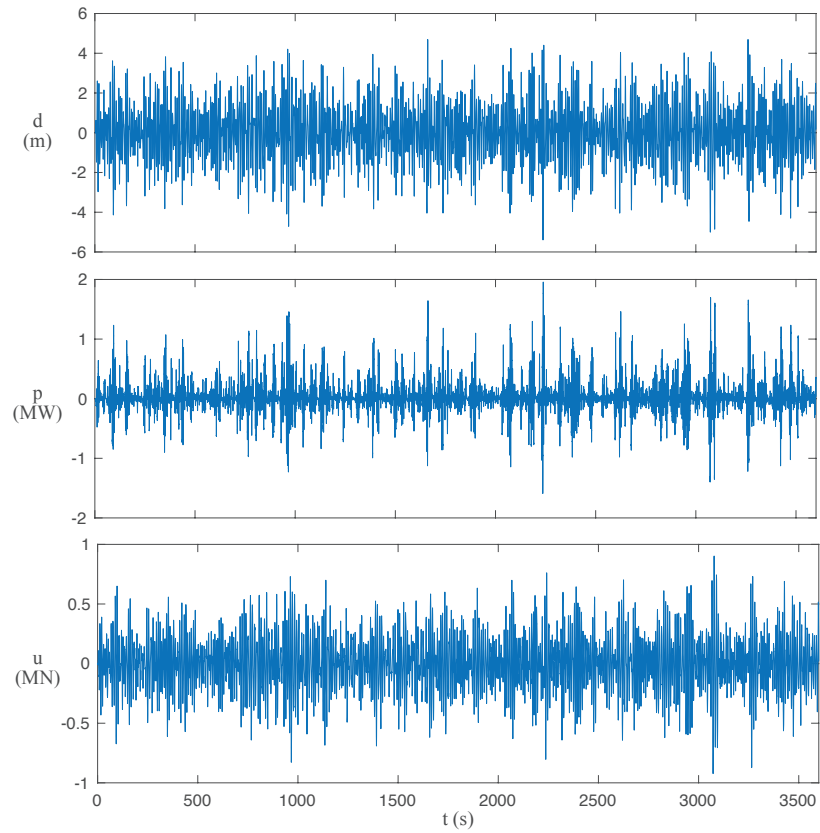
Figure 7.8: Transient responses for linear control design with relaxed stroke constraint: PTO displacement d (top), generated power p (middle), and PTO force u (bottom)

7.6.2 Performance of Nonlinear Controller

To design the nonlinear controller, we take the parameter β (which determines the size of the safe zone in Figure 7.4 to be 0.9. To begin with, we consider the case in which the the nonlinear feedback law is chosen as in (7.117) with δ_k determined as in (7.113); i.e., we set the generalized parameter $\tau = 0$. We also presume Γ to be chosen as in (7.118).

For this scenario, Figure 7.9 shows the PTO displacement, force, and power for one hour of simulation time. As shown, the maximum stroke is maintained at $d_m = 3$m. Performance in this case is largely decreased, with a negative average power generation, which means that the WEC device can not generate energy in this scenario. In Figure 7.9, stroke is protected but in the same time, the controller applies very high PTO forces, which results in the high dissipative power loss and degrades the overall power generation.

In order to increase the average power generation, we need to lower the controller force u and thus increase the value of τ. In Figure 7.10, we can see that the optimal performance that is 28.1kW about 15% reduction in performance is achieved when $\tau = 5T$. As τ increases, the controller becomes so conservative that restrict the movement of the buoy and thus lower the performance. To illustrate this, consider Figure 7.11, which shows transient responses for τ values of T, $5T$, and $50T$. We see that clearly, with $\tau = 5T$, the impulses are virtually eliminated, while still providing (even more cautious) protection of the stroke. For larger τ values, the tradeoff here is that increasing τ will bring lower power generation. Specifically, the mean power generation here in there cases in the figure are 17.0kW, 28.1kW and 11.2kW respectively.
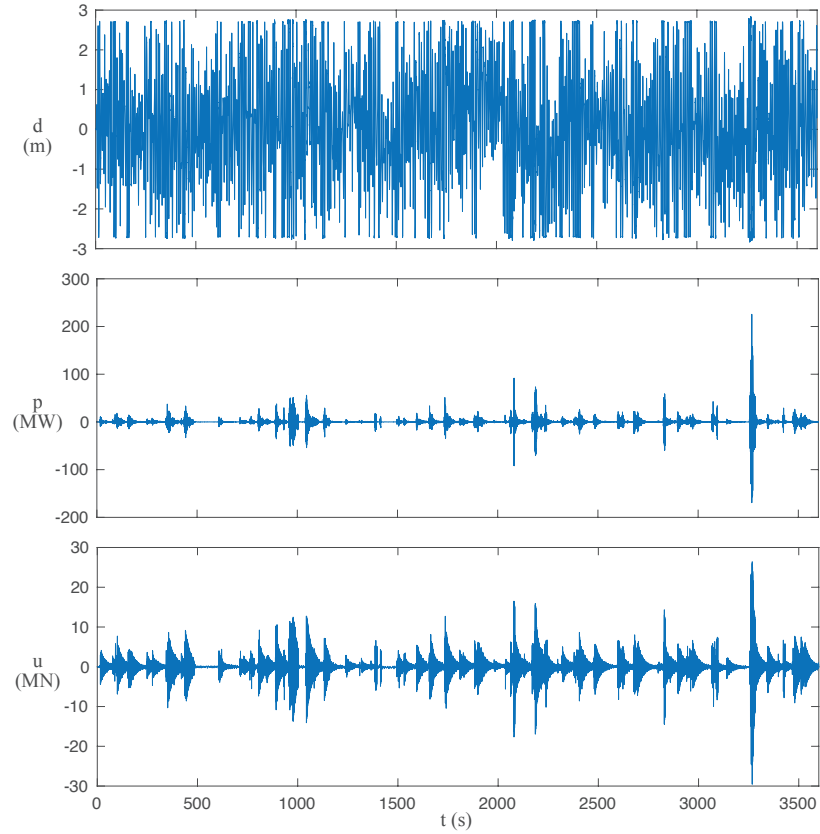
Figure 7.9: Transient responses for linear control design with nonlinear stroke protection, with $\tau = 0$: PTO displacement d (top), PTO force u (middle), and generated power p (bottom)
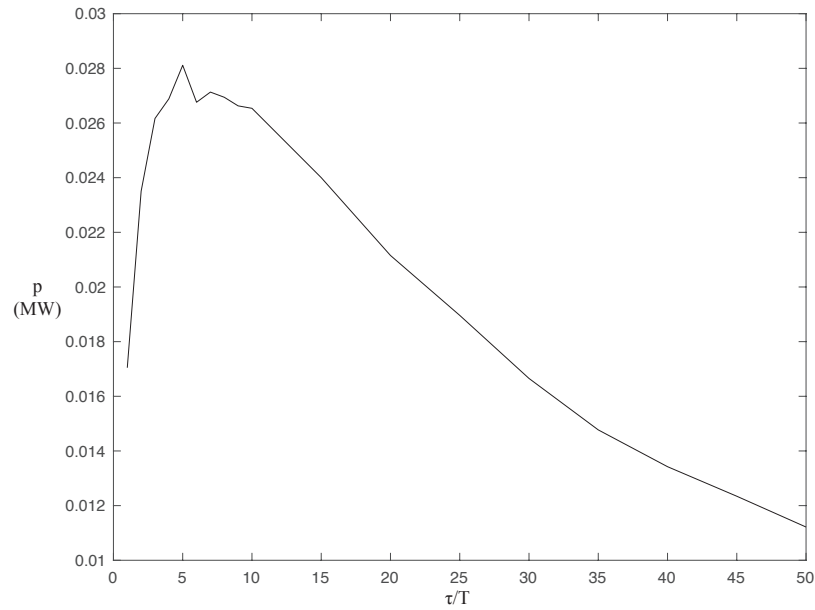

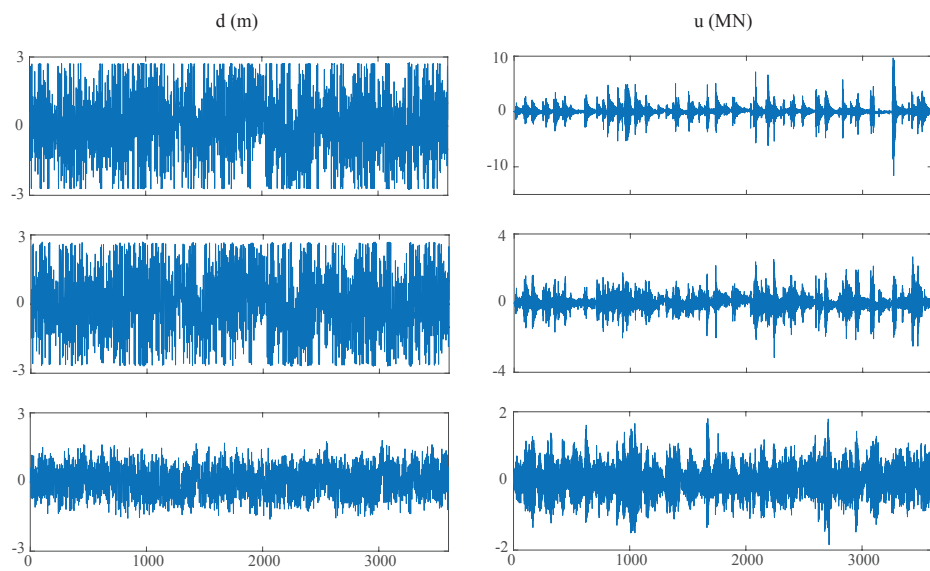Figure 7.10: Average power generation with different values of τ

Figure 7.11: PTO displacement (left) and force (right) trajectories for τ values of T (top), $5T$ (middle), and $50T$.

CHAPTER 8

Robust Control of Wave Energy Converters with Nonlinear Dynamics

8.1 Introduction

A common strategy to design the control system for a WEC is to use the linearized WEC dynamic model around its equilibrium point. The linearized WEC system has many advantages, such as the simple mathematical form and computational efficiency. However, the actual WEC system has a complex dynamic behavior, e.g., the nonlinear viscous drag effect. The use of control techniques has the effect on amplifying the WEC motion to maximize the power generation, which contradicts the small displacement assumption. Some studies reveal that the control system designed without considering the nonlinear WEC dynamics has a lower power capture than expected due to some robustness issues. In this chapter, we considered to design a robust control that preserves the closed-loop system stability while giving a high power generation in the presence of nonlinear effects, in particular the nonlinear viscous damping force. This robust control problem can be formulated as a multi-objective control problem, whose primary objective is to maximize the nominal power generation and the associated objective is to robust stabilize the close-loop system. Unfortunately, this optimization is nonconvex. Here, we use the circle criterion and

Loop Transfer Recovery (LTR) method to give a robust controller design procedure. Although this procedure is sub-optimal, it is easy to be implemented and achieves a high power generation performance.

8.2   Problem Formulation

We will investigate the effect of nonlinear viscous damping in this chapter. An experimental law proposed by Morison [52] describes the viscosity drag force in a quadratic function of the WEC velocity.

$$f_v(t) = \rho \pi r^2 c_d |v(t)| v(t) + \rho \pi r^2 c_i \dot{v}(t) \tag{8.1}$$

where ρ is the water density, r is the cylinder radius, c_d is the drag coefficient and c_i is the inertia coefficient. The experiments generating coefficients c_d and c_i are discussed in [93]. Here, without loss of generality, we can assume that $c_i = 0$ (nonzero value of c_i can be added to the mass term).

Considering the viscosity effect, the dynamic equation of WEC system becomes:

$$[M + M_\infty]\ddot{z}(t) + \int_0^\infty H_r(\tau)v(t - \tau)d\tau + K_v|v(t)|v(t) + Kz(t) = f_f(t) + u(t) \tag{8.2}$$

where $K_v \triangleq \rho \pi r^2 c_d$ is the viscous damping coefficient. The resulting system diagram is in Figure 8.1.

The viscous damping force f_v is a memoryless, time-varying and nonlinear function, which can be proven to satisfy a *sector condition*. Although the WEC motion is irregular and the maximum WEC velocity can be infinity theoretically, from Section 6, we know that the peak stationary response of the WEC velocity can be approximated as Rayleigh-distributed, if $v(t)$ is sufficiently narrowband. The cumulative
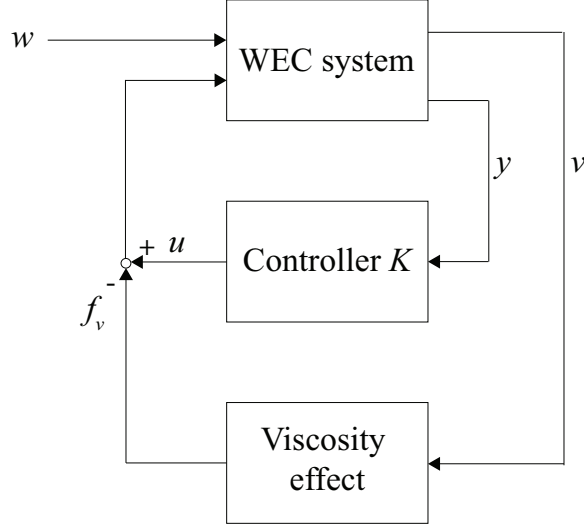
Figure 8.1: Block diagram of the WEC system considering viscosity effect

distribution function of the peak response ϕ is:

$$\Pr[\varphi \leqslant \varphi_0] = 1 - \exp\left\{-\varphi_0^2/2\sigma^2\right\} \tag{8.3}$$

where $\sigma^2 = \mathcal{E}\{v^2\}$. The value of σ is chosen when the LQG controller with velocity feedback is implemented, since the LQG controller amplifies the WEC motion and thus delivers the maximum power generation performance. Here, we choose $\varphi_0 = 3\sigma$ and then the probability that the velocity v exceeds φ_0 is around 1.11%, which is low enough for the robust controller design. Here we denote $K_d \triangleq 3K_v\sigma$,

Definition 8.2.1. A memoryless nonlinearity f_v is said to satisfy a sector condition $[0, K_d]$ if

$$f_v^T[f_v - K_d v] \leqslant 0, \forall v \tag{8.4}$$

for a positive definite matrix K_d.

The power generation $\bar{p}$ of the nominal WEC system is defined in (3.36). We can

175
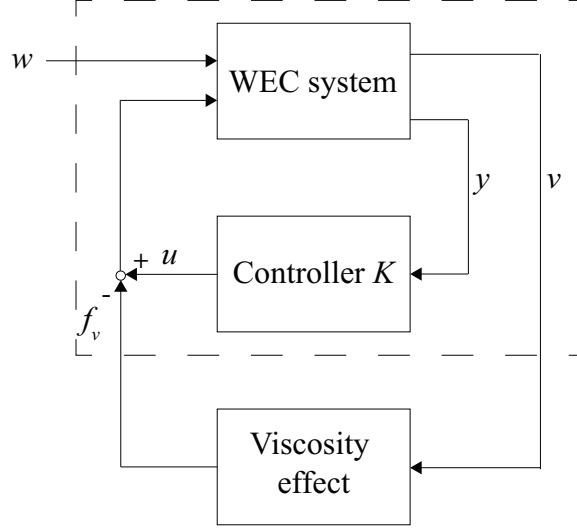
Figure 8.2: Block diagram of the transfer function $G_{f_v v}$

formulate our control problem as an optimization problem.

$$
\text{OP8.1} : \begin{cases}
\text{Maximize:} & \bar{p} \\
\text{Domain:} & \text{causal } \mathcal{K} : y \mapsto u \\
\text{Uncertainty:} & f_v \text{ in sector } [0, K_d]
\end{cases}
$$

This design problem is a multi-objective optimization problem, in which the primary objective is the maximization of the power generation in the nominal system, and the competing objective is to stabilize the closed-loop system in the presence of viscous damping force. The stability constraint can be posed using the circle criterion for absolute stability.

We use the function $G_{f_v v}$ to denote the mapping: $f_v \to v$, which is shown in the dotted line box in Figure 8.2.

Theorem 8.1. *Let assumptions 3.6.1, 3.6.2, and 3.6.3 hold, the closed-loop system is absolutely stable if and only if* $(1 - K_d G_{f_v v}(s))$ *is strictly positive real (SPR)*

Proof. The proof can be found at a number of literatures, e.g., [56]. $\qquad\square$

Based on the above theorem, the robust stability constraint becomes the SPR

176

constraint of the transfer function $(1 - K_d G_{f_v v}(s))$. Specifically, the optimization problem OP8.1 becomes, equivalently,

$$\text{OP8.2}: \begin{cases} \text{Maximize:} & \bar{p} \\ \text{Domain:} & \text{causal } K : y \mapsto u \\ \text{Constraint:} & (1 - K_d G_{f_v v}(s)) \text{ is SPR} \end{cases}$$

8.3 Methodology

Here, we use the LTR method, which increases the covariance of the process noise to make system more robust and is first introduced in [94]. The LQG method in Chapter 5 attains a good performance using the velocity feedback, but it suffers from robustness issues. From Chapter 5, the state-space model of the optimal controller considering the velocity feedback is:

$$\begin{cases} \dot{\hat{x}} = (A + B_u K + L C_v)\hat{x} - Lv \\ u = K\hat{x} \end{cases} \tag{8.5}$$

where K and L can be found in equation (5.15) and (5.24). We can improve the robustness properties of the optimal controller (8.5) using LTR method.

We denote rI as the covariance of the additional process noise. The filter gain is $L = -\Lambda^{-1} S C_v^T$, where S satisfies the filter algebraic Riccati equation:

$$AS + SA^T - SC_v^T \Lambda^{-1} C_v S + EE^T + r B_u B_u^T = 0 \tag{8.6}$$

It has been shown in [55] that as r approaches infinity, the LQG controller approaches the LQR state-feedback controller. In this problem, there is no need to make r close to infinity. Instead, we can increase the value of r until the transfer function $(1 - K_d G_{f_v v}(s))$ satisfies SPR. The LTR approach involves a tradeoff between robustness

and nominal LQG performance, since increasing the system-noise density deteriorates the nominal performance.

To begin with, we have the following theorem

Theorem 8.2. *Let assumptions 3.6.1, 3.6.2, and 3.6.3 hold, Then*

$$\lim_{r \to \infty} G_{f_v v}(s) = -C_v[sI - (A + B_u K)]^{-1} B_u \tag{8.7}$$

Proof. Define the transformation matrix T as

$$T \triangleq \begin{bmatrix} C_v \\ B_\perp \end{bmatrix} \tag{8.8}$$

where $B_\perp$ is chosen such that T is invertible, and $B_\perp B_u = 0$. If $C_v[sI - A]^{-1} B_u$ is passive then it follows that $C_v B_u$ is invertible, and therefore

$$T^{-1} = \begin{bmatrix} B_u(C_v B_u)^{-1} & C_\perp(B_\perp C_\perp)^{-1} \end{bmatrix} \tag{8.9}$$

where $C_\perp$ is such that $C_v C_\perp = 0$. Multiply the Riccati equation from the left by T and from the right by T^T, and we have that

$$
0 = \begin{bmatrix} A_{11} & A_{12} \\ A_{21} & A_{22} \end{bmatrix} \begin{bmatrix} S_{11} & S_{12} \\ S_{12}^T & S_{22} \end{bmatrix} + \begin{bmatrix} S_{11} & S_{12} \\ S_{12}^T & S_{22} \end{bmatrix} \begin{bmatrix} A_{11} & A_{12} \\ A_{21} & A_{22} \end{bmatrix}^T
$$
$$
+ \begin{bmatrix} E_1 \\ E_2 \end{bmatrix} \begin{bmatrix} E_1 \\ E_2 \end{bmatrix}^T + r \begin{bmatrix} C_v B_u \\ 0 \end{bmatrix} \begin{bmatrix} C_v B_u \\ 0 \end{bmatrix}^T - \begin{bmatrix} S_{11} \\ S_{12}^T \end{bmatrix} \Lambda^{-1} \begin{bmatrix} S_{11} & S_{12} \end{bmatrix} \tag{8.10}
$$

178

where

$$
\begin{bmatrix} A_{11} & A_{12} \\ A_{21} & A_{22} \end{bmatrix} = TAT^{-1}
\qquad
\begin{bmatrix} S_{11} & S_{12} \\ S_{12}^T & S_{22} \end{bmatrix} = TST^T
\qquad
\begin{bmatrix} E_1 \\ E_2 \end{bmatrix} = TE
\qquad (8.11)
$$

Let

$$
S = \sqrt{r} \begin{bmatrix} \bar{S}_{11} & 0 \\ 0 & 0 \end{bmatrix} + \begin{bmatrix} 0 & \tilde{S}_{12} \\ \tilde{S}_{12}^T & \tilde{S}_{22} \end{bmatrix}
\qquad (8.12)
$$

and hypothesize that $\bar{S}_{11}$ is finite and $\tilde{S}_{ij}/\sqrt{r}$ is finite. Substitute into the Riccati equation:

$$
\begin{aligned}
0 =\; & \begin{bmatrix} A_{11} & A_{12} \\ A_{21} & A_{22} \end{bmatrix} \begin{bmatrix} 0 & \tilde{S}_{12} \\ \tilde{S}_{12}^T & \tilde{S}_{22} \end{bmatrix} + \begin{bmatrix} 0 & \tilde{S}_{12} \\ \tilde{S}_{12}^T & \tilde{S}_{22} \end{bmatrix} \begin{bmatrix} A_{11} & A_{12} \\ A_{21} & A_{22} \end{bmatrix}^T + \begin{bmatrix} E_1 \\ E_2 \end{bmatrix} \begin{bmatrix} E_1 \\ E_2 \end{bmatrix}^T \\
& + \sqrt{r} \left(\begin{bmatrix} A_{11}\bar{S}_{11} + \bar{S}_{11}A_{11}^T & \bar{S}_{11}A_{21}^T \\ A_{21}\bar{S}_{11} & 0 \end{bmatrix} - \begin{bmatrix} \bar{S}_{11} \\ 0 \end{bmatrix} \Lambda^{-1} \begin{bmatrix} 0 & \tilde{S}_{12} \end{bmatrix} - \begin{bmatrix} 0 \\ \tilde{S}_{12}^T \end{bmatrix} \Lambda^{-1} \begin{bmatrix} \bar{S}_{11} & 0 \end{bmatrix} \right) \\
& - \begin{bmatrix} 0 \\ \tilde{S}_{12}^T \end{bmatrix} \Lambda^{-1} \begin{bmatrix} 0 & \tilde{S}_{12} \end{bmatrix} + r \begin{bmatrix} C_v B_u B_u^T C_v^T - \bar{S}_{11}\Lambda^{-1}\bar{S}_{11} & 0 \\ 0 & 0 \end{bmatrix}
\end{aligned}
\qquad (8.13)
$$

As $r \to \infty$ we have that in order for the (1,1) term to be zero, the (1,1) term in the term that multiplies by r must be zero, i.e.,

$$
\bar{S}_{11} = \Lambda^{1/2} \left[\Lambda^{-1/2} C_v B_u B_u^T C_v^T \Lambda^{-1/2} \right]^{1/2} \Lambda^{1/2}
\qquad (8.14)
$$

and in order for the (1,2) term to be zero as $r \to \infty$,

$$
\left(A_{11} - \sqrt{r}\bar{S}_{11}\Lambda^{-1} \right) \tilde{S}_{12} + \tilde{S}_{12}A_{22}^T + A_{12}\tilde{S}_{22} + E_1 E_2^T + \sqrt{r}\bar{S}_{11}A_{21}^T = 0
\qquad (8.15)
$$

179

As $r \to \infty$, the solution to $\tilde{S}_{12}$ converges to that of the equation

$$\sqrt{r}\bar{S}_{11}\Lambda^{-1}\tilde{S}_{12} = A_{12}\tilde{S}_{22} + \sqrt{r}\bar{S}_{11}A_{21}^T \tag{8.16}$$

But $\bar{S}_{11}$ is invertible, so

$$\tilde{S}_{12} = \frac{1}{\sqrt{r}}\Lambda\bar{S}_{11}^{-1}A_{12}\tilde{S}_{22} + \Lambda A_{21}^T \tag{8.17}$$

In order for the (2,2) term to be zero, the (2,2) term in the term that does not multiply by r must be zero, requiring

$$0 = A_{21}\tilde{S}_{12} + \tilde{S}_{12}^T A_{21}^T + A_{22}\tilde{S}_{22} + \tilde{S}_{22}A_{22}^T + E_2 E_2^T - \tilde{S}_{12}^T \Lambda^{-1} \tilde{S}_{12} \tag{8.18}$$

Substituting the $r \to \infty$ solution for $\tilde{S}_{12}$, we have a Riccati equation for $\tilde{S}_{22}$.

$$0 = A_{22}\tilde{S}_{22} + \tilde{S}_{22}A_{22}^T + A_{21}\Lambda A_{21}^T + E_2 E_2^T - \frac{1}{r}\tilde{S}_{22}A_{12}^T \bar{S}_{11}^{-1}\Lambda^{-1}\bar{S}_{11}^{-1}A_{12}\tilde{S}_{22} \tag{8.19}$$

where we desire the maximizing solution; i.e., the solution with $\tilde{S}_{22} > 0$. As $r \to \infty$, suppose this solution stays finite. Then it is the solution to Lyapunov equation

$$0 = A_{22}\tilde{S}_{22} + \tilde{S}_{22}A_{22}^T + A_{21}\Lambda A_{21}^T + E_2 E_2^T \tag{8.20}$$

The solution to this Lyapunov equation is positive-definite if and only if A_{22} is Hurwitz. But A_{22} is Hurwitz if and only if the transfer function $C_v[sI - A]^{-1}B_u$ is minimum-phase [95]. However, $C_v[sI - A]^{-1}B_u$ is passive, and all passive transfer functions are minimum-phase. Therefore, $\tilde{S}_{22}$ stays finite as $r \to \infty$ and is the solution to Lyapunov equation (8.20).

As $r \to \infty$ the associated partitioned Kalman gain is

$$
L = \begin{bmatrix} S_{11} \\ S_{12}^T \end{bmatrix} \Lambda^{-1}
$$

$$
= - \begin{bmatrix} \sqrt{r}\bar{S}_{11} \\ A_{21}\Lambda \end{bmatrix} \Lambda{-1}
$$

$$
= - \begin{bmatrix} \sqrt{r}\bar{S}_{11}\Lambda^{-1} \\ A_{21} \end{bmatrix} \tag{8.21}
$$

The dynamics of the observer are then governed by

$$
\begin{bmatrix} \dot{\hat{v}} \\ \dot{\hat{x}}_2 \end{bmatrix} = \begin{bmatrix} A_{11} - \sqrt{r}\bar{S}_{11}\Lambda^{-1} & A_{12} \\ 0 & A_{22} \end{bmatrix} \begin{bmatrix} \hat{v} \\ \hat{x}_2 \end{bmatrix} + \begin{bmatrix} C_v B_u \\ 0 \end{bmatrix} u + \begin{bmatrix} \sqrt{r}\bar{S}_{11}\Lambda^{-1} \\ A_{21} \end{bmatrix} v \tag{8.22}
$$

But for all finite s,

$$
\lim_{r \to \infty} \left[sI - \left(A_{11} - \sqrt{r}\bar{S}_{11}\Lambda^{-1} \right) \right]^{-1} \sqrt{r}\bar{S}_{11}\Lambda^{-1} = I \tag{8.23}
$$

so as $r \to \infty$, $\hat{v}(t) \to v(t)$ for all t. Consequently, we have that in the limiting case as $r \to \infty$,

$$
\begin{bmatrix} \dot{v} \\ \dot{\hat{x}}_2 \end{bmatrix} = \begin{bmatrix} A_{11} & A_{12} \\ A_{12} & A_{22} \end{bmatrix} \begin{bmatrix} \hat{v} \\ \hat{x}_2 \end{bmatrix} + \begin{bmatrix} C_v B_u \\ 0 \end{bmatrix} (u - f_v) + \begin{bmatrix} E_1 \\ 0 \end{bmatrix} w
$$

$$
= \begin{bmatrix} A_{11} + C_v B_u K_1 & A_{12} + CB_u K_2 \\ A_{12} & A_{22} \end{bmatrix} \begin{bmatrix} \hat{v} \\ \hat{x}_2 \end{bmatrix} - \begin{bmatrix} C_v B_u \\ 0 \end{bmatrix} f_v + \begin{bmatrix} E_1 \\ 0 \end{bmatrix} w \tag{8.24}
$$

where

$$
\begin{bmatrix} K_1 & K_2 \end{bmatrix} = KT^{-1} \tag{8.25}
$$

181

We conclude that

$$
\hat{v}(s) = - \begin{bmatrix} I & 0 \end{bmatrix} \left(sI - \begin{bmatrix} A_{11} + C_v B_u K_1 & A_{12} + C B_u K_2 \\ A_{12} & A_{22} \end{bmatrix} \right)^{-1}
$$

$$
\left(\begin{bmatrix} C B_u \\ 0 \end{bmatrix} \hat{f}_v(s) + \begin{bmatrix} E_1 \\ 0 \end{bmatrix} \hat{w}(s) \right)
$$

$$
= - C_v [sI - (A + B_u K)]^{-1} \left(B_u \hat{f}_v(s) + T^{-1} \begin{bmatrix} E_1 \\ 0 \end{bmatrix} \hat{w}(s) \right) \tag{8.26}
$$

This proves the claim of the theorem.

□

Using this theorem, we have the following result, which forms the basis for the design methodology.

Theorem 8.3. *Let assumptions 3.6.1, 3.6.2, and 3.6.3 hold. Let K be found as in (5.15), and assume that the transfer function*

$$
H(s) \triangleq C_v [sI - (A + B_u K)]^{-1} B_u \tag{8.27}
$$

is positive real. Let $L = -\Lambda^{-1} S C_v^T$ where S is the solution to (8.6), parametrized by r. Then there exists a finite value of r, above which $1 - K_d G_{f_v v}(s)$ is SPR.

Proof. From Theorem 8.2, it is immediate that $G_{f_v v}(s) \to -H(s)$ as $r \to \infty$. Consequently, the assumption that $T(s)$ is positive real implies that for all $\omega \in \mathbb{R} \cup \{-\infty, \infty\}$,

$$
\lim_{r \to \infty} \left\{ (1 - K_d G_{f_v v}(j\omega)) + (1 - K_d G_{f_v v}(j\omega))^H \right\} = 2 + K_d \left(H(j\omega) + H^H(j\omega) \right) \geqslant 2 > 0 \tag{8.28}
$$

This shows that the limit is strongly positive real. To show that it is strictly positive

182

real, it must be the case that for some $\epsilon > 0$,

$$\lim_{r \to \infty} \left\{ (1 - K_d G_{f_v v}(j\omega - \epsilon)) + (1 - K_d G_{f_v v}(j\omega - \epsilon))^H \right\} \geqslant 0 \qquad (8.29)$$

However, because the above limit is greater than or equal to 2 with $\epsilon = 0$, it is sufficient to show that $G_{f_v v}(s)$ is analytic for all imaginary s. But this is assured because it is known that for K found as in (5.15), it is the case that $A + B_u K$ is Hurwitz. This concludes the proof. $\qquad \square$

Theorem 8.3 requires the assumption to be made that $H(s)$ is positive real. But for a given energy harvesting control problem $H(s)$ is uniquely determined, because K is unique. It is therefore justifiable to ask what can be done if $H(s)$ is found not to be positive real, for a given application. In this case, the LTR method will still yield a finite value of r above which $1 - K_d G_{f_v v}(s)$ is SPR, if K_d is sufficiently small. However, if K_d is above a critical value, then the LTR method cannot be used, irrespective of how large r is made. In order to use LTR in such situations, K would need to be redesigned to be the optimal state-feedback gain that also ensures that $H(s)$ is positive real. This introduces an extra layer of conservatism into the design of the robust controller, and will lead to lower nominal power generation performance.

Interestingly, however, it was found that it is not uncommon for $H(s)$ to be positive real, in applications. Indeed, it appears to be the case (although a proof remains elusive) that $H(s)$ is *always* positive real for applications with only one generator. This claim has been substantiated by randomly generating plant models adhering to the assumption that $C_v[sI - A]^{-1}B_u$ is positive real with A Hurwitz, and searching for a case that does not render $H(s)$ positive real. Despite a rather exhaustive search (millions of randomized models with various state space dimensions) no such case has been found for the single-generator case. For systems with multiple generators, however, it is rather easy to find such cases.
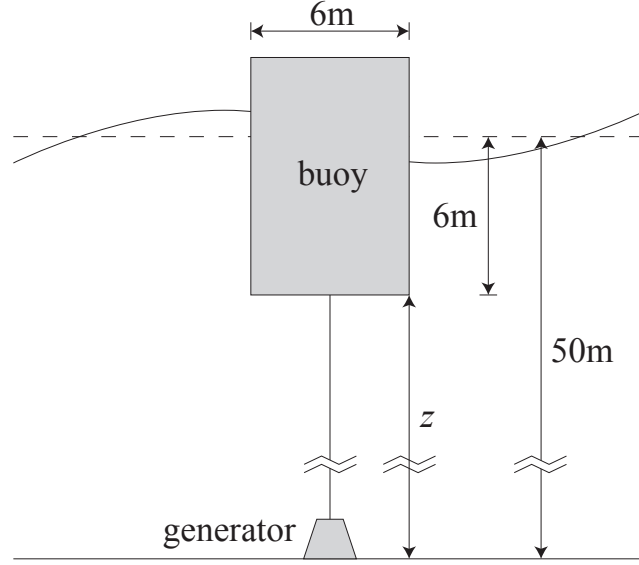
Figure 8.3: Diagram of example WEC

8.4 Numerical Example

We use the same single-degree-of-freedom WEC shown in Figure 8.3 as the one buoy case in the previous chapters. For more details on the modeling of the system in Figure 8.3, and in particular of its finite-dimensional state space model formulation, we refer the readers to the one buoy case in chapter 5. We choose the drag coefficient $c_d = 1$, based on the numerical study in [96]. In the Figure 8.4, we choose the state condition with mean wave period of 9s, significant wave height of 1m and sharpness factor of 1. As we increase φ_0 value, the nominal power generation degrades. When $\varphi_0 = 3\sigma$, the power generation is around 70% of the causal limit, which is acceptable.

In the previous proof, we prove that using LTR method, as $r \to \infty$, the transfer function $-G_{f_v v}$ will become PR. It turns out that increasing r, the LTR controller will make the nominal WEC system more robust, but with the lower nominal power generation performance. In Figure 8.5, we compare the nominal performance of Controller 1 and Controller 2, both of which are generated by LTR method. As we increase r, Controller 1 is the controller which makes $(1 - K_d G_{f_v v})$ SPR. As r approaches infinity,
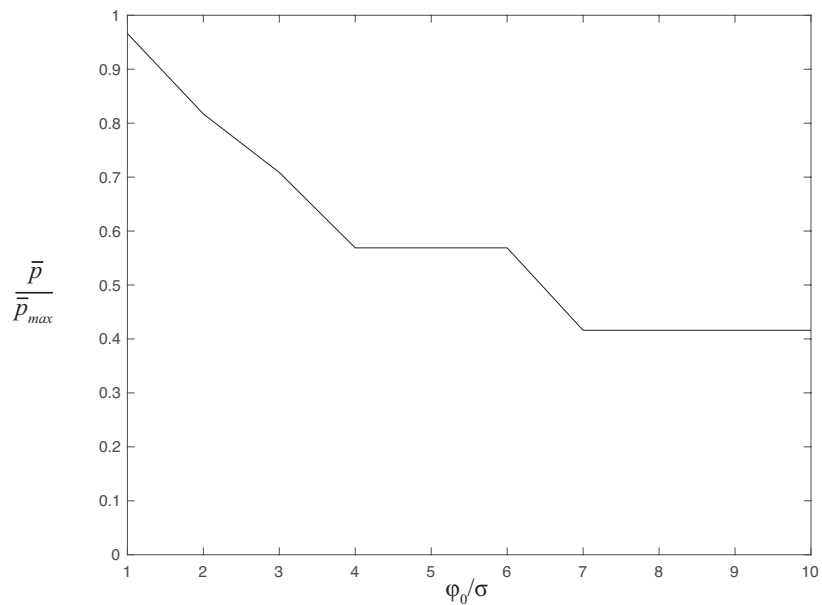
Figure 8.4: Nominal power generation choosing different values of φ_0
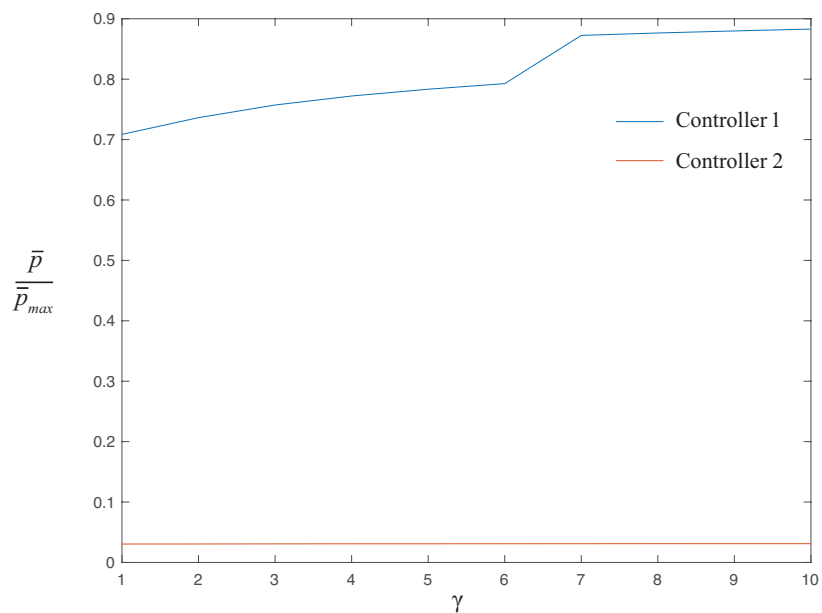
Figure 8.5: Comparison of power generation performance between two controllers under different sharpness factor γ.
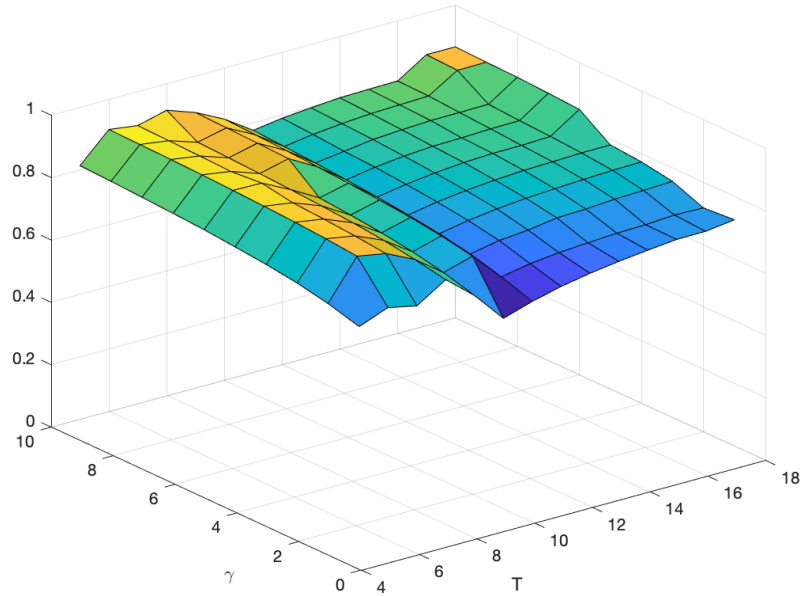
Figure 8.6: The performance of LTR controller under different sea state.

we have the Controller 2 in which the transfer function $-G_{f_v v}$ is PR. The nominal performance of Controller 1 is much higher than Controller 2, which is expected.

We also compare the LTR controller performance with causal power limit on different sea states. In Figure 8.6, we vary the sea state condition, such as changing the sharpness factor γ and mean wave period T. The controller generated using LTR method achieves very good performance, with the lowest power generation equal to 61% of the causal limit and the highest equal to 92%.

186

CHAPTER 9

Conclusions and Future Work

9.1   Conclusions

This dissertation explores the topic of control system design for ocean wave energy converters with the presence of finite stroke and model uncertainty. The main contributions are listed here:

- We propose a modified subspace-based spectral factorization technique whereby the required size of Hankel matrix to be assembled can be significantly reduced, while still attaining high accuracy. This technique can be applied to many other areas besides offshore engineering.

- We develop a nonlinear control design strategy for WEC with stroke saturation. This strategy has three steps: 1) design a linear controller by relaxing the constraint on the displacement variance; 2) augment this linear controller with an extra input channel u^n, in which the mapping $u^n \to v$ is passive; 3) design an outer, passive nonlinear feedback law that ensures the displacement below the stroke limits.

- We extend the above design strategy to the discrete-time WEC system. The main difference is in designing the outer nonlinear feedback controller, which requires a one-step-ahead predictor in the discrete-time domain.

- We demonstrated that a control system designed using LTR method can maximize the nominal power generation performance, in the meantime robustly stabilizing the WEC system in the presence of model uncertainty.

Although this dissertation is mainly about the WEC control system design, the techniques mentioned above can also be applied to other vibration energy harvesting problems.

9.2   Future Work

There are several interesting future extensions to the research presented here:

- The "optimal" subspace-based spectral factorization technique remains an open question. In chapter 4, we choose the index set based on their relative significance to the Markov coefficients. However, this is just one possible way to choose the index set. There may be other schemes that yield even more favorable results.

- One fact we did not consider here is that all the mechanical actuators exhibit force limits. We have assumed these force limits were sufficiently high to be disregarded. Simultaneous satisfaction of stroke saturation and actuator force saturation can be a more realistic and more difficult topic to explore.

- Another future research area is the control system design simultaneously accommodating stroke saturation and model uncertainty. The technique we presented requires precise knowledge of the WEC plant. It remains an open question as to the ramifications when this assumed model differs from reality.

- The LTR method used in chapter 8 is not optimal in any sense. This robust control problem can be formulated as an optimization problem, and unfortunately, this optimization is nonconvex. The possibility of using certain convex

overbounding techniques should be investigated and hopefully we can arrive at a local optimal solution.

- The problem formulated in chapter 8 considers the optimization of *nominal* performance, subject to the constraint that the feedback law is stability-robust in the presence of model uncertainty. However, it would be preferable to formulate the problem such that the feedback law is optimized to be performance-robust; i.e., so that the worst-case power generation performance is optimized. This problem, which is more challenging than the one considered here, remains an item for future work.

APPENDIX

APPENDIX A

Subspace-based System Identification Techniques

Let $\Gamma(s)$ be a generic transfer function whose dimension is $p * m$. And we denote the appoximate transfer function as $\Gamma'(s)$, the procedure of this system identification techniques is below:

1. To begin with, we need to evaluate the transfer function $G(i\omega)$ at the discrete time values of ω. We can generate $M + 1$ frequency response data on a set of uniformly spaced frequencies.

$$\omega_k = \frac{\pi k}{M}, \quad k = 0, \cdots, M$$

$$G_k = G(e^{i\omega_k}), \quad k = 0, \cdots, M \tag{A.1}$$

And we want to extend the data to the full unit circle

$$G_{M+k} = G^*_{M-k}, \quad k = 0, \cdots, M \tag{A.2}$$

where $(\cdot)^*$ denotes the complex conjugate.

2. Copmute the inverse dsicrete Fourier trasnform (IDFT) of frequency response

data:

$$\hat{h}_l = \frac{1}{2M} \sum_{k=0}^{2M-1} G_k e^{i2\pi lk/2M}, \quad l = 0, \cdots, 2M - 1 \tag{A.3}$$

The coefficients $\hat{h}_l$ can be regarded as the approximate discrete time impulse response of the transfer function $\Gamma(i\omega)$.

3. Definite the block Hankel matrix $\hat{H}$ as:

$$\hat{H} = \begin{bmatrix} \hat{h}_1 & \cdots & \hat{h}_r \\ \vdots & \ddots & \vdots \\ \hat{h}_q & \cdots & \hat{h}_{q+r} \end{bmatrix} \tag{A.4}$$

where $q > 0, r > 0, q+r \leq 2M$. There are different ways to assemble the Hankel matrix. One way is to choose the points $\hat{h}_l$ that has the most information about the system dynamics and the size of Hankel matrix can be reduced without lowering accuracy [68].

4. Calculate the singular value decomposition (SVD) of the Hankel matrix

$$\hat{H} = \begin{bmatrix} U_1 & U_2 \end{bmatrix} \begin{bmatrix} \Sigma_1 & 0 \\ 0 & \Sigma_2 \end{bmatrix} \begin{bmatrix} V_1^T \\ V_2^T \end{bmatrix} \tag{A.5}$$

where both Σ_1 and Σ_2 are diagnol and have the singular values in decreasing order. The partitioning of the matrix above is determined such that the singular values in Σ_2 are zero to numerical precision, while those in Σ_1 are significant. The number of the singular values in Σ_1 is noted as n_γ (chosen as 10 for H_r and 20 for W).

5. Construct an approximate finite-dimensional discrete time system as:

$$\hat{\Gamma}'(z) = \hat{D} + \hat{C}[zI - \hat{A}]^{-1}\hat{B} \tag{A.6}$$

192

where

$$\hat{A} = [\text{first}(q-1)p \text{ rows of } U_1]^+ [\text{last}(q-1)p \text{rows of } U_1] \tag{A.7}$$

$$\hat{C} = [\text{first } p \text{ rows of } U_1] \tag{A.8}$$

$$\hat{B} = \left[I - \hat{A}^{2M}\right] \Sigma_1 [\text{first } m \text{ rows of } V_1]^T \tag{A.9}$$

$$\hat{D} = \hat{h}_0 - \hat{C}\hat{A}^{2M-1}\Sigma_1 [\text{first } m \text{ rows of } V_1]^T \tag{A.10}$$

where $(\cdot)^+$ denotes the left pseudoinverse. This is the discrete time transfer function $\hat{\Gamma}'(z)$ and then compute the matrix $\hat{A}$ to see if it is stable (e.g., all the poles are inside the unit disk). Any poles outside the unit disk are radially reflected inside the disk, and then $\hat{B}, \hat{D}$ needs to be recalculated.

6. The matrix parameter $\{A, B, C, D\}$ for the approximate continuous-time transfer function

$$\hat{\Gamma}(s) = D + C[sI - A]^{-1}B \tag{A.11}$$

is then found via the standard bilinear transformation using sampling time T (we choose $T = 0.1s$ in our example), which can be evaluated using the d2c command in Matlab.

7. The approximate transfer function $\Gamma'(s)$ needs to be postive real. We need to check the passivity of $\hat{\Gamma}(s)$ and if it is passive, then $\Gamma'(s) = \hat{\Gamma}(s)$. If not, we can find the new parameters B_{new} and D_{new} to approximate the behavior of the transfer function $\hat{\Gamma}(s)$ while satisfying the passivity constraint: There exists two matrice $P, S > 0$ and a scalar $\gamma \leq 0$, such that

$$\begin{bmatrix} PA^T + AP & B_{\text{new}} - PC^T \\ B_{\text{new}}^T - CP & -D_{\text{new}}^T - D_{\text{new}} \end{bmatrix} \leq 0 \tag{A.12}$$

193

$$\begin{bmatrix} SA^T + AS & B_{\text{new}} - B \\ B_{\text{new}}^T - B^T & -I \end{bmatrix} \leq 0 \qquad\qquad (A.13)$$

$$\begin{bmatrix} CSC^T - \gamma & D_{\text{new}} - D \\ D_{\text{new}}^T - D^T & -I \end{bmatrix} \leq 0 \qquad\qquad (A.14)$$

Our objective is to minimize the value of γ. Since the above constraints are LMI, this optimization is actually a convex optimization, which can solved efficient in Matlab. The approximate continuous time transfer function $\Gamma'(s)$ can be expressed as:

$$\Gamma'(s) = D_{\text{new}} + C[zI - A]^{-1}B_{\text{new}} \qquad\qquad (A.15)$$

BIBLIOGRAPHY

[1] A. Stahl, "The utilization of the power of ocean waves." *Trans Am Soc Mech Eng*, vol. 13, p. 438–506, 1892.

[2] J. Falnes, "A review of wave-energy extraction," *Marine structures*, vol. 20, no. 4, pp. 185–201, 2007.

[3] D. Evans and A. de O Falcao, "Hydrodynamics of ocean wave-energy utilization," Springer-Verlag New York, Inc., New York, NY, Tech. Rep., 1985.

[4] K. Budar and J. Falnes, "A resonant point absorber of ocean-wave power," *Nature*, vol. 256, no. 5517, pp. 478–479, 1975.

[5] M. E. McCormick, *Ocean engineering mechanics: with applications*. Cambridge University Press, 2009.

[6] D. Evans, D. Jeffrey, S. Salter, and J. Taylor, "Submerged cylinder wave energy device: theory and experiment," *Applied Ocean Research*, vol. 1, no. 1, pp. 3–12, 1979.

[7] Y. Masuda, "Experimental full-scale results of wave power machine kaimei in 1978," in *Proc First Symp Wave Energy Utilization, Gothenburg, Sweden*, 1979, pp. 349–63.

[8] F. d. O. Antonio, "Wave energy utilization: A review of the technologies," *Renewable and sustainable energy reviews*, vol. 14, no. 3, pp. 899–918, 2010.

[9] M. Previsic, A. Moreno, R. Bedard, B. Polagye, C. Collar, D. Lockard, W. Toman, S. Skemp, S. Thornton, R. Paasch10 *et al.*, "Hydrokinetic energy in the united states—resources, challenges and opportunities," in *Proceedings of 8th European Wave Tidal Energy Conference*, 2009, pp. 76–84.

[10] U. A. Korde and J. Ringwood, *Hydrodynamic control of wave energy devices*. Cambridge University Press, 2016.

[11] *Power buoys: electricity from waves*. The economist, May 2001, no. 78-79.

[12] R. Pelc and R. M. Fujita, "Renewable energy from the ocean," *Marine Policy*, vol. 26, no. 6, pp. 471–479, 2002.

[13] T. Thorpe, "An overview of wave energy technologies: status, performance and costs," *Wave power: moving towards commercial viability*, vol. 26, pp. 50–120, 1999.

[14] B. Drew, A. R. Plummer, and M. N. Sahinkaya, "A review of wave energy converter technology," 2009.

[15] T. Aderinto and H. Li, "Ocean wave energy converters: Status and challenges," *Energies*, vol. 11, no. 5, p. 1250, 2018.

[16] K. Edwards, M. Mekhiche *et al.*, "Ocean power technologies powerbuoy®: system-level design, development and validation methodology," 2014.

[17] M. Kramer, L. Marquis, P. Frigaard *et al.*, "Performance evaluation of the wavestar prototype," in *Proceedings of the 9th European Wave and Tidal Energy Conference, Southampton, UK*. Citeseer, 2011, pp. 5–9.

[18] R. Henderson, "Design, simulation, and testing of a novel hydraulic power take-off system for the pelamis wave energy converter," *Renewable energy*, vol. 31, no. 2, pp. 271–283, 2006.

[19] J. Cruz, *Ocean wave energy: current status and future prespectives*. Springer Science & Business Media, 2007.

[20] V. L. Neuenschwander, "Wave activated generator," Sep. 3 1985, uS Patent 4,539,485.

[21] H. Polinder, M. E. Damen, and F. Gardner, "Linear pm generator system for wave energy conversion in the aws," *IEEE transactions on energy conversion*, vol. 19, no. 3, pp. 583–589, 2004.

[22] M. Mueller, "Electrical generators for direct drive wave energy converters," *IEE Proceedings-generation, transmission and distribution*, vol. 149, no. 4, pp. 446–456, 2002.

[23] S. H. Salter, "Wave power," *Nature*, vol. 249, no. 5459, pp. 720–724, 1974.

[24] T. Setoguchi and M. Takao, "Current status of self rectifying air turbines for wave energy conversion," *Energy conversion and management*, vol. 47, no. 15-16, pp. 2382–2396, 2006.

[25] A. Tapia, G. Tapia, J. X. Ostolaza, and J. R. Saenz, "Modeling and control of a wind turbine driven doubly fed induction generator," *IEEE Transactions on energy conversion*, vol. 18, no. 2, pp. 194–204, 2003.

[26] T. Ackermann and L. Söder, "Wind energy technology and current status: a review," *Renewable and sustainable energy reviews*, vol. 4, no. 4, pp. 315–374, 2000.

[27] A. F. Falcão and J. C. Henriques, "Oscillating-water-column wave energy converters and air turbines: A review," *Renewable Energy*, vol. 85, pp. 1391–1424, 2016.

[28] A. A. Wells, "Rotary transducers," Sep. 9 1980, uS Patent 4,221,538.

[29] F. d. O. António, "Modelling and control of oscillating-body wave energy converters with hydraulic power take-off and gas accumulator," *Ocean engineering*, vol. 34, no. 14-15, pp. 2021–2032, 2007.

[30] S. H. Salter, J. Taylor, and N. Caldwell, "Power conversion mechanisms for wave energy," *Proceedings of the Institution of Mechanical Engineers, Part M: Journal of Engineering for the Maritime Environment*, vol. 216, no. 1, pp. 1–27, 2002.

[31] M. Greenhow, J. H. Rosen, and M. Reed, "Control strategies for the clam wave energy device," *Applied ocean research*, vol. 6, no. 4, pp. 197–206, 1984.

[32] K. Hasselmann, T. Barnett, E. Bouws, H. Carlson, D. Cartwright, K. Enke, J. Ewing, H. Gienapp, D. Hasselmann, P. Kruseman *et al.*, "Measurements of wind-wave growth and swell decay during the joint north sea wave project (jonswap)," *Ergänzungsheft 8-12*, 1973.

[33] S. Salter, "The development of the duck concept," in *Proc. Wave Energy Conference*, 1978, pp. 17–27.

[34] K. Budal and J. Falnes, "Optimum operation of improved wave-power converter," *Mar. Sci. Commun.;(United States)*, vol. 3, no. 2, 1977.

[35] P. Nebel, "Maximizing the efficiency of wave-energy plant using complex-conjugate control," *Proceedings of the Institution of Mechanical Engineers, Part I: Journal of Systems and Control Engineering*, vol. 206, no. 4, pp. 225–236, 1992.

[36] K. Budal *et al.*, "Interacting point absorbers with controlled motion," 1980.

[37] M. Greenhow and S. White, "Optimal heave motion of some axisymmetric wave energy devices in sinusoidal waves," *Applied Ocean Research*, vol. 19, no. 3-4, pp. 141–159, 1997.

[38] F. d. O. António, "Phase control through load control of oscillating-body wave energy converters with hydraulic pto system," *Ocean Engineering*, vol. 35, no. 3-4, pp. 358–366, 2008.

[39] P. Gieske, "Model predictive control of a wave energy converter: Archimedes wave swing," 2007.

[40] F. Fusco and J. V. Ringwood, "Short-term wave forecasting for real-time control of wave energy converters," *IEEE Transactions on sustainable energy*, vol. 1, no. 2, pp. 99–106, 2010.

[41] J. Cretel, A. Lewis, G. Lightbody, and G. Thomas, "An application of model predictive control to a wave energy point absorber," *IFAC Proceedings Volumes*, vol. 43, no. 1, pp. 267–272, 2010.

[42] T. K. Brekken, "On model predictive control for a point absorber wave energy converter," in *2011 IEEE Trondheim PowerTech*. IEEE, 2011, pp. 1–8.

[43] M. Richter, M. E. Magana, O. Sawodny, and T. K. Brekken, "Nonlinear model predictive control of a point absorber wave energy converter," *IEEE Transactions on Sustainable Energy*, vol. 4, no. 1, pp. 118–126, 2012.

[44] J. Hals, J. Falnes, and T. Moan, "Constrained optimal control of a heaving buoy wave-energy converter," *Journal of Offshore Mechanics and Arctic Engineering*, vol. 133, no. 1, 2011.

[45] ——, "A comparison of selected strategies for adaptive control of wave energy converters," *Journal of Offshore Mechanics and Arctic Engineering*, vol. 133, no. 3, 2011.

[46] F. Fusco and J. Ringwood, "Suboptimal causal reactive control of wave energy converters using a second order system model," in *Proceedings of the 21st (2011) International Offshore and Polar Engineering Conference*. International Society of Offshore and Polar Engineers (ISOPE), 2011, pp. 687–694.

[47] J. Scruggs, S. Lattanzio, A. Taflanidis, and I. Cassidy, "Optimal causal control of a wave energy converter in a random sea," *Applied Ocean Research*, vol. 42, pp. 1–15, 2013.

[48] R. Nie, J. Scruggs, A. Chertok, D. Clabby, M. Previsic, and A. Karthikeyan, "Optimal causal control of wave energy converters in stochastic waves–accommodating nonlinear dynamic and loss models," *International Journal of Marine Energy*, vol. 15, pp. 41–55, 2016.

[49] J. Scruggs and R. Nie, "Disturbance-adaptive stochastic optimal control of energy harvesters, with application to ocean wave energy conversion," *Annual Reviews in Control*, vol. 40, pp. 102–115, 2015.

[50] J. Scruggs, "Multi-objective optimal causal control of an ocean wave energy converter in random waves," in *OCEANS'11 MTS/IEEE KONA*. IEEE, 2011, pp. 1–6.

[51] M. Grant and S. Boyd, "Cvx: Matlab software for disciplined convex programming, version 2.1," 2014.

[52] J. Morison, J. Johnson, S. Schaaf *et al.*, "The force exerted by surface waves on piles," *Journal of Petroleum Technology*, vol. 2, no. 05, pp. 149–154, 1950.

[53] J. Scruggs, "Causal control design for wave energy converters with finite stroke," *IFAC-PapersOnLine*, vol. 50, no. 1, pp. 15 678–15 685, 2017.

[54] G. E. Dullerud and F. Paganini, *A course in robust control theory: a convex approach.* Springer Science & Business Media, 2013, vol. 36.

[55] K. Zhou, J. C. Doyle, K. Glover *et al.*, *Robust and optimal control.* Prentice hall New Jersey, 1996, vol. 40.

[56] H. K. Khalil, *Nonlinear systems.* Prentice hall Upper Saddle River, NJ, 2002, vol. 3.

[57] S. Boyd, S. P. Boyd, and L. Vandenberghe, *Convex optimization.* Cambridge university press, 2004.

[58] S. Boyd, L. El Ghaoui, E. Feron, and V. Balakrishnan, *Linear matrix inequalities in system and control theory.* SIAM, 1994.

[59] J. G. VanAntwerp and R. D. Braatz, "A tutorial on linear and bilinear matrix inequalities," *Journal of process control*, vol. 10, no. 4, pp. 363–385, 2000.

[60] K. Premaratne and E. I. Jury, "Discrete-time positive-real lemma revisited: the discrete-time counterpart of the kalman-yakubovitch lemma," *IEEE Transactions on Circuits and Systems I: Fundamental Theory and Applications*, vol. 41, no. 11, pp. 747–750, 1994.

[61] Y. Lao and J. Scruggs, "Nonlinear control of passive vibratory systems with finite actuation stroke," *Automatica*, vol. 118, p. 109013, 2020.

[62] J. B. Hoagg and D. S. Bernstein, "Nonminimum-phase zeros-much to do about nothing-classical control-revisited part ii," *IEEE Control Systems Magazine*, vol. 27, no. 3, pp. 45–57, 2007.

[63] W. Cummins, "The impulse response function and ship motions," David Taylor Model Basin Washington DC, Tech. Rep., 1962.

[64] J. Falnes, "On non-causal impulse response functions related to propagating water waves," *Applied Ocean Research*, vol. 17, no. 6, pp. 379–389, 1995.

[65] C. J. Damaren, "Time-domain floating body dynamics by rational approximation of the radiation impedance and diffraction mapping," *Ocean Engineering*, vol. 27, no. 6, pp. 687–705, 2000.

[66] O. Faltinsen, *Sea loads on ships and offshore structures.* Cambridge university press, 1993, vol. 1.

[67] T. McKelvey, H. Akçay, and L. Ljung, "Subspace-based multivariable system identification from frequency response data," *IEEE Transactions on Automatic Control*, vol. 41, no. 7, pp. 960–979, 1996.

[68] Y. Lao and J. T. Scruggs, "A modified technique for spectral factorization of infinite-dimensional systems using subspace techniques," in *2019 IEEE 58th Conference on Decision and Control (CDC).* IEEE, 2019, pp. 5412–5419.

[69] S. Mavrakos and P. Koumoutsakos, "Hydrodynamic interaction among vertical axisymmetric bodies restrained in waves," *Applied Ocean Research*, vol. 9, no. 3, pp. 128–140, 1987.

[70] S. Mavrakos, "Hydrodynamic coefficients for groups of interacting vertical axisymmetric bodies," *Ocean Engineering*, vol. 18, no. 5, pp. 485–515, 1991.

[71] K. Kokkinowrachos, S. Mavrakos, and S. Asorakos, "Behaviour of vertical bodies of revolution in waves," *Ocean Engineering*, vol. 13, no. 6, pp. 505–538, 1986.

[72] Y. Goda, "A comparative review on the functional forms of directional wave spectrum," *Coastal Engineering Journal*, vol. 41, no. 1, pp. 1–20, 1999.

[73] M. B. Priestley, *Spectral analysis and time series*. Academic press, 1981.

[74] S. M. Kay, *Modern spectral estimation*. Pearson Education India, 1988.

[75] P. Van Overschee, B. De Moor, W. Dehandschutter, and J. Swevers, "A subspace algorithm for the identification of discrete time frequency domain power spectra," *Automatica*, vol. 33, no. 12, pp. 2147–2157, 1997.

[76] H. AkçAy and S. TüRkay, "Frequency domain subspace-based identification of discrete-time power spectra from nonuniformly spaced measurements," *Automatica*, vol. 40, no. 8, pp. 1333–1347, 2004.

[77] H. Akçay, "Frequency domain subspace-based identification of discrete-time power spectra from uniformly spaced measurements," *Automatica*, vol. 47, no. 2, pp. 363–367, 2011.

[78] ——, "Frequency domain subspace-based identification of discrete-time singular power spectra," *Signal Processing*, vol. 92, no. 9, pp. 2075–2081, 2012.

[79] K. Hinnen, M. Verhaegen, and N. Doelman, "Robust spectral factor approximation of discrete-time frequency domain power spectras," *Automatica*, vol. 41, no. 10, pp. 1791–1798, 2005.

[80] H. Akçay and S. Türkay, "Positive realness in stochastic subspace identification: A regularized and reweighted nuclear norm minimization approach," in *2015 European Control Conference (ECC)*. IEEE, 2015, pp. 1760–1765.

[81] D. MacMartin, D. Miller, S. Hall, C. Rogers, and C. Fuller, "Structural control using active broadband impedance matching," in *Recent Advances in Active Control of Sound and Vibration*, 1991, pp. 604–617.

[82] J. Scruggs, "On the causal power generation limit for a vibratory energy harvester in broadband stochastic response," *Journal of Intelligent Material Systems and Structures*, vol. 21, no. 13, pp. 1249–1262, 2010.

[83] D. W. Miller, S. R. Hall, and A. H. Von Flotow, "Optimal control of power flow at structural junctions," *Journal of Sound and Vibration*, vol. 140, no. 3, pp. 475–497, 1990.

[84] D. S. Bernstein, *Matrix mathematics: theory, facts, and formulas.* Princeton university press, 2009.

[85] K. J. Åström, *Introduction to stochastic control theory.* Courier Corporation, 2012.

[86] B. D. Anderson and J. B. Moore, *Optimal control: linear quadratic methods.* Courier Corporation, 2007.

[87] J. T. Scruggs and Y. Lao, "A new passivity-based nonlinear causal control technique for wave energy converters with finite stroke," in *2019 American Control Conference (ACC).* IEEE, 2019, pp. 5472–5479.

[88] Y.-K. Lin, "Probabilistic theory of structural dynamics(book on probabilistic theory of structural dynamics, analyzing responses of structures to random vibrations)," *NEW YORK, MCGRAW-HILL BOOK CO., 1967. 366 P*, 1967.

[89] J. T. Scruggs, I. L. Cassidy, and S. Behrens, "Multi-objective optimal control of vibratory energy harvesting systems," *Journal of Intelligent Material Systems and Structures*, vol. 23, no. 18, pp. 2077–2093, 2012.

[90] C. Scherer, P. Gahinet, and M. Chilali, "Multiobjective output-feedback control via lmi optimization," *IEEE Transactions on automatic control*, vol. 42, no. 7, pp. 896–911, 1997.

[91] A. J. van der Schaft and A. Van Der Schaft, *L2-gain and passivity techniques in nonlinear control.* Springer, 2000, vol. 2.

[92] B. D. Anderson and J. B. Moore, *Optimal filtering.* Courier Corporation, 2012.

[93] S. Jin, R. J. Patton, and B. Guo, "Viscosity effect on a point absorber wave energy converter hydrodynamics validated by simulation and experiment," *Renewable energy*, vol. 129, pp. 500–512, 2018.

[94] J. Doyle and G. Stein, "Robustness with observers," *IEEE transactions on automatic control*, vol. 24, no. 4, pp. 607–611, 1979.

[95] H. Kwakernaak and R. Sivan, "The maximally achievable accuracy of linear optimal regulators and linear optimal filters," *IEEE Transactions on Automatic Control*, vol. 17, no. 1, pp. 79–86, 1972.

[96] M. A. Bhinder, A. Babarit, L. Gentaz, and P. Ferrant, "Assessment of viscous damping via 3d-cfd modelling of a floating wave energy device," in *Proceedings of the 9th European Wave and Tidal Energy Conference, Southampton, UK*, 2011, pp. 5–9.